İSTANBUL TECHNICAL UNIVERSITY ★ INSTITUTE OF SCIENCE AND TECHNOLOGY

DEVELOPMENT OF A SIMPLIFIED SCHEME FOR INTRINSIC LOW-DIMENSIONAL MANIFOLDS BY EXPLOITING THE HIERARCHICAL STRUCTURES OF HYDROCARBON FUELS

M.Sc. Thesis by

Barış Ali ŞEN, Mech. Eng.

503011002

Date of submission : 05 May 2003

Date of defence examination: 26 May 2003

Supervisor (Chairman): Prof. Dr. İ. Bedii ÖZDEMİR

Members of the Examining Committee Prof.Dr. Ertuğrul ARSLAN (İ.T.Ü.)

Prof.Dr. Rüstem ASLAN (İ.T.Ü.)

MAY 2003

İSTANBUL TEKNİK ÜNİVERSİTESİ ★ FEN BİLİMLERİ ENSTİTÜSÜ

DÜŞÜK BOYUTLU ÇÖZÜM UZAYI YÖNTEMİNİN YÜKSEK HİDROKARBONLU YAKITLARIN HİYERARŞİK YAPILARI KULLANILARAK GELİŞTİRİLMESİ

YÜKSEK LİSANS TEZİ

Mak. Müh. Barış Ali ŞEN
503011002

Tezin Enstitüye Verildiği Tarih : 05 Mayıs 2003
Tezin Savunulduğu Tarih : 26 Mayıs 2003

Tez Danışmanı : Prof. Dr. İ. Bedii ÖZDEMİR
Diğer Jüri Üyeleri Prof.Dr. Ertuğrul ARSLAN (İ.T.Ü.)
Prof.Dr. Rüstem ASLAN (İ.T.Ü.)

MAYIS 2003

ACKNOWLEDGEMENT

I would like to express my gratitude to my supervisor Prof. Dr. İ. Bedii Özdemir, who gave me this interesting and challenging topic to work. I have been working with him for more than three years in the Fluids Laboratories of İTÜ and during all this time his continuous interest on my studies led me to learn many thing. It was a really tough time when I turned back from RWTH-Aachen Universität into İTÜ, and unhesitatingly, he gave me a second chance to rejoin into his group in the mid-year. Also, it was really kind of him that he served all of his opportunities that he could possibly do, including sharing his experience on scientific works and his life. He gave me a lot of freedom than the other researchers of the Fluids Laboratories and waited patiently to find the correct way by myself and finish the work.

I am also pleased to acknowledge Prof. Dr. Dr. h.c. Jürgen Warntaz, for accepting me into his research group in Ruprecht - Karls - Universität Heidelberg, providing a scholarship and let me to use all the availabilities in IWR. Without his kind help it will not be possible to study on this particular subject.

It has been a pleasure to work with many research students and fellows and to benefit from their advice and good friendship. Friendship of M.Sc. Gökhan Özkan, M.Sc. Ömer Dölek, B.Sc. E. Orçun Kozaka in Fluids Laboratories of İTÜ and, Dipl-Chem. Iliyana Naydenova, Dipl-Phys.Berthold Schramm at the IWR of Ruprecht – Karls - Universität Heidelberg is appreciated. Among all the researchers of Fluids Laboratories and IWR I would like to thank first to my friend E. Orçun Kozaka for being always with me and listening to problems related with my research, which was particularly valuable at the moments of disappointment. Also, it was very kind of Iliyana and Alexander Naydenova, to share invaluable moments and for their help even after I turned back to Turkey.

Special thanks goes to Zeynep Didem Çolakel, Barış Beyhan and Eyüp Serdar Öztürk for their friendship and their attempts to lighten the burden of the project by sharing many days with me. These extend to Ömer Dölek, Barbara Werner in that they always helped to resolve problems related with official regulations.

I want to extend my deepest gratitude to my family, my mother Nagihan Şen, my father Mehmet Şen for their encouragement and support throughout the years of my education, and I would like to dedicate my thesis to them. It will not be possible without their mental and financial help to accomplish this work. Finally I would like to thank to my sister Nur Banu Şen, for her patience into my nervous attitudes in home and her help during the preparation of this thesis.

CONTENTS

Page Number

ACKNOWLEDGEMENT……...ii
CONTENTS…….iii
ABBREVATIONS……v
TABLE LIST……...vi
FIGURE LIST……vii
SYMBOL LIST ……...ix
SUMMARY……...xiii
ÖZET……...xv

1. EQUATIONS FOR TURBULENT REACTIVE FLOWS……...1
1.1. Gas Phase Equations……1
1.2. Averaging of the Gas Phase Equations……...4
1.2.1. Reynolds stress model……..8
1.2.2. k - ε model……8

2. CHEMISTRY MODELING FOR REACTIVE FLOWS……...10
2.1. Detailed Reaction Mechanisms……10
2.2. Global Reaction Mechanisms……15
2.3. Steady State and Partial Equilibrium Approximations……..16
2.4. Automatic Reduction of the Reaction Mechanisms……..19
2.5. Effect of Eigenvalues and Eigenvectors on Chemical Kinetics……24

3. CHEMICAL AND PHYSICAL INTERPRETATION OF INTRINSIC LOW DIMENSIONAL MANIFOLDS METHOD……27
3.1. Mathematical Model……..31
3.2. ILDM tables……...49
3.3. Implementation of ILDM into CFD solvers……..55
3.4. Hierarchical Structure of ILDM……61

4. RESULTS AND DISCUSSION……67

5. CONCLUSIONS……79

REFERENCES.……..81

APPENDICES…….83

BIOGRAPHY……...……..98

ABBREVATIONS

CFD	: Computational Fluid Dynamics
DAE	**:** Differential Algebraic Equations
ILDM	: Intrinsic Low-Dimensional Manifolds
LHS	: Left Hand Side
PDF	: Probability Density Function
RAM	: Random Acces Memory
RHS	: Right Hand Side
RPV	: Reaction Progress Variable

LIST OF TABLES

Page Number

Table 1.1. $k - \varepsilon$ turbulence model coefficients 9

LIST OF FIGURES

		Page Number
Figure 2.1.	Schematic representation of the reactions.	12
Figure 2.2.	Concentration variations calculated with detailed mechanism approach.	14
Figure 2.3.	Concentration variations calculated with steady state approach.	18
Figure 2.4.	Concentration variations calculated with eigenvalue approach.	23
Figure 2.5.	Concentration variations calculated with automatic simplification approach.	24
Figure 2.6.	Projection of concentration variations into phase space.	26
Figure 3.1.	Trajectories of the chemical reactions for a stoichiometric methane/air system. Detailed kinetics for all time scales projected on to CO_2-H_2 planes.	29
Figure 3.2.	Trajectories of the chemical reactions for a stoichiometric methane/air system. Detailed reaction mechanism calculation projected on to a) CO_2-H_2O b) H_2O-CO planes.	29
Figure 3.3.	Trajectories of the chemical reactions for a stoichiometric methane/air system. Reduced kinetics obtained by ILDM projected on to a) CO_2-H_2O b) H_2O-CO planes.	30
Figure 3.4.	Trajectories of the chemical reactions for a stoichiometric Methane/Air system obtained by the Equilibrium calculations projected on to a) CO_2 – H_2O, b) H_2O – CO planes.	31
Figure 3.5.	Effect of a perturbation into chemical systems in terms of its eigenvalues.	36
Figure 3.6.	Eigenvalues of methane/air system obtained by ILDM calculations.	37
Figure 3.7.	Flow chart of the ILDM code.	43
Figure 3.8.	Flow chart of the outer loop for the modified version of ILDM code.	46
Figure 3.9.	Flow chart of the inner loop for the modified version of ILDM code.	47
Figure 3.10.	Flow chart for the modified version of ILDM code.	48
Figure 3.11.	Mass fraction variation of the species projected into H_2O space for a synthesis gas/oxygen combustion. (ζ=0.3)	50
Figure 3.12.	Mass fraction variation of the species projected into CO_2-H_2O space for methane/air combustion. (ζ=0.3)	52
Figure 3.13.	Mass fraction variation of the species projected into CO_2-H_2O space for methane/air combustion. (ζ=0.2)	53

Figure 3.14.	Mass fraction variation of the species projected into CO_2-H_2O space for a methane/air combustion. (ζ=0.5)	54
Figure 3.15.	Schematic illustration for PDF of mixture fraction in a turbulent non-premixed combustion configuration.	57
Figure 3.16.	Burke-Schumann solution for the variation of CO_2 and H_2O with respect to mixture fraction.	59
Figure 3.17.	Schematic representation of the C_1 and C_2 hydrocarbon oxidation.	63
Figure 3.18.	Low Dimensional Manifolds for different fuels projected into H_2O_2-CO_2-H_2O space.	66
Figure 3.19.	Low Dimensional Manifolds for different fuels projected into OH-CO_2-H_2O space.	66
Figure 4.1.	Mass fraction variation of the species projected into CO_2-H_2O space, calculated for synthesis gas/oxygen with classical approach.	70
Figure 4.2.	Mass fraction variation of the species projected into CO_2-H_2O space, calculated for methane/oxygen with hierarchical approach.	71
Figure 4.3.	Mass fraction variation of the species projected into CO_2-H_2O space, calculated for methane/oxygen with classical approach.	72
Figure 4.4.	Mass fraction variation of H with respect to CO_2 obtained for four different cross sections.	75
Figure 4.5.	Mass fraction variation of CO with respect to CO_2 obtained for four different cross sections.	76
Figure 4.6.	Mass fraction variation of H_2O_2 with respect to CO_2 obtained for four different cross sections.	77
Figure 4.7.	Mass fraction variation of OH with respect to CO_2 obtained for four different cross sections.	78

LIST OF SYMBOLS

a_i	:Reaction coefficient of species i
B_b	:Frequency factor for the backward reaction
Bc	:Control matrix
B_f	:Frequency factor for the forward reaction
c	:Local error vector
c_c	:Central manifold for the error vector
c_i	:Inertial manifold for the error vector
c_p	:Specific heat
C_k	:Diffusion term coefficient of the TKE equation
C_ε	:Diffusion term coefficient of the dissipation equation
$C_{\varepsilon 1}$	:Production term coefficient of the dissipation equation
$C_{\varepsilon 2}$	:Destruction term coefficient of the dissipation equation
D_{AB}	:Diffusion coefficient
E	:Internal energy
E_B	:Activation energy for backward reaction
E_F	:Activation energy for forward reaction
E_i	:Eigenvector matrix corresponding the slow system
$\tilde{\tilde{E}}$	:Favre Mean of the internal energy
err	:Error
$\vec{F}$	:Rate of change of the state vector
h_i	:Specific enthalpy of species *i*
h^{ref}	:Reference value for enthalpy
J	:Jacobian
$\vec{J}$	:Heat flux vector
$\vec{J}_i$	:Diffusion flux density of species *i*
k	:Turbulent kinetic energy
k_b	:Backward reaction coefficient
k_c	:Thermal conductivity
kf	:Forward reaction coefficient
l	:Kolmogorov length scale
Mi	:Molar mass of species *i*
n	:Number of the reactants
n_b	:Temperature exponent for the backward reaction

n_f :Temperature exponent for the forward reaction
n_s :Number of species
P :Pressure
P_c :Central manifold for parameter matrix
P_i :Inertial manifold for parameter matrix
Pr :Prandtl number, α / υ
$\overline{\overline{p}}$:Pressure tensor
$P(\rho, T)$:Probability density function
$\vec{\vec{P}}(\vec{\psi})$:Parameter equations
P^{ref} :Reference value for pressure
q_i :Schur vectors
Q :Schur matrix
$\dot{Q}^C$:Source due to chemical reactions
R_0 :Ideal gas constant
$\vec{s}^{\varepsilon}$:Initial perturbation
$\vec{s}^{0}$:Equilibrium state of perturbation
$\vec{S}(\vec{\Psi}(\vec{x}, t))$:Rate of formation due to chemical kinetics
Sc :Schmidt number, α / D_{AB}
S_α :Source term for general form of the conservation equation
t :Time
T :Temperature
$\widetilde{T}''^2$:Variance of temperature
u :x component of the velocity field
$\overline{U}$:x component of the mean velocity
U' :x component of the fluctuation velocity
$\vec{U}$:Velocity field
$\widetilde{U}$:x component of the Favre mean velocity
$\vec{\overline{U}}$:Mean component of the velocity field
$\vec{U}'$:Fluctuation component of the velocity field
$\vec{\widetilde{U}}$:Favre mean component of the velocity field
$\vec{U}''$:Favre fluctuation component of the velocity field
v :y component of the velocity field
$\overline{V}$:y component of the mean velocity
V' :y component of the fluctuation velocity
$\widetilde{V}$:y component of the Favre mean velocity
w :z component of the velocity field
w_B :Reaction rate of backward reaction

w_F	:Reaction rate of forward reaction
w_R	:Reaction rate
$\overline{W}$	:*z* component of the mean velocity
W'	:*z* component of the fluctuation velocity
$\widetilde{W}$	:*z* component of the Favre mean velocity
Yi	:Mass fraction of species *i*
$\widetilde{Y}_i$	:Favre mean of mass fraction of species *i*
$\dot{Y}_i$	:Rate of change of species *i*
Z_f	:Schur vectors corresponding the fast part
Zs	:Schur vectors corresponding the slow part
δ_{iL}	:Cronecker delta
$\Delta h^0{}_f$	:Standard enthalpy of formation
ε	:Dissipation rate of the turbulence kinetic energy
ϕ''	:*y* component of the Favre fluctuation velocity
Φ_i	:Specific mass fraction of species i
ϑ_i	:Eigenvectors
φ''	:*x* component of the Favre fluctuation velocity
Γ	:Eigenvector matrix
Γ_f	:Eigenvectors corresponding the fast part
Γ_s	:Eigenvectors corresponding the slow part
Γ_α	:Diffusion coefficient for dummy variable
γ	:Error vector, without any control
γ_c	:Error vector, without any control, projected in to central manifold
γ_i	:Error vector, without any control, projected in to inertial manifold
κ	:Constant for proportional controller
Λ	:Eigenvalues matrix
Λ_f	:Eigenvalues corresponding the fast part
Λ_s	:Eigenvalues corresponding the slow part
λ_i	:Eigenvalues
μ	:Dynamic viscosity
θ	:Parameterization vector
θ_c	:Central manifold of the parameterization vector
θ_i	:Inertial manifold of the parameterization vector
ρ	:Density
ρ_i	:Density of species *i*

$\overline{\rho}$	:Mean of density
$\dot{\rho}$	:Rate of change of density
τ	:Constant for integral controller
τe	:Initial value for elements
τ_C	:Initial value for element *C*
τ_H	:Initial value for element H
τ_N	:Initial value for element N
τ_O	:Initial value for element O
ν	:Kinematic viscosity
υ_i'	:Stoichiometric coefficient for reactants side *i*
υ_i''	:Stoichiometric coefficient for products side i
$\vec{\Xi}\left(\vec{\Psi}(\vec{x},t)\right)$	:Rate of formation due to physical kinetics
$\vec{\psi}$	:Parameterized form of the state vector
$\vec{\psi}_0$	:Equilibrium point
ψ''	:z component of the Favre fluctuation velocity
$\vec{\Psi}$	:State vector
ζst	:Stoichiometric mixture fraction
$\widetilde{\zeta''^2}$	:Variance of mixture fraction

DEVELOPMENT OF A SIMPLIFIED SCHEME FOR INTRINSIC LOW-DIMENSIONAL MANIFOLDS BY EXPLOITING THE HIERARCHICAL STRUCTURES OF HYDROCARBON FUELS

SUMMARY

In recent years, there has been an increasing attempt to improve techniques used in the simulation of the reactive flows, where the turbulent combustion processes are of greater importance. Apart from the difficulty imposed by the turbulent flow field, which can be resolved by using appropriate procedures such as Reynolds averaged Navier-Stokes or large eddy simulations, the combustion processes add further intricacy into the governing equations in that the reactions occurring within the combustion zone effects the chemical source terms of the species. Even though the source terms can be calculated by tracking the elementary reactions, this procedure may end up with a detailed investigation of thousands of reactions with many species, which is beyond the current capacity of the most of the computer storages, especially for 3-D turbulent reactive flow applications. Thus, it is highly desirable to develop methods that can simplify the reaction kinetics without loss of accuracy. In this respect, the Intrinsic Low-Dimensional Manifolds (ILDM) method is a promising procedure, which can be used for simplifying the chemical kinetics, based on the dynamical system approach. However, simulation of the reactive flows with ILDM is still a challenging task compared with the conventional simplification methods. Apart from its advantages, some aspects of the ILDM require improvement, in particular, for high hydrocarbon fuels. It is known that, as the complexity of the fuel increases, the number of the reactions involved in the combustion also increases, resulting in a much more stiff equation system. Sensitivity analyses, performed for different hydrocarbon fuels to understand the overall kinematics of the combustion processes show that the rate-limiting part of the detailed mechanisms is the oxidation of the CH_3 and C_2H_5 radicals. Thus, the strategy in the development of detailed reaction mechanisms for high hydrocarbons is to use the C_1-C_4 reaction mechanism and to add additional reactions for the specific system. Then it is possible to state that, if the eigenvalues, corresponding to the additional reaction mechanisms, have smaller values than the C_1-C_4 mechanism, both the original and the reduced schemes should represent the same topology in the phase space. In this way, mechanisms developed, for example, for C_8H_{18} combustion will also be applicable to the calculation of the CH_4 flames. It is because of this hierarchical structure, the ILDM calculation performed for different combustion systems usually show the same characteristics; they tend to reach into their equilibrium point regardless of the dimensionality of the simulation.

In an attempt to generate result tables with ILDM methodology for the simulation of reactive flows where high hydrocarbon fuels are used as the fuel, the existing code have been modified in a way based on the hierarchical structure of the chemical kinetics. The

modified version of the program is capable of generating subsequent result tables starting from the simpler ones like synthesis gas, and ending in the desired fuel composition. The existing datasets in the result tables, which belongs to a simpler fuel, is used as initial guesses for the next calculation. The accessible area characterized by the mass fractions of the species may not be closed region, or may contain zones where it is not possible to generate a result. Since the classical approach of ILDM does not have any insight about the chemical aspects of the combustion, most of the time required for the construction of result tables is spend on those regions. On the other hand with the modified version, it is possible to set proper initial conditions for an ILDM simulation, which dictates the zones available for calculation, and serves relaxed state vectors as initial guesses.

Within the concept of the thesis the subroutines of the existing ILDM code is modified and its accuracy is validated with a set of calculation for synthesis gas and methane combustion systems. Results showed that both the altered and classical versions of ILDM represent the same distribution in the phase space. Also it was interesting to see that even tough the computational area exhibits a larger area for simpler fuel, the accessible area obtained by the hierarchical calculation matches perfectly with the classical approach. Thus, it is possible to state that the effect of the initial guesses does not force the simulation to produce wrong results. Also, for further error analyzing the results obtained by the calculations are compared within each other to get the error. It was observed that the local error of the modified version remains %0.5-1 for small values of H2O mass fraction. The increase in the mass fraction value of H2O results an increase in the error as well but not exceeding a maximum of %9.

DÜŞÜK BOYUTLU ÇÖZÜM UZAYI YÖNTEMİNİN YÜKSEK HİDROKARBONLU YAKITLARIN HİYERARŞİK YAPILARI KULLANILARAK GELİŞTİRİLMESİ

ÖZET

Günümüzde, çalkantılı yanma işlemlerinin baskın olduğu, reaktif akışların sayısal gerçeklenmesi uygulamalarında kullanılmak üzere basitleştirilmiş modellerin geliştirilmesi konusunda yoğun olarak çalışmalar gerçekleştirilmektedir. Bu tür akışlarda oluşan çalkantı yapılarının Reynolds ortalamalı Navier-Stokes veya büyük akım paketçikleri gibi çeşitli yöntemlerle elde edilmesi olanaklıyken yanma doğasının temel denklemlerde kaynak terimlerini oluşturması çözümleri daha da zorlaştırmaktadır. Her ne kadar kimyasal kaynak terimlerinin yanma esnasında oluşan bütün tepkimelerin ve bileşenlerin incelenmesi yardımıyla elde edilmesi mümkün olsa da, bu tür bir çalışma binlerce reaksiyonun ve bir o kadar da bileşenin incelenmesini gerektirdiği için özellikle de 3 boyutlu, çalkantılı reaktif akışların modellenmesi uygulamalarında günümüz bilgisayarlarının işlemci ve depolama kapasitesini kat be kat aşmaktadır. Bu açıdan akış fiziğinin yanı sıra kimya kinetiğinin de basitleştirilmesi gereklilik kazanmaktadır. Düşük boyutlu çözüm uzayı (DBÇU) yöntemi kimya kinetiğini dinamik sistem olarak algılayarak basitleştirilmiş kimyasal kaynak terimlerinin elde edilmesine olanak sağlamaktadır. Ancak, reaktif akışların DBÇU ile basitleştirilmesi halen özellikle yüksek hidrokarbonlu yakıtların yanması için geliştirilmesi gereken bir yöntemdir. Yanma uygulamalarında yakıt sistemi karmaşıklaştıkça oluşan ara tepkimelerin sayısı da çözümü zorlaştıracak bir şekilde artmaktadır. Yanma işlemlerinin kinetiğinin anlaşılması için çeşitli hidrokarbon yakıtları için gerçekleştirilen hassaslık analizleri CH_3 ve C_2H_5 radikallerinin oksidasyonunun bütün sistemin hızını belirlediğini göstermektedir. Bu açıdan yüksek hidrokarbonlu yakıtların detaylı yanma mekanizmalarının oluşturulması sırasında izlenen yöntem C_1-C_4 tepkime mekanizmalarının üzerine yakıta ait özel tepkimelerin eklenmesidir. Bu durumun bir sonucu olarak, mekanizmaya sonradan eklenen tepkimelerin yol açtığı özdeğerlerin C_1-C_4 mekanizmasından elde edilenlerden küçük olması durumunda çözüm uzayında benzer yüzey özellikleri göstermektedir. Bu hiyerarşik yapı, CH_4 için elde edilen detaylı yanma mekanizmalarının C_8H_{18} yakıtı için de kullanılabileceğini göstermektedir. Değişik yanma sistemleri için gerçekleştirilen sayısal gerçekleme uygulamalarında aynı karakteristik eğrilerin görülmesi de hidrokarbonlu yakıtların detaylı mekanizmalarının hiyerarşik yapıları ile açıklanmaktadır.

DBÇU yönetemi ile yüksek hidrokarbonlu yakıtların sayısal gerçeklenmesine imkan tanıyacak şekilde kimyasal kinetiğin hiyerarşik yapısı da kullanılarak basitleştirilmiş bir model geliştirilmiştir. Bu model yardımıyla DBÇU programı basit yakıtlarla başlayıp istenen yakıtta biten ardışık sayısal gerçeklemeler yapabilmekte ve çözüm tablolarında basit yakıtlar için bulunan veri kalıplarının bir sonraki hesaplama için de kullanabilmektedir. Çözüm uzayında kütle oranları ile ifade edilen çözüm bölgeleri içinde hesaplama yapmanın mümkün olmadığı bölgeler bulunbilmektedir. Klasik DBÇU yöntemi sayısal gerçeklemenin kimyası hakkında bir fikir sahibi

olmadığından dolayı çözüm tablolarının oluşturulması sırasında zamanın büyük bir bölümünü bu tür bölgelerde hesaplama yapmakla geçirmektedir. Değiştirilmiş modelde yüksek hidrokarbonlu yakıtlar için DBÇU sayısal gerçeklemesi sırasında, basit yakıtlar için elde edilen veri kalıplarının başlangıç koşulları olarak kullanılması yardımıyla bu tür bölgelerin önceden algılanarak çözüm zamanını oldukça düşürülmesi öngörülmektedir.

Yüksek lisans tezi kapsamında, DBÇU yönteminin elde var olan kaynak kodu değiştirilmiş ve doğruluğu değişik yakıt sistemleri için çalıştırılarak test edilmiştir. Sonuçlar değiştirilmiş programın gerçeğe çok yakın doğrulukta çözümler verdiğini göstermektedir. Ayrıca basit yakıtlar için elde edilen sonuç tabloları çözüm uzayında büyük bir alan işgal ederken, değiştirilmiş model gerçek sistemdeki sınırları da büyük bir hassaslıkta yakalayabilmektedir. Bu açıdan başlangıç değerlerinin sonucu yanlış yerlere doğru götürmediğini görmek sevindirici bir sonuçtur. Hata irdelemeleri sonucunda H_2O kütle oranının düşük değerleri için hatanın % 0.5 ile 1 arası gelmekte olduğu görülmüştür. H_2O kütle oranın artışı ise yerel hata değerlerini %9 mertebesine doğru çekmektedir.

1. EQUATIONS FOR TURBULENT REACTIVE FLOWS

1.1 Gas Phase Equations

The physical concepts of the combustion processes requires the determination of the conserved variables associated with the fluid flow and combustion, by the equations of the continuum mechanics, the so-called conservation equations and the state relation of the thermodynamics. The conservation equations for a reactive flow are, conservation of species mass, conservation of total mass, conservation of momentum and finally, the conservation of energy. It should be noted that, associated with the release of thermal energy and increase in temperature, there is a local decrease in density which in turn affects the momentum balance. Therefore, all these equations are loosely coupled to each other (Peters 2000). For a conserved variable Φ, the general form of the conservation equations is,

$$\frac{\partial(\rho\Phi)}{\partial t} + \nabla(\rho\vec{U}\Phi) = \nabla(\Gamma_{\Phi}\,\mathrm{grad}\Phi) + S_{\Phi} \tag{1.1}$$

in that, first term on the left hand side (LHS) of the equation is the accumulation of the variable Φ within the control volume, where as the second term represents the convection of Φ with the velocity field $\vec{U}$. First term that can be seen in the right hand side (RHS) is associated with the diffusion of Φ. The molecular diffusion of the conserved variable is proportional with a diffusion coefficient Γ_{Φ}. Finally, last term is the source term for Φ (Versteeg and Malalasekera 1996).

The velocity field $\vec{U}$ in the above formulation is considered as,

$$\vec{U} = u\vec{i} + v\vec{j} + w\vec{k} \tag{1.2}$$

in that *u*, *v* and *w* are the components of the velocity field in three orthogonal directions of the Cartesian coordinate system.

The conserved variable for the conservation of species mass equation is $\frac{\rho_i}{\rho}$ and the diffusion coefficient Γ_Φ is denoted as D_{AB}. Using this terminology, the equation for conservation of species mass turns out to be,

$$\frac{\partial \rho_i}{\partial t} + \nabla\left(\rho_i \vec{U}\right) = \nabla\left(\rho D_{AB} \nabla\left(\frac{\rho_i}{\rho} \right)\right) + \dot{\rho}_i \tag{1.3}$$

It is assumed that all the species have the equal diffusivities given by,

$$D_{AB} = \frac{\mu}{\rho S_C} \tag{1.4}$$

where μ is the dynamic viscosity and Sc is the Schmidt number.

To represent the conservation equation in terms of the mass fractions, $Y_{i,}$ of the species *i*, is a more preferred way. So, in terms of the mass fraction, equation (1.3), can be derived by replacing the partial mass per unit volume, $\rho_i = \rho Y_i$. The resulting equation is as follows.

$$\rho \frac{\partial Y_i}{\partial t} + \nabla\left(\rho Y_i \vec{U}\right) = \nabla\left(\rho D_{AB} \nabla\left(Y_i\right)\right) + \rho \dot{Y}_i \tag{1.5}$$

Conserved variable Φ for the conservation of total mass is 1. Since the production of mass is not possible for a closed control volume, the RHS of the equation is zero. General form of the conservation of mass equation for an unsteady, three-dimensional, compressible fluid flow can be seen below,

$$\frac{\partial \rho}{\partial t} + \nabla\left(\rho \vec{U}\right) = 0 \tag{1.6}$$

Conservation of momentum is the application of Newton's second law into the fluid dynamics. It is well known that, Newton's second law states that the rate of change of momentum of a particle equals the sum of the forces acting on the particle (Versteeg and Malalasekera 1996). The conserved form of the momentum equation for an inviscid, incompressible and free from gravitational effects can be represented as,

$$\frac{\partial(\rho\vec{U})}{\partial t}+\nabla(\rho\vec{U}\vec{U})=-\nabla P+\nabla(\mu\nabla\vec{U}) \tag{1.7}$$

Similarly, by neglecting the body forces, e.g. buoyancy and curvature effects, the momentum equation can be written more explicitly for three orthogonal directions of the Cartesian coordinate system,

x: $$\frac{\partial(\rho u)}{\partial t}+\nabla(\rho u\vec{U})=-\frac{\partial P}{\partial x}+\nabla(\mu\nabla u) \tag{1.8}$$

y: $$\frac{\partial(\rho v)}{\partial t}+\nabla(\rho v\vec{U})=-\frac{\partial P}{\partial y}+\nabla(\mu\nabla v) \tag{1.9}$$

z: $$\frac{\partial(\rho w)}{\partial t}+\nabla(\rho w\vec{U})=-\frac{\partial P}{\partial z}+\nabla(\mu\nabla w) \tag{1.10}$$

The equation for the specific internal energy *E*, excluding the heats of formation of the species involved, is

$$\frac{\partial(\rho E)}{\partial t}+\nabla(\rho\vec{u}E)=-P\nabla(\vec{u})-\nabla(\vec{J})+\rho\varepsilon+\dot{Q}^{C} \tag{1.11}$$

The term $\rho\varepsilon$ represents the energy source due to the turbulence where $\dot{Q}^{C}$ is the source due to the chemical reactions. ε is the dissipation rate of the turbulent kinetic energy. The heat flux vector $\vec{J}$ is the sum of contributions due to heat conduction and enthalpy diffusion,

$$J=-K\nabla T-\rho D\sum_{i}h_{i}\nabla\left(\frac{\rho_{i}}{\rho}\right) \tag{1.12}$$

where *T* is the fluid temperature, *K* is the thermal conductivity and h_i is the specific enthalpy of species *i*. *K* is calculated from the Prandtl number, Pr, and the specific heat at constant pressure *cp* using

$$K=\frac{\mu cp}{\mathrm{Pr}} \tag{1.13}$$

where the specific heat of the mixture is calculated using,

$$c_P(T) = \sum_i \frac{\rho_i}{\rho} c_{Pi}(T) \tag{1.14}$$

The specific enthalpies h_i in equation (1.12) and the specific heats of the species c_{pi} in equation (1.14) are obtained from the JANAF tables as functions of temperature (Stull and Prophet 1971).

The state relations are assumed to be of an ideal gas, giving equations for the temperature and the pressure as

$$T = \frac{1}{R_0} \sum_i M_i \left[h_i(T) - \frac{\rho_i}{\rho} E(T) \right] \tag{1.15}$$

$$P = R_0 T \sum_i \frac{\rho_i}{M_i} \tag{1.16}$$

where M_i is the molar mass of species i, and R_0 is the ideal gas constant.

1.2 Averaging of the Gas Phase Equations

The gas phase conservation equations and the state relation include all the information required for understanding the physics of the fluid flow and reactions in a certain reactive flow application. To solve the equations directly is possible and yet it is sufficient to evaluate the velocity, temperature and density fields. It should be noted that the equations are in general non-linear and coupled with each other. From the view of a mathematician, this fact may seem as a problem while trying to reach a result from the given boundary and initial conditions, but it can be overcome by using special numerical discretisation methods. The main difficulty arises from the physics of the problem itself. The practical fluid flow applications require the solution for the turbulence flow scales. Turbulence is an irregular motion, which in general makes its appearance in fluids when they flow over solid surfaces or streams of different speeds. Irregularity is the most important feature and because of this it is impossible to describe all the details of the motion as functions of space and time coordinates (Tennekes and Lumley 1973). The turbulent flow imposes different structures ranging from the largest scale, which is associated with the principle

dimensions of the flow field, to the smallest scale of the eddies referred as the Kolmogorov scaling. In order to get exact results, one should consider the spatial and time scale dimension of the eddies in the Kolmogorov scale as well as the large scales. Thus, the logical mesh size restriction imposed by the physics of the fluid flow, requires large amount of computer storage. Since it exceeds the storage and CPU capacity of the computers, a simplification procedure should be accomplished on the simulating techniques. Commonly used procedure is to apply a time averaging on the turbulent structures of the flow field, which means an assumption of the time dependent eddies are frozen at any time, and using coarser meshes than the Kolmogorov scale (Tennekes and Lumley 1973; Pope 2000). To get the exact form of the conservation equations for the simulation of a turbulent flow, replacing the mean and fluctuation terms of the conserved variables, a time averaging procedure is accomplished.

Then, the final form of the conservation of momentum equation in the closed form for turbulent flow is,

$$\frac{\partial\left(\vec{\bar{U}}\right)}{\partial t}+\nabla\left(\rho\vec{\bar{U}}\vec{\bar{U}}\right)=-\frac{1}{\rho}\nabla P+\upsilon\left(\nabla^2\vec{\bar{U}}\right)-\nabla\left(\overline{U_i'U_j'}\right) \tag{1.17}$$

where $\vec{\bar{U}}$ and $\vec{U}'$ represents the mean and fluctuation components of the velocity field, each given in equation (1.18) and (1.19) respectively,

$$\vec{\bar{U}}=\overline{U}\vec{i}+\overline{V}\vec{j}+\overline{W}\vec{k} \tag{1.18}$$

$$\vec{U}'=U'\vec{i}+V'\vec{j}+W'\vec{k} \tag{1.19}$$

The new components arising on the right hand side of the equation (1.17) are called the “Reynolds Stresses”, and are due to the momentum, which is generated by the velocity fluctuations due to the turbulent flow (Chen and Jaw 1998). The rest of the equation resembles to the one that was introduced for the mean flow in equation (1.7). Then, in a similar way, the momentum equation in terms of the mean and fluctuation components of the velocity field can be represented in the three directions of the coordinate system as follows,

x: $$\frac{\partial \overline{U}}{\partial t}+\nabla\left(\overline{V}\vec{\overline{U}}\right)=-\frac{1}{\rho}\frac{\partial P}{\partial x}+\upsilon\nabla^2\left(\overline{U}\right)-\left[\frac{\partial \overline{U'U'}}{\partial x}+\frac{\partial \overline{U'V'}}{\partial y}+\frac{\partial \overline{U'W'}}{\partial z}\right] \quad (1.20)$$

y: $$\frac{\partial \overline{V}}{\partial t}+\nabla\left(\overline{V}\vec{\overline{U}}\right)=-\frac{1}{\rho}\frac{\partial P}{\partial y}+\upsilon\nabla^2\left(\overline{V}\right)-\left[\frac{\partial \overline{V'U'}}{\partial x}+\frac{\partial \overline{V'V'}}{\partial y}+\frac{\partial \overline{V'W'}}{\partial z}\right] \quad (1.21)$$

z: $$\frac{\partial \overline{W}}{\partial t}+\nabla\left(\overline{W}\vec{\overline{U}}\right)=-\frac{1}{\rho}\frac{\partial P}{\partial z}+\upsilon\nabla^2\left(\overline{W}\right)-\left[\frac{\partial \overline{W'U'}}{\partial x}+\frac{\partial \overline{W'V'}}{\partial y}+\frac{\partial \overline{W'W'}}{\partial z}\right] \quad (1.22)$$

Apart from the mathematical calculations of the conservation equations for a turbulent reactive flow application; one important point that has to be cleared out associated with the averaging of the equations, is the effect and the role of the density gradient. The large variation of the temperature in the combustion chambers strongly affects the density field. Thus, in order to avoid the terms involving density fluctuations, a density-weighted averaging, namely the Favre averaging, should be introduced into the conservation equations (Warnatz *et al.* 2001). Using Favre averaging, a variable Φ can be split into its Favre mean ($\tilde{\Phi}$) and Favre fluctuating (Φ'') terms as follows,

$$\Phi=\tilde{\Phi}+\Phi'' \quad (1.23)$$

where the Favre mean component is defined as,

$$\tilde{\Phi}=\frac{\overline{\rho\Phi}}{\overline{\rho}} \quad (1.24)$$

Introducing the new averaging technique into the conservation equations and the state relation, the final form of the equations governing the turbulent flow field, turns out to be;

Conservation of species mass

$$\frac{\partial \overline{\rho}\tilde{Y}_i}{\partial t}+\nabla\left(\overline{\rho}\tilde{Y}_i\vec{\tilde{U}}\right)=\nabla\left(\overline{\rho D\nabla Y_i}-\overline{\rho\vec{U}''Y''}_i\right)+\overline{\dot{\rho Y}_i} \quad (1.25)$$

Conservation of total mass

$$\frac{\partial \overline{\rho}}{\partial t} + \nabla\left(\overline{\rho}\vec{\tilde{U}} \right) = 0 \tag{1.26}$$

Conservation of momentum

$$\frac{\partial\left(\overline{\rho}\vec{\tilde{U}} \right)}{\partial t} + \nabla\left(\overline{\rho}\vec{\tilde{U}}\vec{\tilde{U}} \right) = -\nabla P + \mu\nabla^2\left(\vec{\tilde{U}} \right) - \nabla\left(\overline{\rho\vec{U}''\vec{U}''} \right) \tag{1.27}$$

Conservation of energy

$$\frac{\partial\left(\overline{\rho}\tilde{E} \right)}{\partial t} + \nabla\left(\overline{\rho}\vec{\tilde{U}}\tilde{E} \right) = -P\nabla\vec{\tilde{U}} - \nabla\left(\vec{\bar{J}} + \rho\vec{U}''E'' \right) + \overline{\rho}\overline{\varepsilon} + \overline{\dot{Q}} \tag{1.28}$$

State relations

$$\tilde{T} = \frac{1}{R_0}\sum_i M_i\left[h_i\left(\tilde{T}\right) - \frac{\overline{\rho_i}}{\overline{\rho}}\tilde{E}\left(\tilde{T}\right) \right] \tag{1.29}$$

$$\tilde{P} = \frac{\overline{\rho}R_0\tilde{T}}{\overline{M}} \tag{1.30}$$

The main difficulty in the solution of the turbulent flows arises when the fluctuating components of the velocity field are introduced in the conservation equations. The second correlations of the fluctuation velocities, the Reynolds stresses, impose new unknowns into the equation set. The number of unknowns introduced in the Favre averaged conservation equations ($\tilde{U},\tilde{V},\tilde{W},\overline{\varphi''\varphi''},\overline{\varphi''\phi''},\overline{\varphi''\psi''},\overline{\phi''\phi''},\overline{\phi''\psi''},\overline{\psi''\psi''},P,\tilde{T},\varphi''\tilde{T},\phi''\tilde{T},\psi''\tilde{T}$), becomes much larger than the total number of the conservation equations and, as a result, the equation set is not closed, which this is called turbulence closure problem. In order to solve the problem, the second correlations of the fluctuation terms need to be modeled with appropriate assumptions. Most widely used modeling techniques, among the one-equation and two-equation models, are the Reynolds Stress Model and the k - ε model. A brief explanation for the each modeling technique can be found on the next subsections.

1.2.1 Reynolds stress model

One approach to solve the turbulence closure problem is to derive extra equations from the momentum equation, for the Reynolds stresses and to solve the new set of governing equations. The Reynolds stress model works fairly good when there is a large velocity gradient in the flow field (Fluent users manual). The equation derived for the Reynolds stresses can be seen below,

$$\frac{D\overline{U_i''U_j''}}{Dt} = \frac{\partial}{\partial x_L}\left[-\overline{U_i''U_j''U_L''} - \frac{P}{\rho}\left(\delta_{jL}U_i'' + \delta_{iL}U_j''\right) + \upsilon\frac{\partial\left(\overline{U_i''U_L''}\right)}{\partial x_L}\right]$$

$$+\left[\overline{U_i''U_L''}\frac{\partial\tilde{U}_j}{\partial x_L} + \overline{U_j''U_L''}\frac{\partial\tilde{U}_i}{\partial x_L}\right] - 2\upsilon\overline{\frac{\partial U_i''}{\partial x_L}\frac{\partial U_j''}{\partial x_L}} + \frac{P}{\rho}\left(\overline{\frac{\partial U_i''}{\partial x_j}} + \overline{\frac{\partial U''j}{\partial xi}}\right) \qquad (1.31)$$

where, the first term on the LHS is the molecular diffusion of the Reynolds stresses, second one the production, third one dissipation and the last one is the pressure strain term.

1.2.2 k - ε model

Another technique used in turbulence modeling is the k - ε model. Solution methodology generally compromises of solving two additional equations, one for the kinetic energy of the flow field induced by turbulence, and the other is for the dissipation of the turbulent kinetic energy (TKE).

"k", Turbulent Kinetic Energy Equation

$$\frac{Dk}{Dt} = \frac{\partial}{\partial x_L}\left[-\overline{k'U_L''} - \overline{\frac{PU_L''}{\rho}} + \upsilon\frac{\partial k}{\partial x_L}\right] - \overline{u_i u_L}\frac{\partial\tilde{U}_i}{\partial x_L} - \varepsilon \qquad (1.32)$$

First two terms on the LHS represent the turbulent diffusion of the TKE. Third term is the diffusion of the TKE with the molecular transport. The forth term is the production of the TKE with the fluctuations and, the last term is the dissipation of the TKE.

TKE equation can be modeled as,

$$\frac{Dk}{Dt} = \frac{\partial}{\partial x_L}\left[C_k \frac{k^2}{\varepsilon}\frac{\partial k}{\partial x_L} + \upsilon \frac{\partial k}{\partial x_L} \right] - \overline{U_i'' U_L''}\frac{\partial \tilde{U}_i}{\partial x_L} - \varepsilon \qquad (1.33)$$

"ε", Rate of Dissipation Equation

$$\frac{D\varepsilon}{Dt} = \frac{\partial}{\partial x_L}\left[-\overline{\varepsilon' u_L} - \frac{2\upsilon}{\rho}\overline{\frac{\partial U_L''}{\partial x_j}\frac{\partial P}{\partial x_j}} + \upsilon \frac{\partial \varepsilon}{\partial x_L} \right] + \left[-2\upsilon \overline{U_L''\frac{\partial U_L''}{\partial x_j}\frac{\partial^2 \tilde{U}_i}{\partial x_L \partial x_j}} \right.$$
$$\left. + 2\upsilon \frac{\partial U_i''}{\partial x_j}\left[\overline{\frac{\partial U_L''}{\partial x_i}\frac{\partial U_L''}{\partial x_j}} + \overline{\frac{\partial U_i''}{\partial x_L}\frac{\partial U_j''}{\partial x_L}} \right] \right] + \left[-2\upsilon \overline{\frac{\partial U_i''}{\partial x_j}\frac{\partial U_i''}{\partial x_L}\frac{\partial U''j}{\partial x_L}} - 2\upsilon \overline{\left(\frac{\partial^2 U_i''}{\partial x_L \partial x_L} \right)^2} \right] \qquad (1.34)$$

First two terms on the LHS represents the turbulent diffusion, where the third term is the molecular diffusion of the dissipation term. The fourth and fifth terms are related with the production of the dissipation and the sixth and seventh terms are associated with the destruction of dissipation.

Modeled equation is

$$\frac{D\varepsilon}{Dt} = \frac{\partial}{\partial x_L}\left[C_\varepsilon \frac{k^2}{\varepsilon}\frac{\partial \varepsilon}{\partial x_i} + \upsilon \frac{\partial \varepsilon}{\partial x_L} \right] - C_{\varepsilon 1}\frac{\varepsilon}{k}\overline{U_i'' U_j''}\frac{\partial U_i''}{\partial x_j} - C_{\varepsilon 2}\left(\frac{\varepsilon}{k} \right)\varepsilon \qquad (1.35)$$

The coefficients of the modeled TKE and Dissipation are generally used as,

Table 1.1 k - ε turbulence model coefficients

Coefficients	C_k	C_ε	$C_{\varepsilon 1}$	$C_{\varepsilon 2}$
Suggested Values	0.09-0.11	0.07-0.09	0.07-0.09	0.07-0.09

2. CHEMISTRY MODELING FOR REACTIVE FLOWS

The concept and the solution methodology of the reactive flows are complicated, and the complication arises by the source terms, which were introduced in the conservation of the species mass equation and the conservation of the energy equation. The source terms in those equations need to be handled carefully similar to the Reynolds stresses of the conservation of momentum equation. The source term in the conservation of species mass equation is associated with the consumption or production of the each species during the chemical reactions. Determination of the source or destruction term in the conservation of species mass equation can be fulfilled either by using the detailed mechanisms, or the reduced kinetic models of. Reduced models can be derived by investigating all individual reaction that take place during the combustion process, in the basis of the chemical kinetics. On the following sections solution procedures, which are widely used in the current combustion investigations, are given. These are detailed reaction mechanisms, global reaction rate mechanisms, quasi-steady state mechanisms, partial equilibrium chemistry and finally the automatic reduction of the reaction mechanisms.

2.1 Detailed Reaction Mechanisms

Detailed reaction mechanism calculations are based on solving the conservation equations for all species involved in the combustion process. The source terms arising on the conservation of species mass and conservation of energy equations needs to be evaluated for all species, which in turns requires a careful handling of the chemical kinetics of the elementary reactions. The source terms $\dot{\rho}_i$ of the equation (1.3) and $\dot{Q}$ of equation (1.11) can be calculated as follows,

$$\dot{\rho}_i = M_i \sum_r \left(\upsilon_i'' - \upsilon_i' \right) w_R \tag{2.1}$$

$$\dot{Q} = \sum_r w_R \sum_i (\upsilon_i'' - \upsilon_i')\left(\Delta h^0{}_f\right)_i \tag{2.2}$$

In the equations, w_R represents the reaction rate, which determines the progress rate of the reaction R, and υ_i', υ_i'' are the stoichiometric coefficients for the reactants side, and product side respectively. Let us demonstrate the calculation for a simple bi molecular reaction of the form,

$$\upsilon_A' \mathrm{A} + \upsilon_B' \mathrm{B} \xrightarrow{kf} \upsilon_C'' \mathrm{C} + \upsilon_D'' \mathrm{D}$$

where k_f is the forward reaction coefficient. The rate at which species A is consumed can be calculated as,

$$\left(\frac{d[A]}{dt}\right)_f = -\upsilon_A' kf [A]^{\upsilon_A'} [B]^{\upsilon_B'} = \upsilon_A w_F \tag{2.3}$$

A more compact form is,

$$w_F = k_f [A]^{\upsilon_A'} [B]^{\upsilon_B'} \tag{2.4}$$

Similar calculations can be done for a reaction of n reactants,

$$w_F = k_f \prod_{j=1}^{n} [Y_j]^{\upsilon_j'} \tag{2.5}$$

In the same manner, the production rate of the species A for the backward reaction is calculated as,

$$\upsilon_A' \mathrm{A} + \upsilon_B' \mathrm{B} \xleftarrow{k_b} \upsilon_C'' \mathrm{C} + \upsilon_D'' \mathrm{D}$$

$$\left(\frac{d[A]}{dt}\right)_b = -\upsilon_A' k_b [C]^{\upsilon_C''} [D]^{\upsilon_D''} = \upsilon_A w_B \tag{2.6}$$

where k_b is the reaction rate of the backward reaction. Then, the reaction rate of the backward reaction turns out to be,

$$w_B = k_b [C]^{\upsilon_C''} [D]^{\upsilon_D''} \tag{2.7}$$

and in a more general way for m products,

$$w_B = k_b \prod_{j=1}^{m} [Y_j]^{\upsilon_j''} \tag{2.8}$$

As a result, for an elementary reaction, containing an arbitrary number of reactants *n*, and products *m*, the reaction rate can be calculated by combining both forward and backward reactions as,

$$w_R = k_f \prod_{j=1}^{n} \left[Y_j\right]^{\upsilon_j'} - k_b \prod_{j=1}^{n} \left[Y_j\right]^{\upsilon_j''} \tag{2.9}$$

The rate coefficients of the forward and backward reactions, *kf* and k_b, are functions of temperature. They represent the frequency at molecular collision between molecules and the probability that a collision will lead a chemical reaction (Peters 2000). Even tough the exact values of the coefficients can only be obtained by experimental methods; there are also few mathematical expressions, which can be used in calculations of the chemical kinetics. The most widely used model, suggested by Arrhenius, can be seen in equations (2.10) and (2.11).

$$k_f(T) = B_f T^{n_f} e^{-\left(\frac{E_F}{RT}\right)} \tag{2.10}$$

$$k_b(T) = B_b T^{n_b} e^{-\left(\frac{E_b}{RT}\right)} \tag{2.11}$$

In the equations, B_f and B_b are the frequency factors, containing information about spatial configurations of the molecules during the reactions. They represent the probability of two molecules to collide and start a reaction. E_f and E_b are the activation energy corresponding to an energy barrier which has to be overcome. Finally n_f and n_b are the temperature exponents of the forward and backward reactions respectively.

As a result, the detailed mechanism calculations require the solution of a set of n_s non-linear and coupled differential equations derived for the consumption/production rates of the species. In order to clarify the solution procedure, a simple example will be given on a fictious 4-step reaction mechanism, which can be seen below

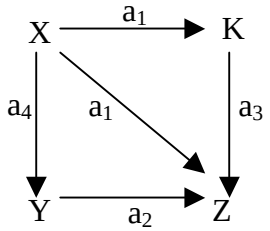


Figure 2.1 Schematic representation of the reactions

The consumption or the production of the each species during the chemical reaction can be written as follows,

$$\frac{d[X]}{dt} = -a_1 X - a_4 X - a_5 X \tag{2.12}$$

$$\frac{d[Y]}{dt} = a_1 X - a_2 Y \tag{2.13}$$

$$\frac{d[Z]}{dt} = a_2 Y + a_3 K + a_5 X \tag{2.14}$$

$$\frac{d[K]}{dt} = a_4 X - a_3 K \tag{2.15}$$

For the simplicity, reactions are assumed to be proceeding only in the forward direction, and the reaction rate coefficients are constant. In this case, the rate laws can be considered as a linear set of differential equation with constant coefficients, and can be solved with the appropriate initial conditions. Let us assume that in the initial stage, there exists only the species X in the reactor. Then, the initial conditions can be written as, $[X]_{t=0} = X_0$, $[Y]_{t=0} = 0$, $[Z]_{t=0} = 0$ and $[K]_{t=0} = 0$. The concentration variation of each species can be derived by solving the following differential equation

$$\begin{bmatrix} -(a_1 + a_4 + a_5) & 0 & 0 & 0 \\ a_1 & -a_2 & 0 & 0 \\ a_5 & a_2 & 0 & a_3 \\ a_4 & 0 & 0 & -a_3 \end{bmatrix} \begin{bmatrix} X \\ Y \\ Z \\ K \end{bmatrix} = \begin{bmatrix} \dot{X} \\ \dot{Y} \\ \dot{Z} \\ \dot{K} \end{bmatrix} \tag{2.16}$$

The solution can be calculated in the form of,

$$\vec{X} = e^{\lambda t} \vec{\vartheta} \tag{2.18}$$

where λ and $\vec{\vartheta}$ represents the eigenvalue and its eigenvector respectively. In this way, the general solution for the differential equation can be given as,

$$\vec{X} = C_1 e^{\lambda_1 t} \vec{\vartheta}_1 + C_2 e^{\lambda_2 t} \vec{\vartheta}_2 + C_3 e^{\lambda_3 t} \vec{\vartheta}_3 + ... + C_{n_s} e^{\lambda_{n_s} t} \vec{\vartheta}_{n_s} \tag{2.19}$$

The solution for the concentration of the species, calculated by this method, can be seen in equations (2.20), (2.21), (2.22) and (2.23)

$$X(t) = C_1 e^{-(a_1+a_4+a_5)t} \tag{2.20}$$

$$Y(t) = C_1\left(\frac{-a_1}{-a_2+a_1+a_4+a_5}\right)e^{-(a_1+a_4+a_5)t} + C_2 e^{-a_2 t} \tag{2.21}$$

$$Z(t) = C_1\left(\frac{-a_5+\left(a_1a_2 \diagup -a_2+a_1+a_4+a_5\right)+\left(a_3a_4 \diagup -a_3+a_1+a_4+a_5\right)}{(a_1+a_4+a_5)}\right)e^{-(a_1+a_4+a_5)t} + C_4 e^{-a_3 t} \tag{2.22}$$

$$K(t) = C_1\left(\frac{-a_4}{-a_3+a_1+a_4+a_5}\right)e^{-(a_1+a_4+a_5)t} + C_4 e^{-a_3 t} \tag{2.23}$$

The coefficients C_1, C_2 and C_4 can be calculated by applying the appropriate initial conditions, and are given in equation (2.24),

$$C_1 = x_0,\ C_2 = \frac{a_1 x_0}{-a_2+a_1+a_4+a_5},\ C_4 = \frac{-a_4 x_0}{-a_3+a_1+a_4+a_5} \tag{2.24}$$

The graphical representation of the solution can be seen in figure (2.2)

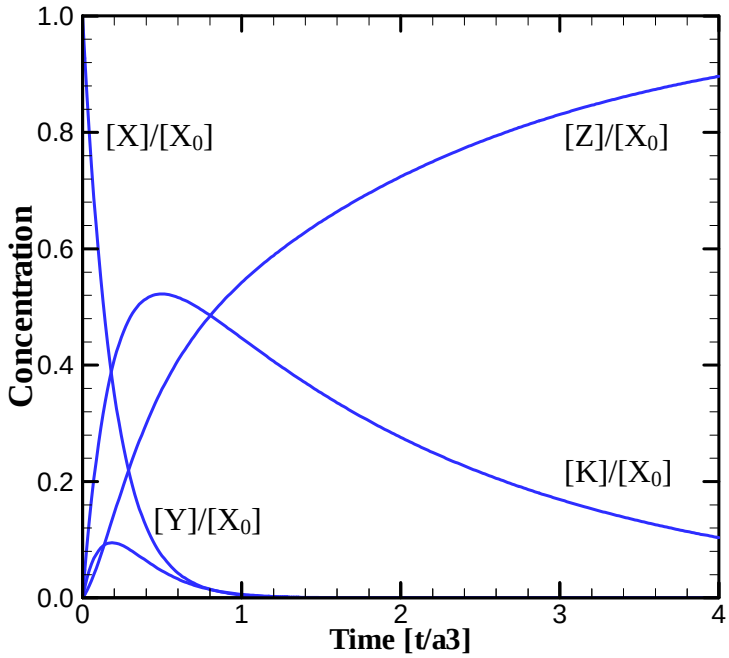


Figure 2.2 Concentration variations calculated with detailed mechanism approach

In the numerical calculation, species Y is assumed to be reactive and thus has a very short lifetime. This was verified by setting $a_2 >> a_3$.

2.2 Global Reaction Mechanisms

The combustion processes are usually involved with many species and elementary reaction steps. The combustion of n-heptane/air mixture, where the detailed mechanism contains 620 species and approximately 2400 reactions, can be given as a typical example (Chevalier et.al. 1992). For a 3-D turbulent reactive flow, calculation of the source terms given in the conservation of species mass transfer and conservation of energy equations, for each species, is not feasible by using the detailed reaction mechanism calculations. Also, in some cases the information for the chemical kinetics can be insufficient, or the intermediate species may not play an important role on the overall mechanism (Warnatz et. al. 2001). So, instead of focusing on each individual elementary reaction steps in deriving the source terms, defining a few rate-determined stable steps and performing the calculations on these global reactions is a more frequently used technique. Those global reactions should represent the stoichiometric relations among major species including fuel, oxidizer and the most stable combustion products. A simple example for this methodology can be seen below for a combustion process of methane/air system,

$$CH_4 + 2O_2 + 7.5\ N_2 \longrightarrow CO_2 + 2H_2O + 7.5\ N_2$$

Using the formulation of the chemical kinetics, the consumption of fuel with respect to the species involved in the global reaction can be calculated as,

$$\frac{d[CH_4]}{dt} = B_f T^{n_F} e^{\frac{-E_A}{R_0 T}} [CH_4][O_2]^2 [N_2]^{0.375} \qquad (2.25)$$

Apart from its advantage, which permits the demonstration of the chemical kinetics in terms of one or more few global steps, the global reaction methodology has many disadvantages, especially when an accurate scientific simulation is desired. Since many of the elementary reactions are not taken into consideration, the consumption or production of the elementary species and the radicals are not calculated. This fact reduces the information gained by tracking the concentration of species that plays important role in the combustion dynamics. CO concentration, which supplies

information for the ignition timing, or OH concentration, which gives further insight in the soot formation, cannot be get by the global reaction mechanisms. Another disadvantage of the methodology arises from the fact that the global mechanism steps are fictive reactions, which never happen or do not play an important role in the detailed mechanisms. Since they are not real, the coefficients and the concentration dependencies for each species involved in the global reaction are needed to be re calculated for successive simulations (Correa 2000). Due to the limited availability of the data, these values may only be applicable in a very narrow temperature range and some important species may be omitted (Maas and Pope 1992a).

2.3 Steady State and Partial Equilibrium Approximations

Most common used techniques for reducing chemical kinetics are the steady state and equilibrium approximations. The steady state solution procedure stems from investigating the intermediate species and determining the consumption or production rates of some of them experimentally, before the simulation. The main idea is nothing more than application of the assumption of; slow rate-limiting reactions determine the overall rate of the global reactions (Warnatz 2001). So, it can be concluded that the fast processes do not have much importance, compared with the slow processes, on the overall chemical kinetics of the combustion. Careful investigation of the reactions reveals that *a certain number of the intermediate species* are responsible for the occurrence of slow or fast reactions. Determination of the reactive elements, which have very short lifetime during the combustion, and setting their consumption rate to zero, forms the basis of the methodology. In this way it is possible to reduce the dimension of the differential equations representing the chemical kinetics, by turning them into simple algebraic equations.

Let us re calculate the concentration variations for the fictious reaction mechanism that was introduced in section (2.1). In this particular example the steady state assumption is valid for species Y. Applying the assumption of $\frac{dY}{dt} = 0$ to equation (2.13), the rate of concentration change for Y can be calculated as,

$$\frac{d[Y]}{dt} = a_1 X - a_2 Y = 0 \tag{2.26}$$

which in turn leads to an algebraic equation that in terms of *X* and *Y*. Then the set of governing equation turns out to be,

$$\frac{dX}{dt} = -(a_1 + a_4 + a_5)X \tag{2.27}$$

$$\frac{dZ}{dt} = (a_1 + a_5)X + a_3 K \tag{2.28}$$

$$\frac{dK}{dt} = a_4 X - a_3 K \tag{2.29}$$

and an additional algebraic equation for Y,

$$a_1 X = a_2 Y\ ,\ Y = \frac{a_1}{a_2} X \tag{2.30}$$

The set of linear differential equation can be written and solved by the same initial conditions given in the previous application.

$$\begin{bmatrix} -(a_1 + a_4 + a_5) & 0 & 0 \\ (a_1 + a_5) & 0 & a_3 \\ a_4 & 0 & -a_3 \end{bmatrix} \begin{bmatrix} X \\ Z \\ K \end{bmatrix} = \begin{bmatrix} \dot{X} \\ \dot{Z} \\ \dot{K} \end{bmatrix} \tag{2.31}$$

and the solution calculated for each species is,

$$X(t) = C_1 e^{-(a_1+a_4+a_5)t} \tag{2.32}$$

$$Z(t) = C_1 \left(\frac{\left(\frac{a_4 a_3}{-a_3 + a_1 + a_4 + a_5} \right) - (a_1 + a_5)}{a_1 + a_4 + a_5} \right) e^{-(a_1+a_4+a_5)} + C_2 + C_3 e^{-a_3 t} \tag{2.33}$$

$$K(t) = C_1 \left(\frac{-a_4}{-a_3 + a_1 + a_4 + a_5} \right) e^{-(a_1+a_4+a_5)} - C_3 e^{-a_3 t} \tag{2.34}$$

where the coefficients are,

$$C_1 = X_0 \tag{2.35}$$

$$C_2 = -X_0\left(\frac{\left(\frac{a_4 a_3}{-a_3+a_1+a_4+a_5}\right)-(a_1+a_5)}{a_1+a_4+a_5}\right) - X_0\left(\frac{-a_4}{-a_3+a_1+a_4+a_5}\right) \quad (2.36)$$

$$C_3 = X_0\left(\frac{-a_4}{-a_3+a_1+a_4+a_5}\right) \quad (2.37)$$

The concentration variations calculated with steady state species assumption can be seen in the figure (2.3). It can be clearly stated out that except for the early stages of concentration of species *Y*, the trajectories show similar behavior with the values that was derived from the detailed reaction mechanism technique.

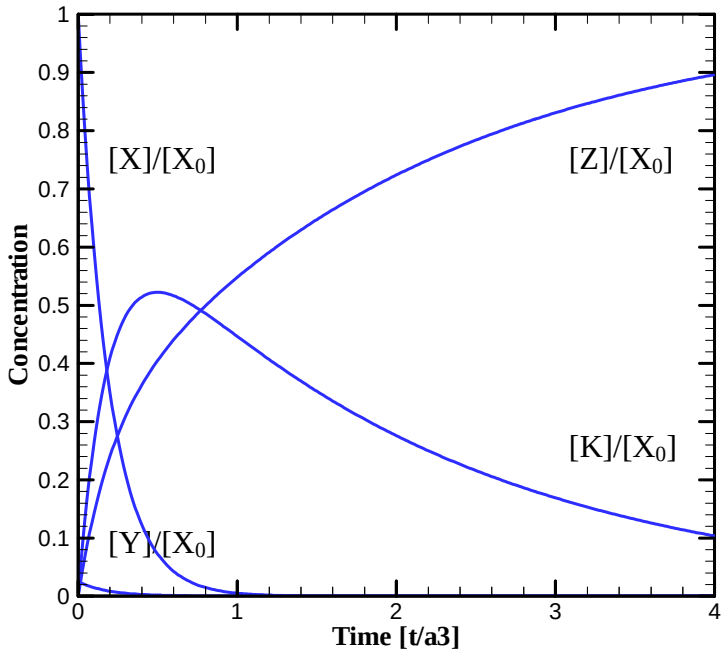


Figure 2.3 Concentration variations calculated with steady state approach

The partial equilibrium approximation assumes that the forward and the backward reaction rates of *a certain number of the reactions* are equal in specific conditions, and thus the rates of the forward and backward reactions are assumed to be equal (Rawath 1997). An example for such a case can be given from the reaction mechanism of the hydrogen combustion. An analysis of experiments shows that for

the temperature values above1800 K at 1 bar pressure, the reaction rates of the forward and backward reactions are so fast, that one obtains partial equilibria for the reactions,

$$H + O_2 \longrightarrow OH + O$$

$$O + H_2 \longrightarrow OH + H$$

$$OH + H_2 \longrightarrow H_2O + H$$

(Warnatz 2001). In this case, the set of differential equation that needed to be solved for the calculation of the consumption rates turns out to be an algebraic equations in terms of the intermediate species, by using the assumption of,

$$k_1[H][O_2] = k_2[OH][O]$$

$$k_3[O][H_2] = k_4[OH][H]$$

$$k_5[OH][H_2] = k_6[H_2O][H]$$

The final mechanism consists of set differential equations plus algebraic equations.

2.4 Automatic reduction of the reaction mechanisms

Simplification of the reaction kinetics by steady state, global reaction or equilibrium processes, in combination with global reactions, is widely used in combustion simulations. They are able to provide accurate and rapid results. But to simplify the reaction kinetics by using one of these techniques, the physics of the reaction mechanism should be well defined. For the application of the steady state assumption, the species which have very short lifetime must be determined prior to the simulation. Determination of those pre requisites for the equilibrium processes may be easy for simple combustion processes, like the combustion of synthesis gas, which involves 67 elementary reactions and 13 species (Maas and Pope, 1992a). But for the cases like combustion of methane/air or dodecane/air systems, which involves 295 and 888 elementary reactions respectively (Warnatz 1992), it is very difficult to track the reaction mechanism and specify the assumptions. So an automatic simplification methodology, which is capable of defining the reactive species and

equilibrium reactions, is highly desirable. The eigenvalue and eigenvector analysis of the reaction mechanism can be used to get the information required for the different time scales of the combustion. Another difficulty imposed by the chemical system is that the consumption or production rate of each species is coupled with each other. Thus, sometimes it is even impossible to reach a solution if the mechanism is not greatly simplified. This can also be resolved by the eigenvalue analysis of the reaction system. The set of reactions can be generally expressed as,

$$\vec{F} = J\vec{\psi} \tag{2.38}$$

where $\vec{\psi}$ is the species vector, $\vec{F}$ represents the vector of the rate of change of the concentrations and J is the Jacobian matrix composed of the forward and backward rate coefficients. The eigenvalues of the Jacobian matrix should satisfy the following eigenvalue equation,

$$J = \Gamma\Lambda\Gamma^{-1} \tag{2.39}$$

in that, Γ is the matrix composed of the eigenvectors of the Jacobian and Λ is a diagonal matrix containing the eigenvalues. Inserting equation (2.39) into the equation (2.38) yields,

$$\vec{F} = \Gamma\Lambda\Gamma^{-1}\vec{\psi} \tag{2.40}$$

and by multiplying both sides with the inverse of the eigenvector matrix from left,

$$\Gamma^{-1}\vec{F} = \Lambda\Gamma^{-1}\vec{\psi} \tag{2.41}$$

The final form of the equation set represents a set of ordinary differential equations of the form,

$$\frac{dy}{dt} = const.y \tag{2.42}$$

and the solution can be calculated easily as,

$$y(t) = y_0 \exp(const \times t) \tag{2.43}$$

Next, a simple example for the calculation of the species concentrations with the automatic reduction of the reaction mechanism will be given for the fictitious reaction mechanism, which was introduced in figure (2.1).

The reactions form the set of equations,

$$\begin{bmatrix} \dot{X} \\ \dot{Y} \\ \dot{Z} \\ \dot{K} \end{bmatrix} = \begin{bmatrix} -(a_1 + a_4 + a_5) & 0 & 0 & 0 \\ a_1 & -a_2 & 0 & 0 \\ a_5 & a_2 & 0 & a_3 \\ a_4 & 0 & 0 & -a_3 \end{bmatrix} \begin{bmatrix} X \\ Y \\ Z \\ K \end{bmatrix} \tag{2.44}$$

where, the eigenvalues of the Jacobian matrix is calculated as,

$$\Lambda = \begin{bmatrix} 0 & 0 & 0 & 0 \\ 0 & -a_3 & 0 & 0 \\ 0 & 0 & -(a_1 + a_4 + a_5) & 0 \\ 0 & 0 & 0 & -a_2 \end{bmatrix} \tag{2.45}$$

Note that the eigenvalues are sorted with decreasing real parts. Then, the corresponding eigenvectors are,

$$\Gamma = \begin{bmatrix} 0 & 0 & 1 & 0 \\ 0 & 0 & \dfrac{a_1}{a_2 - (a_1 + a_4 + a_5)} & -1 \\ 1 & -1 & \dfrac{\left[-a_5 + \dfrac{a_2 a_1}{a_1 + a_4 + a_5 - a_2} + \dfrac{a_3 a_4}{a_1 + a_4 + a_5 - a_3} \right]}{(a_1 + a_4 + a_5)} & 1 \\ 0 & 1 & \dfrac{a_4}{a_3 - (a_1 + a_4 + a_5)} & 0 \end{bmatrix} \tag{2.46}$$

and its inverse is,

$$\Gamma^{-1} = \begin{bmatrix} 1 & 1 & 1 & 1 \\ \dfrac{a_4}{a_1 + a_4 + a_5 - a_3} & 0 & 0 & 1 \\ 1 & 0 & 0 & 0 \\ \dfrac{a_1}{a_2 - (a_1 + a_4 + a_5)} & -1 & 0 & 0 \end{bmatrix} \tag{2.47}$$

The RHS of the equation (2.41) can be calculated as equation (2.48),

$$\Lambda\Gamma^{-1} = \begin{bmatrix} 0 & 0 & 0 & 0 \\ a_3 \times \dfrac{\left[-a_5 + \dfrac{a_2 a_1}{a_1 + a_4 + a_5 - a_2} + \dfrac{a_3 a_4}{a_1 + a_4 + a_5 - a_3}\right]}{(a_1 + a_4 + a_5)} & 0 & 0 & -a_3 \\ -(a_1 + a_4 + a_5) & 0 & 0 & 0 \\ \dfrac{a_2 a_1}{a_1 + a_4 + a_5 - a_2} & a_2 & 0 & 0 \end{bmatrix} \tag{2.48}$$

Then equation (2.48) yields four differential equations, (2.49), (2.50), (2.51) and (2.52), which are all decoupled from each other

$$\dot{X} + \dot{Y} + \dot{Z} + \dot{K} = 0 \tag{2.49}$$

$$-C_1 \times \dot{X} + \dot{K} = -a_3(-C_1 \times X + K) \tag{2.50}$$

$$\dot{X} = -(a_1 + a_4 + a_5)X \tag{2.51}$$

$$\frac{a_1}{a_2 - (a_1 + a_4 + a_5)}\dot{X} - \dot{Y} = -a_2\left(\frac{a_1}{a_2 - (a_1 + a_4 + a_5)}X - Y\right) \tag{2.52}$$

for C_1 being,

$$C_1 = a_3 \times \frac{\left[-a_5 + \dfrac{a_2 a_1}{a_1 + a_4 + a_5 - a_2} + \dfrac{a_3 a_4}{a_1 + a_4 + a_5 - a_3}\right]}{(a_1 + a_4 + a_5)} \tag{2.53}$$

The solution of the equations (2.49), (2.50), (2.51) and (2.52), is very simple, and they form four algebraic equations, (2.54), (2.55), (2.56) and (2.57),

$$X + Y + Z + K = X_0 + Y_0 + Z_0 + K_0 \tag{2.54}$$

$$-C_1 \times X + K = -a_3(-C_1 \times X_0 + K_0) \times \exp(-a_3 t) \tag{2.55}$$

$$X = X_0 \times \exp(-(a_1 + a_4 + a_5) \times t) \tag{2.56}$$

$$\frac{a_1}{a_2 - (a_1 + a_4 + a_5)}X - Y = \left(\frac{a_1}{a_2 - (a_1 + a_4 + a_5)}X_0 - Y_0\right) \times \exp(-a_2 t) \tag{2.57}$$

The results obtained from the automatic reduction of the reaction mechanism technique can be seen in figure (2.4). Both figures (2.2) and (2.3) show similar patterns, which means that the solution calculated by this method is correct.

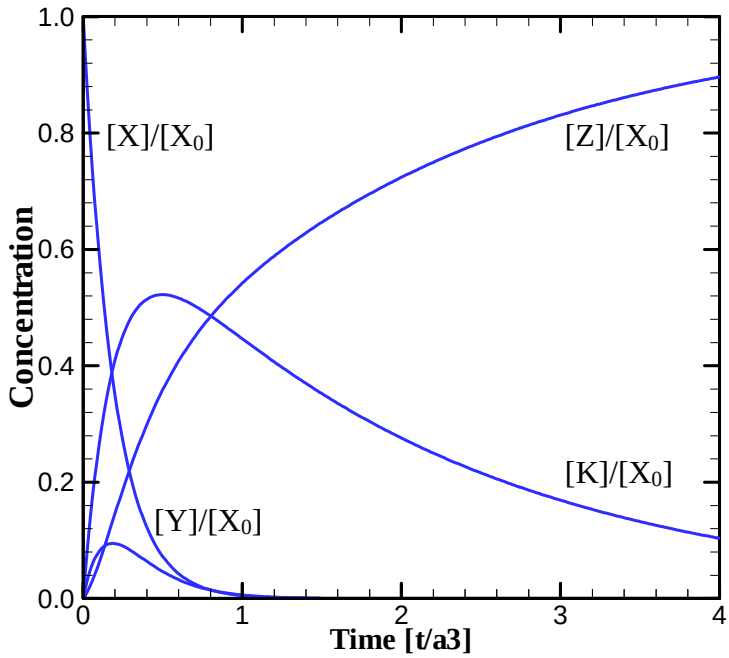


Figure 2.4 Concentration variations calculated with eigenvalue approach

As a result, the assumption made on the previous section, that species Y is reactive, can be reached automatically by this method. The eigenvalues of the Jacobian appear in the exponential term of the solution equations. The smallest eigenvalue $-a_2$, then drives the left hand side of equation (2.56) go to small values very rapidly, which means that the its reaction rate is very small. Then the LHS of equation (2.56) can be equilibrated to zero which yields an equation of the form,

$$\frac{a_1}{a_1-(a_1+a_4+a_5)}\dot{X}-\dot{Y}=0 \qquad (2.58)$$

Equation (2.58) can be solved to get an expression between the concentration of species X and Y

$$\dot{Y} = \frac{a_1}{a_1 - (a_1 + a_4 + a_5)} \dot{X} \tag{2.59}$$

$$\dot{Y} = \frac{a_1 X_0 t}{a_1 - (a_1 + a_4 + a_5)} \times \exp(-(a_1 + a_4 + a_5) \times t) \tag{2.60}$$

Similar to the solution that we get from the steady state assumption, the set of equation is turned out to be 3 equations, plus one equation for species Y in terms of species X. The change of the concentration of the species with respect to time, calculated with this method, can be seen in figure (2.5).

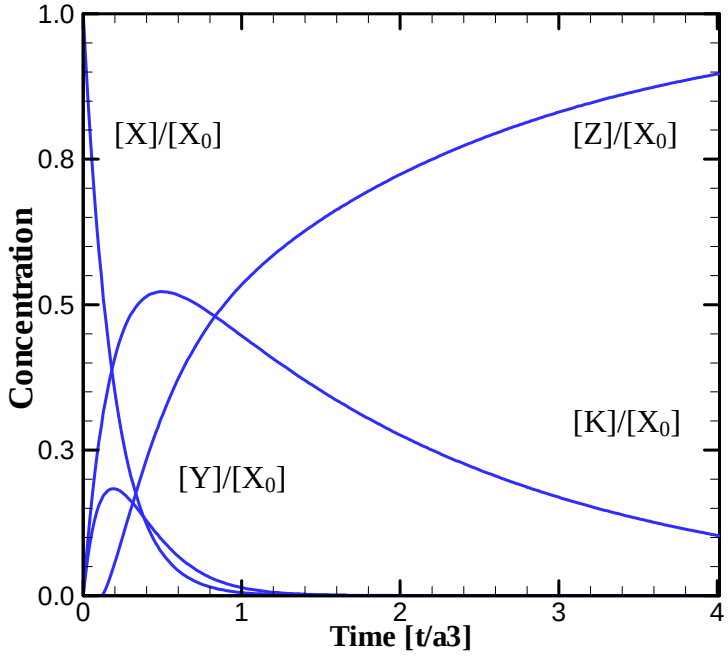


Figure 2.5 Concentration variations calculated with the automatic simplification approach

2.5 Effect of Eigenvalues and Eigenvectors on the Chemical Kinetics

Any distribution, even the chaotic ones that is very difficult to characterize in time domain, can be well investigated in the phase space with respect to its eigenvalues and eigenvectors (Glendinning 1999). Following this idea, further insight can be obtained for the concentration variation of species by constructing their basis in the phase space. As it was outlined in section (2.1), the solution for a linear differential equation system with constant coefficients can be calculated with equation (2.19.). In

this equation the exponential terms, whose powers are the eigenvalues are multiplied with their corresponding eigenvectors. This refers that the change of any species can be calculated with a superimposition of different exponential functions. The decaying limits of those exponential functions are characterized by the eigenvalues, whereas the eigenvectors represents the characteristic directions in the phase space. In this respect, eigenvectors belong to the negative eigenvalues denote the local tangential lines of the trajectories where they tend to convergence, and for positive ones it is nothing more than the asymptotes (Percival and Richards 1989). Different trajectories calculated in the phase space for different initial conditions of species X can be seen in figure (2.6). It is a common feature in all graphs that each variation shows similar patterns, which are characterized by their eigenvectors. Those shapes of the trajectories are not affected by the initial values, except for being shifted. It is also possible to say that, even tough all the trajectories start from distinct locations in the phase space, they more or less tend to bunch and end in a fixed state. The fast processes drive the system to the end points where as slow processes are responsible for the movements on this specific part of the phase space. Then, it is possible to divide the phase space into two regions as slow and fast subspaces spanned by various eigenvectors. Indeed the concept of automatic simplification procedure, outlined in section (2.4), stems from this phenomenon. With this method, instead of obtaining the whole distribution for various initial conditions, the fast species are detected by an eigenvalue analysis, and calculations are done only on for the bunched trajectories by neglecting the fast reactions. This can be simply accomplished by assuming that the rates of the fast reactions are zero on the direction of their eigenvectors. In this way, the effect of the reactive species is removed from the system automatically, and it is only controlled by the slow processes.

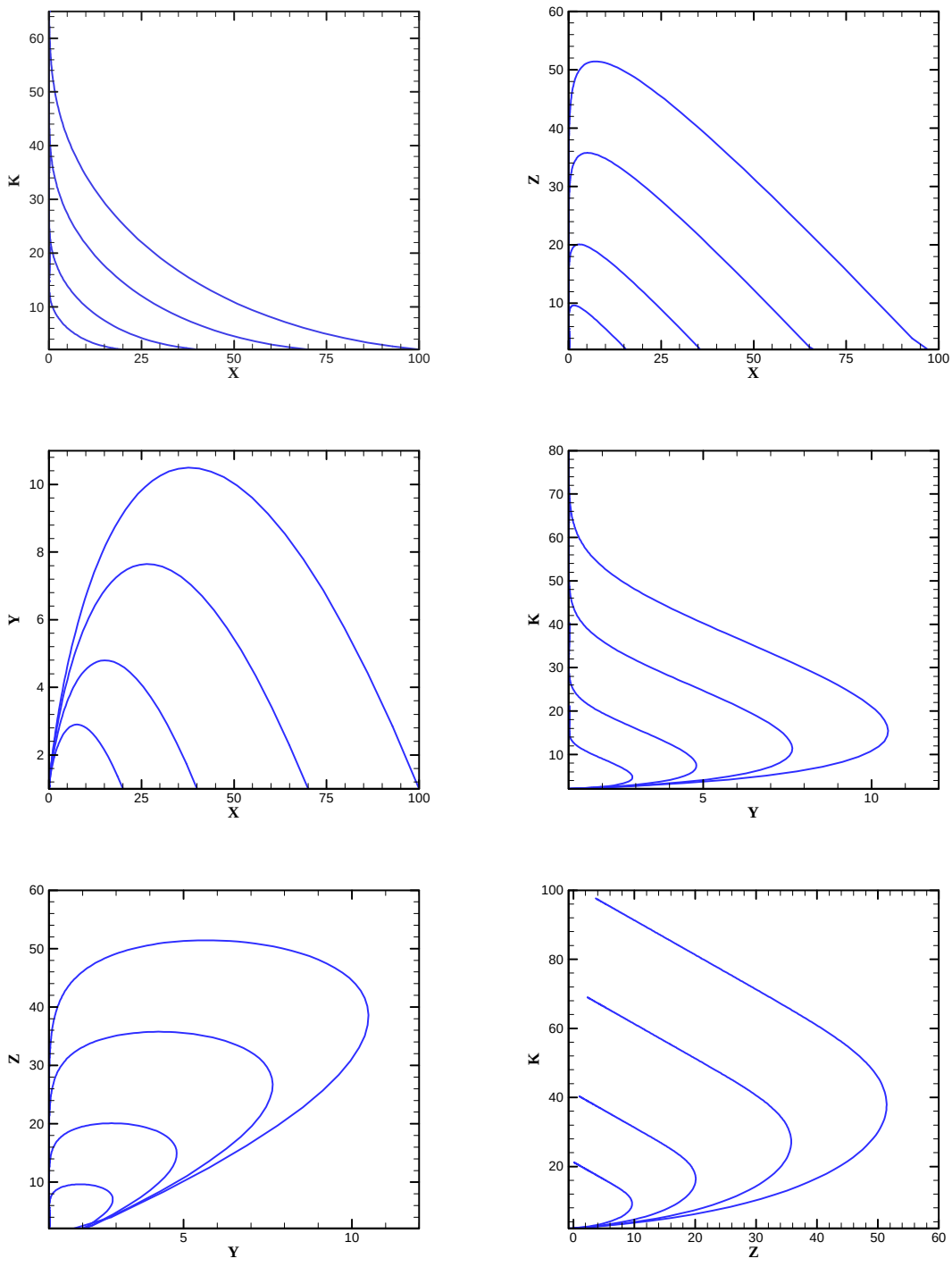


Figure 2.6 Projection of concentration variations into phase space

3. CHEMICAL AND PHYSICAL INTERPRETATION OF INTRINSIC LOW-DIMENSIONAL MANIFOLDS METHOD

The simulation of 3-D turbulent reactive flows typically occurring in gas turbine combustors requires effective models for the combustion processes. Combustion can be simulated perfectly with detailed mechanisms, which contains the information of every single reaction step associated with intermediate species and the radicals, but unfortunately this procedure far more exceeds the current capacity of the computers. This fact arises the need for developing simplified but still accurate models for the simulation of combustion. The partial equilibrium and steady state assumptions are widely used especially in commercial computational fluid dynamics (CFD) codes for the reactive flow applications. The simplified schemes are able to predict the consumption or production rates of the major species, which permits us to evaluate their composition within the combustion field. Moreover, it is also possible to represent the enthalpy or pressure field with the simplified mechanisms. Although those steady state and partial equilibrium assumptions are quite convenient to use, they have one major disadvantage, namely the explicitly imposed assumption. In order to use the reduced mechanisms, a case-by-case understanding of different chemical reaction system is needed, which invokes the need for investigating each single step in the detailed mechanism (Maas and Pope 1992a). So, only after a careful inspection of the detailed mechanism to examine each single reaction and to track all the species involved in the reactions, it can be possible to exploit the steady state and partial equilibrium assumptions respectively. Under these conditions, for each fuel and oxidizer system a considerable amount of human time and labor is required to reach a, for example, two-step or four-step reduced mechanism (Maas and Pope 1992b). Also the partial equilibrium and steady state assumptions can be applied under specific conditions of mixture composition and temperature. So, even for a reduced mechanism, which is generated for a specific fuel and oxidizer system, the assumption of steady state or equilibrium, may just work in a certain domain of the composition or temperature space. Those difficulties are resolved by the intrinsic

low-dimensional manifolds (ILDM) methodology, which can predict the steady state species and equilibrium reactions by simply using the time scale information of the system obtained by the eigenvalue analysis of the detailed mechanism.

The dynamics of the detailed mechanism can be divided into two groups as the fast and slow processes, where, the time scale information of the process, which can be calculated with a local eigenvalue analysis of the equation system, may reveal the kinematical characteristics of the different chemical processes occurring within the combustion zone (Maas and Pope 1992a; Maas and Pope 1992b; Maas and Pope 1994; Warnatz *et al.* 2001). The time scale information of the combustion for hydrocarbon fuels is usually as follows; first, fuel is consumed into minor intermediate species by the fast chain breaking processes, and then the intermediate species tend to unite with each other by slow time scale reactions (Schmidt 1996). The kinematical characteristics can be well defined by examining the reaction trajectories calculated starting from distinct points in the state space, representing different initial composition of the species, and is shown in figure (3.1) It is a common characteristic in the graph is that the initial processes, which occur in a very short time corresponding to the formation of radicals and intermediate species with fast reactions, are tend to unite in a specific portion of the state space. This portion of the space is related with the slow time scale processes and most of the important reactions occur within this range of the species mass fractions. ILDM methodology makes use of this hierarchical structure of the timescale information of reactions, and automatically seeks for the fast processes, which have very high reaction rates. On the next step, the fast processes are decoupled with the slow reactions and the overall chemical kinetics is represented by the slow processes. The timescale information needed to identify these processes is obtained by a local eigenvalue and eigenvector analysis of the governing equations of the system.

The concept of low-dimensional manifolds will be shown for a specific methane/air combustion system, which can be seen in figure (3.2) a) and b), in which the reaction trajectories are projected into H_2O- CO and CO_2 planes respectively. Both a) and b) represents the results of a simulation done by using a detailed mechanism calculations performed on a homogenous isobaric system for the same enthalpy, pressure and mixture fraction values, but different initial compositions. The equilibrium point is marked with a circle in both graphs. A careful inspection of the

combustion process clearly shows that the trajectories tend to bunch on a portion of the solution space as can be seen in the figure

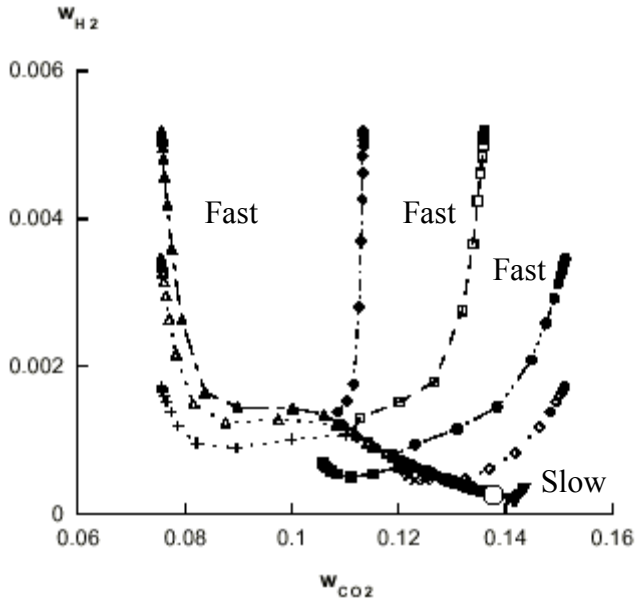


Figure 3.1 Trajectories of the chemical reactions for a stoichiometric methane/air system. Detailed kinetics for all timescales, projected on to CO_2 – H_2 planes (Schmidt 1996).

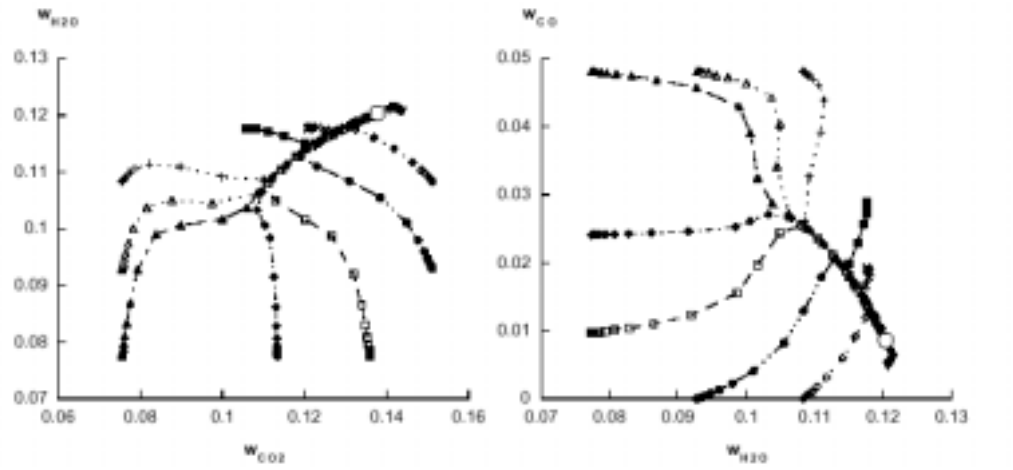


Figure 3.2 Trajectories of the chemical reactions for a stoichiometric methane/air system. Detailed reaction mechanism calculation projected on to a) CO_2 – H_2O, b) H_2O – CO planes (Schmidt 1996).

This observation shows the existence of an intrinsic subspace that is free from the initial conditions, which attracts the solution space to itself. The low dimensional manifold get for the same calculation can be seen in figure (3.3)

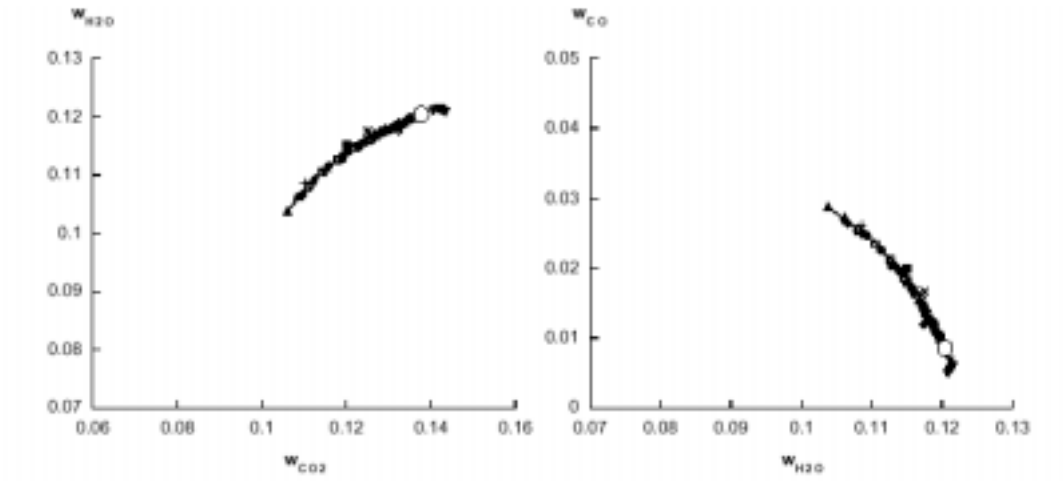


Figure 3.3 Trajectories of the chemical reactions for a stoichiometric methane/air system. Reduced kinetics obtained by ILDM projected on to a) CO_2 – H_2O, b) H_2O – CO planes (Schmidt 1996).

The effect of the conventional reduced mechanisms on the chemical kinetics of the detailed mechanism calculations can also be illustrated on the phase space. Detailed mechanism calculations define the phase space for all time scales and possible mass fractions. Figure (3.2) can be given as an example for the case. A more interesting feature of the solution space can be get by using conventional reduced mechanism for the simulation. The partial equilibrium methodology makes use of the, roughly speaking, "mix is burned" assumption by suppressing the most of the time scales; and is concerned only with the slow main reactions. Therefore, the mechanism get by this assumption can access only to a very small part, or simply a point, in the solution space, by neglecting all the dynamics of the system, which is indeed a crude over-simplification (Schmidt *et al.* 1996). The portion of the state space, which can be accessed by the equilibrium calculation, can be seen in figure (3.4)

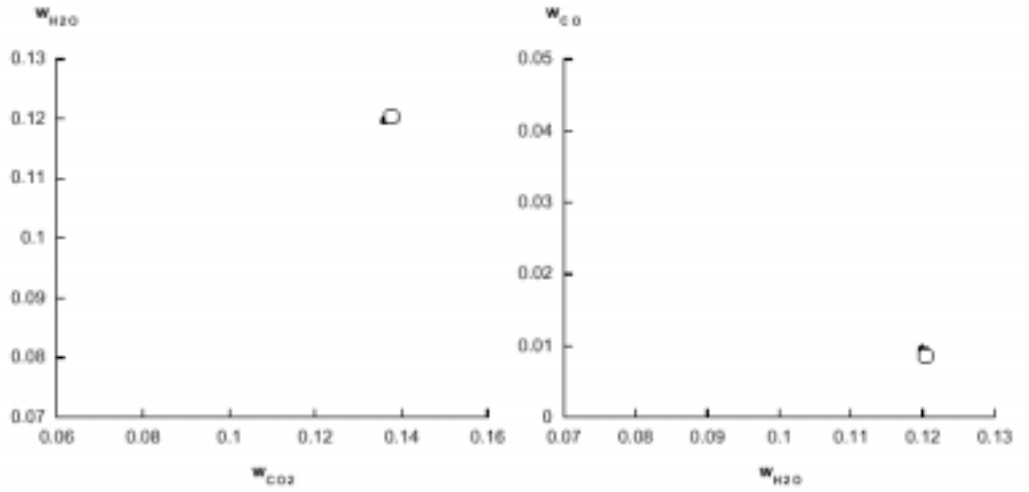


Figure 3.4 Trajectories of the chemical reactions for a stoichiometric methane/air system obtained by the Equilibrium calculations projected on to a) CO_2 – H_2O, b) H_2O – CO planes (Schmidt 1996).

3.1 Mathematical Model

In the previous section it was explained thoroughly, for simple examples that, based on a timescale analysis of the governing equations in a homogenous chemical reaction system, it is possible to identify low dimensional subspaces of the composition space that may be used to simplify the complicated chemical systems. On the following section methods used to calculate timescale information and to simplify the reaction system will be discussed.

Reacting flow simulations are based on the numerical simulation of the partial differential equation system for the scalar field of $\vec{\Psi}(x,t) = \left(h, P, \Phi_1, \Phi_2, \Phi_3, ..., \Phi_{ns}\right)^T$ and the velocity field $\vec{U}(x,t)$, where Φ_i represents the specific mass fraction of species *i*, which is defined by $\Phi_i = Y_i / M_i$, for Y_i being the mass fraction of species *i*.

The governing equations for the scalar field are the conservation of the species mass, conservation of energy and the conservation of total mass. In vectorial formulation the equations for the scalar field are written as

$$\frac{\partial \vec{\Psi}(\vec{x},t)}{\partial t} = \vec{S}\left(\vec{\Psi}(\vec{x},t)\right) + \vec{\Xi}\left(\vec{\Psi}(\vec{x},t)\right) \tag{3.1}$$

where $\vec{S}$ are the rates of formation due to the chemical kinetics and $\vec{\Xi}$ the rates of change due to physical processes, like molecular transport, convection etc. These expressions can be given explicitly as follows,

$$S_h = 0 \qquad \Xi_h = \frac{f_p}{\rho} - \vec{v}\nabla h - \frac{1}{\rho}\nabla \vec{q} - \frac{1}{\rho}\overline{\overline{p}} : \nabla \vec{v} + \frac{1}{\rho}\nabla(\rho \vec{v}) + \frac{w_h}{\rho} \tag{3.2}$$

$$S_P = 0 \qquad \Xi_P = f_p \tag{3.3}$$

$$S_{\Phi_i} = \frac{w_i}{\dot{\rho}} \qquad \Xi_{\Phi_i} = -\frac{1}{\rho M_i}\nabla \vec{J}_i - \vec{v}\nabla \Phi_i \qquad i=1, 2, 3,\ldots, n_s \tag{3.4}$$

where, $\overline{\overline{p}}$ denotes the pressure tensor, $\vec{J}_i$ diffusion flux density of species *i*, and finally ":" represents the twofold contraction of two tensors. The term f_p describes the time behavior of the pressure (Maas and Pope 1994). Since a constant pressure is used quite often in flame calculations this term shall not be written explicitly in the concept of the thesis.

Assuming that the velocity field does not play any role on the combustion, the whole equation set for the chemical kinetics can be shown in a more compact form as follows

$$\frac{\partial \vec{\Psi}}{\partial t} = \vec{F}\left(\vec{\Psi}\right) \tag{3.5}$$

The data can be obtained and tabulated by solving equation (3.5) with assumptions of ILDM, and can be used successively in the CFD solvers by reading the reaction rates when needed. In order to find the mass fraction variation of the species for the combustion application, the conservation equations for all the species should be solved. Then, for example the case when a synthesis gas/air system is used, the number of the species involved in the detailed mechanism is 13, which requires the solution of 13 equations for the conservation of species mass transport in the CFD code. As the complexity of the reaction mechanism is increased by using different fuel/oxidizer compositions, the total number of the species involved in the detailed

mechanism also increases. Then, for example, simulation of a dodecane/air combustion system requires the solution of 90 differential equations by the CFD solver, which are non linear in general. To overcome this problem, CFD simulations are done for limited number of species, and thus the dimension of the governing equations are reduced in terms of the specific variables, which can represent the scalar field effectively. The choice of the representative variables, so called reaction progress variables (RPVs), and their number (nrpv) are important parameters for the accuracy of the solution in that the governing equations are solved only for them. This requires constructing the low-dimensional subspace in terms of the RPVs, which can represent the components of the scalar field, enthalpy, pressure and the specific mass fractions (Schmidt *et al.* 1996). By the use of RPVs the scalar variable vector $\vec{\Psi}(x,t) = \left(h, P, \Phi_1, \Phi_2, \Phi_3, ..., \Phi_{ns}\right)^T$ is transformed into a reduced form, which can be shown as $\vec{\psi}(x,t) = \left(h, P, \Phi_1, \Phi_2, \Phi_3, ..., \Phi_{ns-nrpv}\right)^T$. All other variables, like enthalpy h($\vec{\psi}$), pressure P($\vec{\psi}$), and mass fractions of the species $\Phi_i(\vec{\psi})$ are known functions of the RPV. In this case, the parameterized field of the scalars evolves according to

$$\frac{\partial \vec{\psi}(\vec{x},t)}{\partial t} = \vec{P}(\vec{\psi}(\vec{x},t)) + \vec{\Gamma}(\vec{\psi}(\vec{x},t)) \tag{3.6}$$

In the final form of the equation, which is parameterized and represented in terms of the RPVs, the basic idea to find the low-dimensional attracting manifold, is to seek for the points in the state space, where in the direction of certain eigenvectors vanish, which are associated with the eigenvalues, corresponding to the fast time scales (Maas and Pope 1992a). This concept requires the representation of the phase space not by the variables of the state vector, but with a modified coordinate system of the eigenvectors, which allows us to track more efficiently the fast processes

Recall the compact form of the equations of the scalar field, but this time written in terms of the reduced scalar field,

$$\frac{\partial \vec{\psi}}{\partial t} = \vec{F}(\vec{\psi}) \tag{3.7}$$

For linear equations, the timescale analysis can be obtained simply by investigating the term $\vec{F}(\vec{\psi})$, but in most cases the equation system is nonlinear and the eigenvalue

analysis should be accomplished on the linearized form of the equation. The general formula for the linearization can be obtained by using the Taylor series expansion,

$$f(t) = f(t_0) + \left.\frac{\partial f}{\partial t}\right|_{t_0} (t - t_0) + \left.\frac{\partial^2 f}{\partial t^2}\right|_{t_0} (t - t_0)^2 + \ldots \tag{3.8}$$

Then, the set of equations can be linearized as follows,

$$\frac{\partial \vec{\psi}}{\partial t} = \vec{F}(\vec{\psi}_0) + \left.\frac{\partial \vec{F}}{\partial \vec{\psi}}\right|_{\psi_0} (\vec{\psi} - \vec{\psi}_0) \tag{3.9}$$

where the higher order terms are neglected. $\vec{\psi}_0$ is a solution for the equation system and hence, is a stable point for the phase space, that attracts the solution to itself. Then, the term $\vec{F}(\vec{\psi}_0)$ vanishes and the system reduces to,

$$\frac{\partial \vec{\psi}}{\partial t} = \left.\frac{\partial \vec{F}}{\partial \vec{\psi}}\right|_{\psi_0} (\vec{\psi} - \vec{\psi}_0) \tag{3.10}$$

Finally, the eigenvalues and the eigenvectors of the Jacobian $J = \left.\frac{\partial \vec{F}}{\partial \vec{\psi}}\right|_{\psi_0}$ should fulfill the eigenvalue equation (Golub and Loan 1989),

$$J\Gamma = \Gamma\Lambda \tag{3.11}$$

Where Γ corresponds the matrix formed by the eigenvectors, ordered according to decreasing values of the real parts of the corresponding eigenvalues.

$$\Gamma = \begin{pmatrix} . & . & . & . & . \\ \vartheta_1 & \vartheta_2 & . & . & \vartheta_n \\ . & . & . & . & . \end{pmatrix} \tag{3.12}$$

and its inverse

$$\Gamma^{-1} = \begin{pmatrix} . & \tilde{\vartheta}_1 & . \\ . & \tilde{\vartheta}_2 & . \\ . & . & . \\ . & . & . \\ . & \tilde{\vartheta}_n & . \end{pmatrix} \tag{3.13}$$

whereas Λ holds the eigenvalues of the Jacobain on its diagonal,

$$\Lambda = \begin{pmatrix} \lambda_1 & & 0 \\ & \lambda_2 & \\ & . & \\ 0 & & . \\ & & \lambda_n \end{pmatrix}_{n \times n} \tag{3.14}$$

So, the Jacobian is,

$$J = \Gamma \Lambda \Gamma^{-1} \tag{3.15}$$

A more explicit form of the Jacobian ($J=\frac{\partial \vec{F}}{\partial \vec{\Psi}}$) can be seen in equation (3.16)

$$J = \frac{\partial \vec{F}}{\partial \vec{\Psi}} = \begin{bmatrix} \frac{\partial \dot{h}}{\partial h} & \frac{\partial \dot{h}}{\partial P} & \frac{\partial \dot{h}}{\partial \Phi_1} & . & . & \frac{\partial \dot{h}}{\partial \Phi_{ns}} \\ \frac{\partial \dot{P}}{\partial h} & \frac{\partial \dot{P}}{\partial P} & \frac{\partial \dot{P}}{\partial \Phi_1} & . & . & \frac{\partial \dot{P}}{\partial \Phi_{ns}} \\ \frac{\partial \dot{\Phi}_1}{\partial h} & \frac{\partial \dot{\Phi}_1}{\partial P} & \frac{\partial \dot{\Phi}_1}{\partial \Phi_1} & . & . & \frac{\partial \dot{\Phi}_1}{\partial \Phi_{ns}} \\ & & & . & . & \\ \frac{\partial \dot{\Phi}_{ns}}{\partial h} & \frac{\partial \dot{\Phi}_{ns}}{\partial P} & \frac{\partial \dot{\Phi}_{ns}}{\partial \Phi_1} & . & . & \frac{\partial \dot{\Phi}_{ns}}{\partial \Phi_{ns}} \end{bmatrix} \tag{3.16}$$

The existence of a low dimensional subspace should be also clearly stated out before going no further in the mathematical modeling. The dynamical system approach is the main tool used in the ILDM technique in two ways. By a simple eigenvalue analysis of the Jacobian of the system, first, the slow and fast time scaled reactions, occurring in the physical domain can be defined. This would help to understand the kinematics of the reactions and thus to decouple the slow reactions with the fast reactions. Secondly the response of the system to a small perturbation can be investigated as well, which allows the construction of the basis with attractors on the phase space.

Let us assume a single initial perturbation $\vec{s}^{\,\varepsilon}$ to the reactive system, which lies on its stable point, the equilibrium point, denoted with $\vec{s}^{\,0}$. The development of the perturbation within the phase space can be calculated with a Modal analysis. Let us

rewrite the linearized form of the governing equation system shown on equation (3.9),

$$\frac{d}{dt}\left(\vec{s}^{\,\varepsilon}-\vec{s}^{\,0}\right)=F_s\left(\vec{s}^{\,0},h,P\right)\left(\vec{s}^{\,\varepsilon}-\vec{s}^{\,0}\right) \tag{3.17}$$

F_s denotes the Jacobian $\frac{\partial F}{\partial s}$, with a variable change of $\vec{\varepsilon}=\left(\vec{s}^{\,\varepsilon}-\vec{s}^{\,0}\right)$, the equation reads

$$\frac{d\vec{\varepsilon}}{dt}=F_s\left(\vec{s}^{\,0},h,P\right)\vec{\varepsilon} \tag{3.18}$$

Suppose that the initial perturbation is given by $\vec{\varepsilon}^{\,0}$. Then $\vec{\varepsilon}$ develops according to

$$\vec{\varepsilon}(t)=e^{F_s t}\vec{\varepsilon}^{\,0} \qquad \ldots. \tag{3.19}$$

If we define the perturbations in terms of the eigenvectors of the Jacobian, we finally end up with a very simple equation for the development of the perturbations where the variables are decoupled,

$$\vec{\varepsilon}_i(t)=e^{\lambda_i t}\vec{\varepsilon}_i^{\,0} \tag{3.20}$$

where i=1, 2, 3, ….n_s, λ_i denotes the eigenvalues of the Jacobian and $\vec{\varepsilon}_i$, the components in the basis of the eigenvectors. Final form reveals that the behavior of the dynamical system to a perturbation evolves with respect to eigenvalues in 3 different ways as it can be seen in figure (3.5)

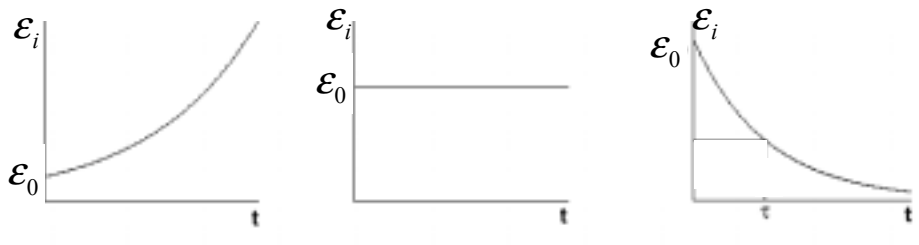


Figure 3.5 Effect of a perturbation into chemical systems in terms of its eigenvalues (Niemann 2002).

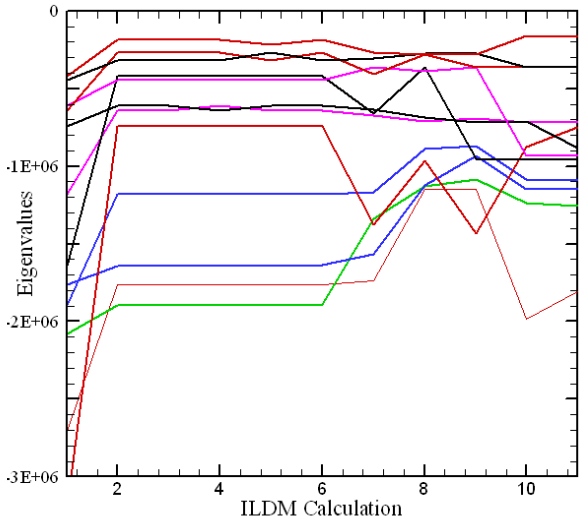


Figure 3.6 Eigenvalues of methane/air system obtained by ILDM calculations.

The eigenvalues having a positive real part will cause the perturbation to grow rapidly in the direction of its eigenvector. On the other hand the negative eigenvalues will damp the $e^{\lambda_i t}$ term. This would cause the perturbation to become small as the time proceeds. Combination of this information with the chemical system reveals interesting results. The eigenvalue analysis of a combustion system shows that nearly al of the eigenvalues have a negative real part, as can be seen in figure (3.6). As a result, a perturbation given to a variable will be conducted to the others and most of them would try to suppress the perturbation in the direction of their eigenvectors, which would result in a movement to a specific portion of the solution space. Thus a low dimensional subspace exists where all the reactions tend go on the direction of their eigenvectors and with the speed determined by their eigenvalues. Then, it is possible to modify the phase space in such a way that, representing the evolvement of the different processes will be available in the eigenvector basis.

Let us continue in deriving the mathematical formulation of the ILDM with the equation (3.9), by applying a variable change of the form,

$$\vec{\varphi} = \vec{\psi} - \vec{\psi}_0 \tag{3.21}$$

Where, $\vec{\psi}_0$ is the solution and $\vec{\psi}$ is the calculated guess value, which is supposed to be on the low-dimensional manifold. Then equation (3.9) takes the form of,

$$\frac{\partial \vec{\varphi}}{\partial t} = \vec{F}(\vec{\psi}_0) + F_{\psi}\Big|_{\vec{\psi}_0} \vec{\varphi} \tag{3.22}$$

If Γ is defined as the matrix whose column partitions are the basis vectors, namely the eigenvectors, the variables $\vec{\varphi}$ are transformed into $\vec{\xi}$ according to the equation (3.23).

$$\vec{\varphi} = \Gamma \vec{\xi} \tag{3.23}$$

Then the main equation turns out to be,

$$\Gamma \frac{\partial \vec{\xi}}{\partial t} = \vec{F}(\vec{\psi}_0) + F_{\psi}\Big|_{\vec{\psi}_0} \Gamma \vec{\xi} \tag{3.24}$$

Multiply the equation with Γ^{-1} from left side,

$$\frac{\partial \vec{\xi}}{\partial t} = \Gamma^{-1}\vec{F}(\vec{\psi}_0) + \Gamma^{-1}F_{\psi}\Big|_{\vec{\psi}_0} \Gamma \vec{\xi} \tag{3.25}$$

The final form of the equation is,

$$\frac{\partial \vec{\xi}}{\partial t} = \Gamma^{-1}\vec{F}(\vec{\psi}_0) + \Lambda \vec{\xi} \tag{3.26}$$

where it can be decomposed into two set of equations for the slow (3.27), and fast (3.28), time scales

$$\frac{\partial \vec{\xi}_s}{\partial t} = \Gamma_s{}^{-1}\vec{F}(\vec{\psi}_0) + \Lambda_s \vec{\xi}_s \tag{3.27}$$

$$\frac{\partial \vec{\xi}_f}{\partial t} = \Gamma_f{}^{-1}\vec{F}(\vec{\psi}_0) + \Lambda_f \vec{\xi}_f \,. \tag{3.28}$$

First $n - n_f$ eigenvectors are related with the slow, where the remaining n_f vectors represent the fast timescales, and their corresponding eigenvalues. Accordingly, the eigenvectors, associated with the fast and slow timescales are,

$$\Gamma_s = \begin{pmatrix} . & . & . & . & . \\ \vec{\varphi}_1 & \vec{\varphi}_2 & . & . & \vec{\varphi}_{n-n_f} \\ . & . & . & . & . \end{pmatrix}_{n\times(n-n_f)} \tag{3.29}$$

$$\Gamma_f = \begin{pmatrix} . & . & . & . \\ \vec{\varphi}_{n-n_f+1} & \vec{\varphi}_{n-n_f+2} & . & . & \vec{\varphi}_n \\ . & . & . & . & . \end{pmatrix}_{n\times n_f} \tag{3.30}$$

Similarly, the eigenvalue matrix, Λ, can also be divided into two parts for the slow and fast processes as,

$$\Lambda_s = \begin{pmatrix} \lambda_1 & & & 0 \\ & \lambda_2 & & \\ & & . & \\ & & & . \\ 0 & & & \lambda_{n-n_f} \end{pmatrix}_{n\times(n-n_f)} \tag{3.31}$$

$$\Lambda_f = \begin{pmatrix} \lambda_{n-n_f+1} & & & 0 \\ & \lambda_{n-n_f+2} & & \\ & & . & \\ & & & . \\ 0 & & & \lambda_n \end{pmatrix}_{n\times n_f} \tag{3.32}$$

The concept of the low dimensional manifold exploits the fact that, the fast processes evolve very rapid, and tend to derive the system to the slow processes. This means that, in order to get the low-dimensional manifold on the phase space, one should look for the rates, which have low values on the direction of the eigenvectors corresponding the fast processes. This procedure can be get mathematically by looking for the solution of the following equation,

$$\Gamma_f^{-1}\vec{F}(\vec{\psi}_0) = 0 \tag{3.33}$$

where matrix Γ_f^{-1} is obtained by eliminating the first 2 + n_e + n_c rows, corresponding the conserved variables h/T, P, element composition (n_e), and the RPVs. So, the rows of the matrix correspond to the fast processes and since they evolve very rapidly, their rates can be set to zero. In this case, the set of equations for the slow and fast timescale processes becomes,

$$\frac{\partial \vec{\xi}_s}{\partial t} = U_s{}^{-1}\vec{F}(\vec{\psi}_0) + \Lambda_s \vec{\xi}_s \tag{3.34}$$

and

$$\Gamma_f^{-1}\vec{F}(\vec{\psi}_0) = 0 \tag{3.35}$$

The approach of working on the basis of the eigenvectors, has the following disadvantages. The eigenvalues of $\lambda_{2+ne+nc}$ and $\lambda_{2+ne+nc+1}$ may form a complex pair, or they can be equal to each other. Thus, it is useful to work on another basis, the basis of the so-called Schur vectors (Maas and Pope 1992a).

Let $Q^T F_\psi Q = N$ denote the real Schur decomposition of the Jacobian, such that the eigenvalues appear in the diagonal of *N*. Then the matrix *Q* can be written as follows,

$$Q = \begin{pmatrix} . & . & . & . & . \\ \vec{q}_1 & \vec{q}_2 & . & . & \vec{q}_n \\ . & . & . & . & . \end{pmatrix} \tag{3.36}$$

where $\vec{q}_i$ is defined as the Schur vectors. Following the same procedure done on the previous section, the decomposition of the set of equation into slow and fast part, matrix *Q* can be separated into two different parts. One corresponding processes with fast time scales and the other with slow processes. Then the decomposition of the Jacobian in terms of Schur vectors can be rewritten as,

$$\begin{pmatrix} Z_s^T \\ Z_f^T \end{pmatrix} F_\psi \begin{pmatrix} Zs & Z_f \end{pmatrix} = \begin{pmatrix} N_s & 0 \\ 0 & N_f \end{pmatrix} \tag{3.37}$$

Continue with equation (3.38) for the construction of low-dimensional manifold,

$$\frac{\partial \vec{\varphi}}{\partial t} = \vec{F}(\vec{\psi}_0) + F_\psi\big|_{\vec{\psi}_0}\vec{\varphi} \tag{3.38}$$

$$\frac{\partial}{\partial t}\left(Z_f^T\vec{\varphi}\right) = Z_f^T\vec{F}(\vec{\psi}_0) + Z_f^T F_\psi\big|_{\vec{\psi}_0}\vec{\varphi} \tag{3.39}$$

In this case the low-dimensional space is governed by m_f-dimensional equation system,

$$Z_f^T(\vec{\psi})\vec{F}(\vec{\psi}_0) = 0 \tag{3.40}$$

for n unknowns. In principle equation (3.40) is a quite simple equation system. Its solution, however, is complicated by several facts. The governing equation represents a n_f-dimensional set of equations for n unknowns. Therefore additional equations for the parameters should be also introduced. It is a complicated non-linear equation system where both Z_f and F depend non-linearly on $\vec{\psi}$. And finally, the state variable $\vec{\psi}$ is bounded by physical constraints (positiveness of mass fractions and temperature), thus the solution domain is bounded also (Maas 1997). By adding the parameterization equations, the equations get the final form of the

$$\vec{\tilde{P}}(\vec{\psi}) = 0 \tag{3.41}$$

$$Z_f^T(\vec{\psi})\vec{F}(\vec{\psi}) = 0 \tag{3.42}$$

Let us summarize that in order to obtain the manifold, we now have to solve the following equation system,

$$Z_f^T(\vec{\psi})\vec{F}(\vec{\psi}) = 0 \tag{3.43}$$

$$g(\vec{\psi}, \vec{\tau}_e) = 0 \tag{3.44}$$

$$rpv(\vec{\psi}, \vec{\tau}_{rpv}) = 0 \tag{3.45}$$

for equation (3.43) defines the manifold and (3.44) with (3.45) closes the equation system by n_e+2+nrpv equations. The parameter equations (3.44) and (3.45) can be written in an explicit manner as,

$$h - h^{ref} = 0 \tag{3.46}$$

$$P - P^{ref} = 0 \tag{3.47}$$

$$X_H(\vec{\Phi}) - \tau_H = 0 \tag{3.48}$$

$$X_C(\vec{\Phi}) - \tau_C = 0 \tag{3.49}$$

$$X_O(\vec{\Phi}) - \tau_O = 0 \tag{3.50}$$

$$X_N\left(\vec{\Phi}\right) - \tau_N = 0 \tag{3.51}$$

$$\Phi_{H_2O} - \tau_{N_2O} = 0 \tag{3.52}$$

$$\Phi_{CO_2} - \tau_{CO_2} = 0 \tag{3.53}$$

where equations (3.46), (3.47) represents the parameter equations for temperature/enthalpy and pressure respectively. Equations (3.48) – (3.51) are the element compositions and finally (3.52) – (3.53) are for the RPVs. Then to get the solution, the initial conditions for the state vector, h^{ref}, P^{ref}, $\tau_e\left(\vec{\Phi}\right)$ and $\tau_{rpv}\left(\vec{\Phi}\right)$, are needed, which fulfills the equation (3.43). Therefore, the initial state vector should represent any point that lies on the manifold, and starting from the initial state, it will be possible to construct the low-dimensional manifold in the phase space. In order to give further insight in how a point is calculated with ILDM, a flow chart is prepared and can be seen in figure (3.7) The calculation is started by an initial guess value for the state vector $\vec{\psi}(h, P, \Phi_i)$. On the next step, the linearization of the governing equations is accomplished on the neighborhood of the initialization vector, and the Jacobian is calculated. Also, the Schur decomposition of the Jacobian, to get the eigenvalues and the eigenvectors of the fast processes, is fulfilled. By the use of the Schur decomposition, equations (3.41) and (3.42) are solved up to a steady state result is obtained. For this purpose, on each calculation step, the increments on the state vector are compared with a convergence criteria ε. If the convergence is satisfied, then the new calculated data is stored in the memory, and the procedure continues with the calculation of another point. Incase it will not be possible to obtain a solution, the decomposition and solution of the governing equation is repeated for several of steps and program stops.

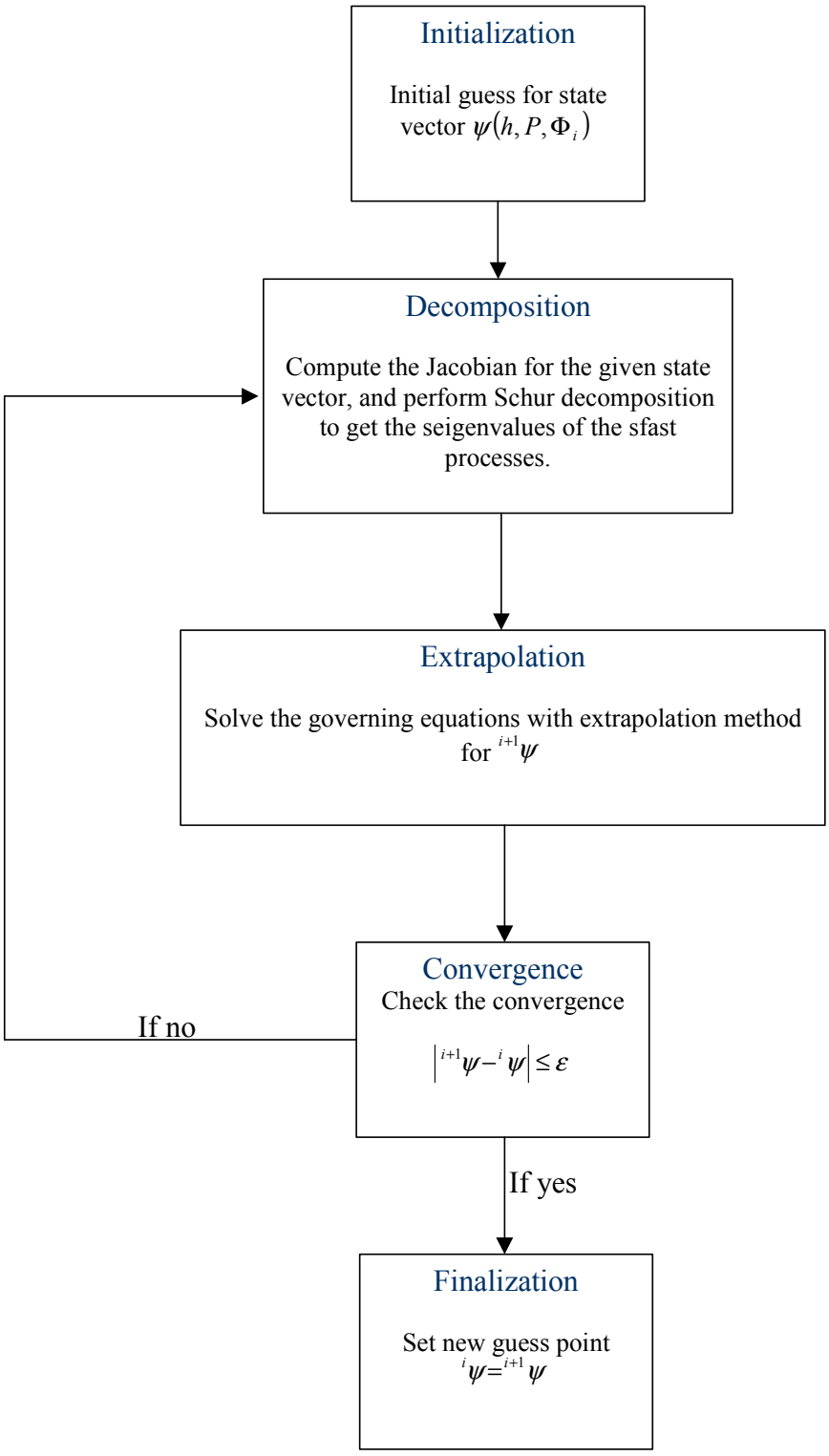


Figure 3.7 Flow chart of ILDM code.

In recent years there have been numerous attempts to increase the efficiency of the classical ILDM approach, either to decrease the calculation time (Maas 1997; Blasenbrey *et al.* 1999; Maas 2002), or to let the program be able to perform calculations for high hydrocarbon fuels (Blasenbrey 2000; Blasenbrey and Maas 2000; Şen *et al.* 2003). Since, the scope of this thesis is not concerned with the evaluation of the ILDM method and the effect of different algorithms on reactive flow calculations, only, the new algorithm introduced by Niemann (2002) will be discussed. Recall the governing equation to calculate the low-dimensional manifold,

$$Z_f^T(\vec{\psi})\vec{F}(\vec{\psi}) = 0 \tag{3.54}$$

which can be rewritten as,

$$Z_f^T(\vec{\psi})\vec{F}(\vec{\psi}) + Z_f^T(\vec{\psi})Z_s(\vec{\psi})c = 0 \tag{3.55}$$

$$\vec{F}(\vec{\psi}) + Z_s(\vec{\psi})c = 0 \tag{3.56}$$

where c is the local error of the parameter vector and $Z_s(\vec{\psi})$ represents the eigenvalues associated with the slow system. The parameter vector defines the variables, which are being solved by the parameter equations, namely the variables of the slow subsystem, and it can be calculated by the dot multiplication of the parameter matrix with the state vector as,

$$\theta = P^T\psi = \begin{pmatrix} T/h & P & H & C & O & N & rpv1 & . & rpv2 \end{pmatrix}. \tag{3.57}$$

So, definition of the low-dimensional manifold is nothing more than a coordinate transform in the phase space from the state vector to the parameter vector. In this calculation parameter matrix is used for the coordinate transformation. The vector c is defined as the local distance of parameter vector to the desired state, which is indeed the error. It is obvious that for any state of the phase space calculated by ILDM, a coordinate transformation is valid by the use of the parameter matrix. Since the element composition remains the same for a closed system it should not change at any state. Also, the ILDM calculations are generally performed for isobaric systems. Then for the given value of the RPVs, and for the given initial value of the parameter vector, the best trajectory to follow can be adapted on each successive calculation by checking the difference between the parameter vector of the current step and the desired step.

The formulation for the error analysis can be given as,

$$err = ({}^{i}\theta - \theta) = \left(P^{T\,i}\psi(t) - \theta\right) \tag{3.58}$$

The local error control of the state vector is a classical control problem, referred as error minimization, and to increase the efficiency of the calculations a PI control algorithm is used.

$$c(t) = \begin{pmatrix} c_c(t) \\ c_i(t) \end{pmatrix} = \kappa\left(\gamma(t) + \frac{1}{\tau}\int_0^t \gamma(t)dt\right) \tag{3.59}$$

$$\gamma(t) = \begin{pmatrix} \gamma_c(t) \\ \gamma_i(t) \end{pmatrix} = \begin{pmatrix} P_c^T B_c & \\ & P_i^T E_i \end{pmatrix}\begin{pmatrix} P_c^T\psi(t) - \theta_c \\ P_i^T\psi(t) - \theta_i \end{pmatrix} \tag{3.60}$$

for κ and τ being the constants for the Proportional and Integral controllers, and are locally calculated in the ILDM. It should be noted that the parameter vector consists of two subspaces, namely the central and the inertial manifolds. Central manifold represents the conserved scalars of temperature, pressure and the element composition, which does not change during the ILDM calculation. On the other hand the composition part associated with reaction progress variables and corresponding eigenvalues & eigenvectors are changed on each calculation step. This means that the error vector has also two distinct parts, which should be considered separately. Then the equation (3.56) reads,

$$\dot{\psi} = \vec{F}(\vec{\psi}) + B_c c_c(t) + E_i(\psi)c_i(t) \tag{3.61}$$

where B_c is the control matrix which represents only the H, C, O and N carrier species and else zero, and E_i is the eigenvectors of the RPVs. With the assumption of PI algorithm the error vectors can be written in a more explicit manner as,

$$c_c(t) = \kappa\left[P_c^T B_c\left(P_c^T\psi(t) - \theta_c\right) + \frac{1}{\tau_c}\int_o^t P_c^T B_c\left(P_c^T\psi(t) - \theta_c\right)dt\right] \tag{3.62}$$

$$c_i(t) = \kappa\left[P_i^T E_i\left(P_i^T\psi(t) - \theta_i\right) + \frac{1}{\tau_i}\int_o^t P_i^T E_i\left(P_i^T\psi(t) - \theta_i\right)dt\right] \tag{3.63}$$

The final form allows the definition of LDM not in terms of the vast number of fast processes, but in a more compact way, by the slow processes with n_e+2+nrpv equations.

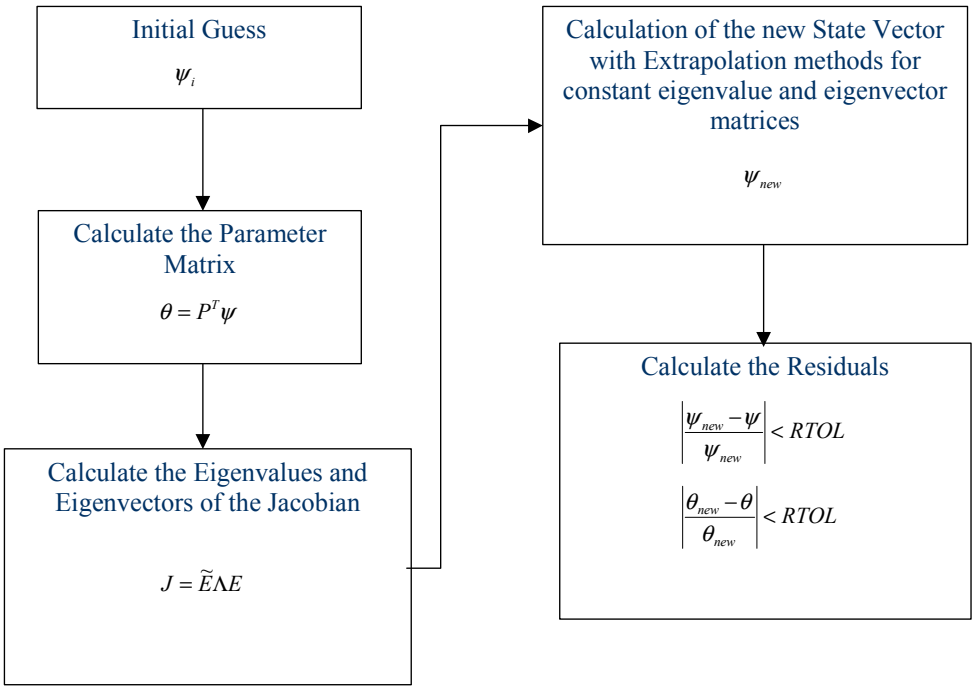


Figure 3.8 Flow chart of the outer loop for the modified version of ILDM code.

In this respect the calculation procedure for the ILDM that was introduced in figure (3.7) have some slight changes with the new approach. The ILDM calculation this time is divided into two loops, namely the outer and the inner loop. The flow chart represented in figure (3.8) demonstrates the outer loop for an ILDM calculation, which is indeed not so different from the algorithm introduced by Maas and Pope (1992a, 1992b). The calculation of a point on the low dimensional manifold starts with an initial value, which is already on the manifold. The usual procedure is to use the equilibrium point. Incase of the existence of a table, which was generated before, the closest point to the desired calculation is selected automatically by the program. Then, the parameter vector and the eigenvalues, eigenvectors of the Jacobian are calculated. The inner loop calculates the new state vector by Extrapolation methods and the residuals between the new state vector and old one is calculated. If it is below a desired value and is the first calculation, program either stops the simulation, or seeks for better initial guesses, the points which are closer to the desired value.

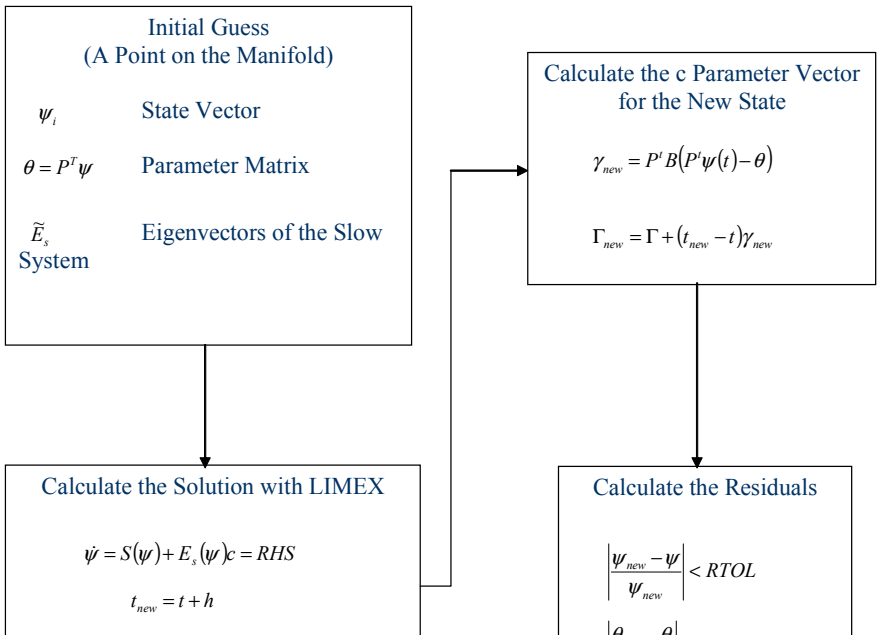


Figure 3.9 Flow chart of the inner loop for the modified version of ILDM code.

Refinement of the mesh is also possible when it is required. Thus for the zones where ILDM fails to calculate the points, a local mesh refinement is adapted automatically by the program. The flow chart for inner loop can be seen in figure (3.9). The inner loop performs the calculations for constant parameter matrix, eigenvalues and eigenvectors of the Jacobian. Although the best way to calculate the points seems to re evaluating the parametrizing matrix and decomposing the Jacobian in each step, this would cause the program to work slowly. For the ranges of the mass fraction of RPVs where ILDM produces good results, skipping the re evaluation of the matrices in each step would be useful. In this respect, the code is capable of changing its status between the constant and variable matrices. The set of differential algebraic equation (DAE) is solved by XLIMEX. XLIMEX exploits the extrapolation method, which produces fair good results for DAEs where the RHS of the system can be calculated and tabulated explicitly. The RHS of the governing equation for different step sizes are supplied to XLIMEX to get the solution. The constant part of the RHS, corresponding the chemical source terms, can be obtained by calculating the reaction rates by the Arrhenius expression.

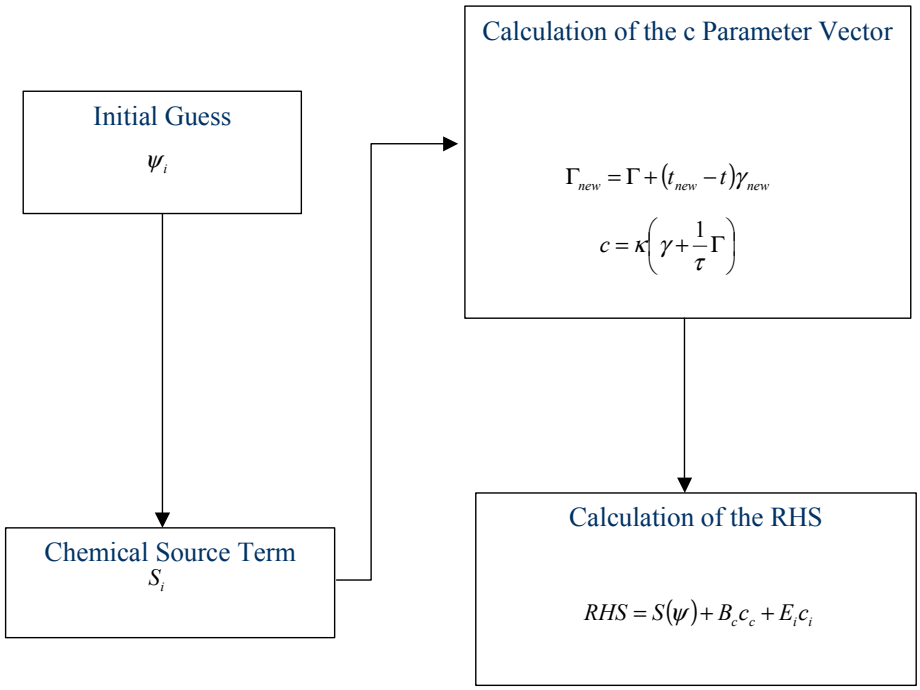


Figure 3.10 Flow chart for the modified version of ILDM code.

c local error matrix is evaluated by using the PI control. The PI control parameters are re calculated in each step. Final form of the RHS is obtained by adding the error vector to the chemical source terms.

3.2 ILDM Tables

For the simulation of combustion processes, ILDM methodology can be used with different Fuel/Oxidizer combinations with various number of reaction progress variables, including the Temperature and Mixture Fraction also as additional coordinates. Tables generated for different RPVs can be later used for the PDF calculations to close the production terms associated with the combustion. In this section of the thesis some sample calculations of ILDM for both 2-D and 3-D ILDM tables will be given as example.

Figure (3.11) represents the 2-D ILDM results obtained from the simulation of a synthesis gas/oxygen combustion system. In this particular example, the synthesis

gas composition is chosen to be consist of with CO and H_2 mixture where, corresponding mass fraction values are 0.667 and 0.333. The combustion for the synthesis gas is assumed to be including the C_1 mechanism, thus the mechanism prepared by Warnatz and Karbach is used, which consists of 13 species; H, H_2, O_2, O, H_2O, OH, HO_2, H_2O_2, CO, CO_2, CH_2O, CHO, N_2, and 72 reactions. The reactions and the associated rate coefficients can be seen in Appendix I. Since, the number of the species and the reactions exhibit small number compared with the other combustion systems, the overall equation system can be represented by few RPVs, which results a rapid simulation. In this respect H_2O is chosen as the RPV. In figure (3.11), the variation of the specific mass fraction of the species H, OH, CO, H_2O_2, CH_2O and CHO with respect to H_2O is illustrated. The enthalpy and mixture fraction is assumed to be constant during the simulation and are maintained at 2000 J/kg and 0.2 respectively. In the figure, the intermediate species OH, H_2O_2, CH_2O, CHO are all reach into their maximum values for the range of 0.2-0.3 of H_2O. On the other hand the combustion product CO_2 shows an increasing variation with respect to the H_2O as it is expected. The specific mass fraction distribution of H is inversely correlated with the H_2O distribution.

Figures (3.12), (3.13) and (3.14) shows the variation of the specific mass fractions of the species H, OH, CO, H_2O_2, CH_3 and CH_4, projected into the CO_2, H_2O plane, for a methane/oxygen combustion. In this specific example, the detailed reaction mechanism of C_1-C_2 chemistry, generated by Warnatz and Karbach, is used for the simulation. The detailed mechanism consists of 35 species, being H, H_2, O_2, O, H_2O, OH, HO_2, H_2O_2, CO, CH_4, CH_3, $3CH_2$, $1CH_2$, C, CH, CH_3OH, CH_3O, CH_2OH, CH_2O, CHO, CH_3O_2H, CH_3O_2, C_2H_6, C_2H_5, C_2H_4, C_2H_3, C_2H_2, C_2H, HCCO, CH_2CO, CH_2CHO, CH_3CHO, CH_3CO, CO_2, N_2, and 305 reactions, including the C_1 and C_2 reactions like, CH_3, C_2H_4 reactions. Detailed mechanism is available in Appendix II. H_2O and CO_2 is selected as the RPVs for the simulation, in that they can represent effectively the slow processes and thus be able to sweep the phase space more accurately than the intermediate species. Detailed mechanism is available in Appendix II. H_2O and CO_2 is selected as the RPVs for the simulation, in that they can represent effectively the slow processes and thus be able to sweep the phase space more accurately than the intermediate species.

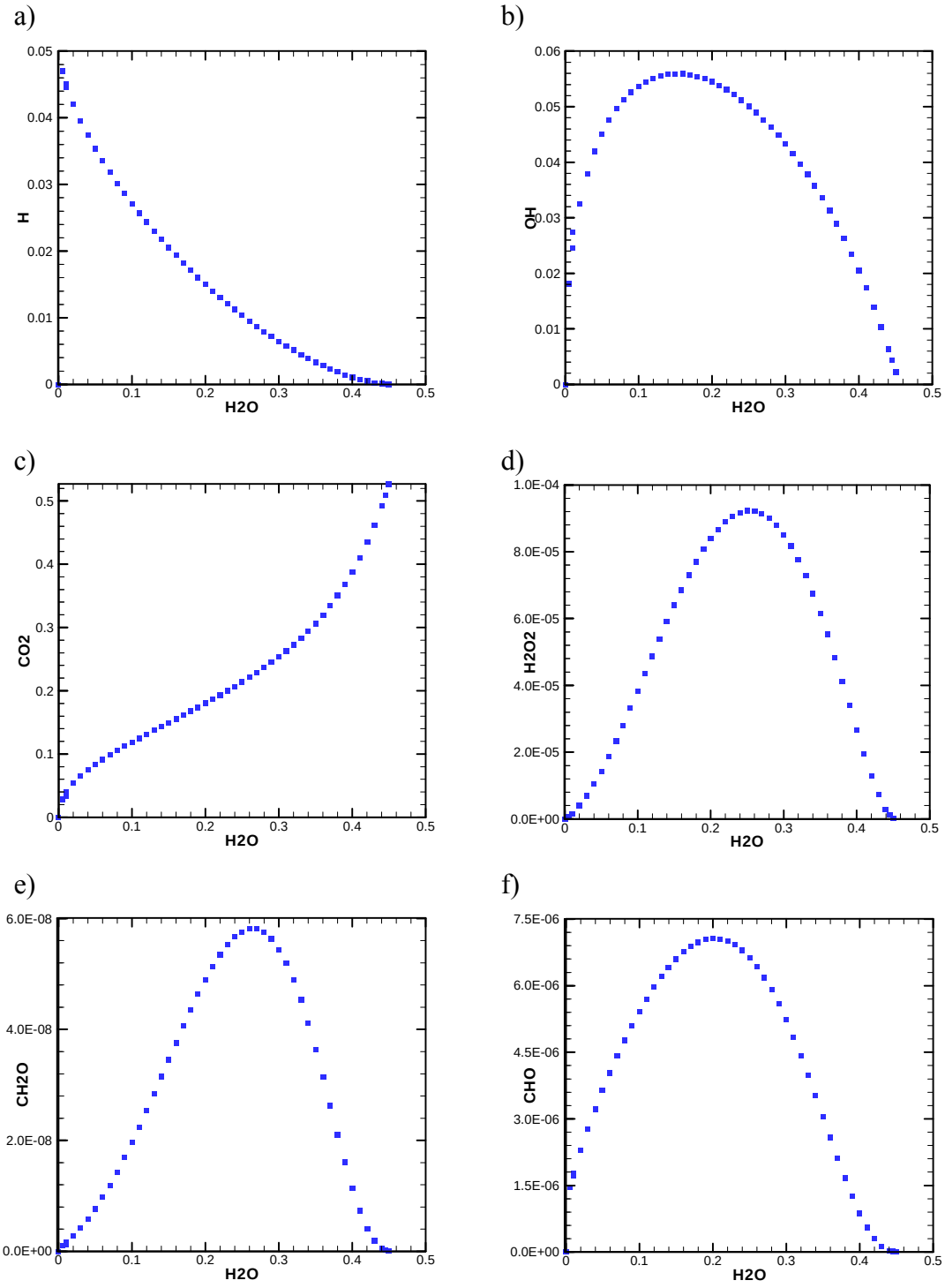


Figure 3.11 Mass fraction variation of the species projected into H_2O space, for a synthesis gas/oxygen combustion. (ζ= 0.3)

For a more detailed investigation, species like O_2, or CO can be also used as RPV, which belong to the C_1 mechanism. To increase the accuracy of the calculation and to implement the ILDM table to the CFD solver, the additional coordinates to RPVs are chosen to be Temperature and the Mixture Fraction. The table is generated by seeking the points that lie on the Low-Dimensional Manifolds for the mesh generated in the range of 300 - 5100 K for Temperature, 0 - 0.95 for mixture fraction, and 0 - 0.95 for CO_2 and H_2O. On each level of Temperature, mixture fraction and RPVs, the step sizes are chosen to be 25, 0.020 and 0.025 respectively. In the figures, it is a common feature that the variation of the species mass fractions generally show the same structure for different values of mixture fraction. The only difference imposed by the mixture fraction is that it strongly affects the area, and thus the number of ILDM points, that is calculated by the method. 3-D Low-Dimensional Manifolds can be generated for the area that lies in the range of 0.0 and 0.5 for both CO_2 and H_2O mass fractions. As deviations occur from the stoichiometric mass fraction value to rich or lean regimes, the accessible area by the ILDM confines to a rather small field which lies between 0.0 - 0.1 for CO_2 and 0.0 - 0.3 for H_2O. A more interesting result can be observed for figure (3.14) Even though the value of mixture fraction corresponds to a fuel rich portion, the accessible area seems to be increased to the specific mass fraction values of both CO_2 and H_2O to 0.0 - 0.8. Indeed, in this part, the variation shows a peak value in a very narrow area, and then quickly relaxes to the values on the order of zero. Thus, the area for this configuration is rougher than the other two. Especially the area in between 0.4 - 0.7 for CO_2 and 0.0 - 0.2 for H_2O seems to be a really problem for calculation. The specific mass fraction variation of Carbon carrier species like CO, CH_3 and CH_4 are highly affected by the variation of CO_2, and for the increasing values of CO_2, the variation also steeps up. A common behavior can be also spoken for the variation of H, in that it increases linearly with the increasing values of H_2O.

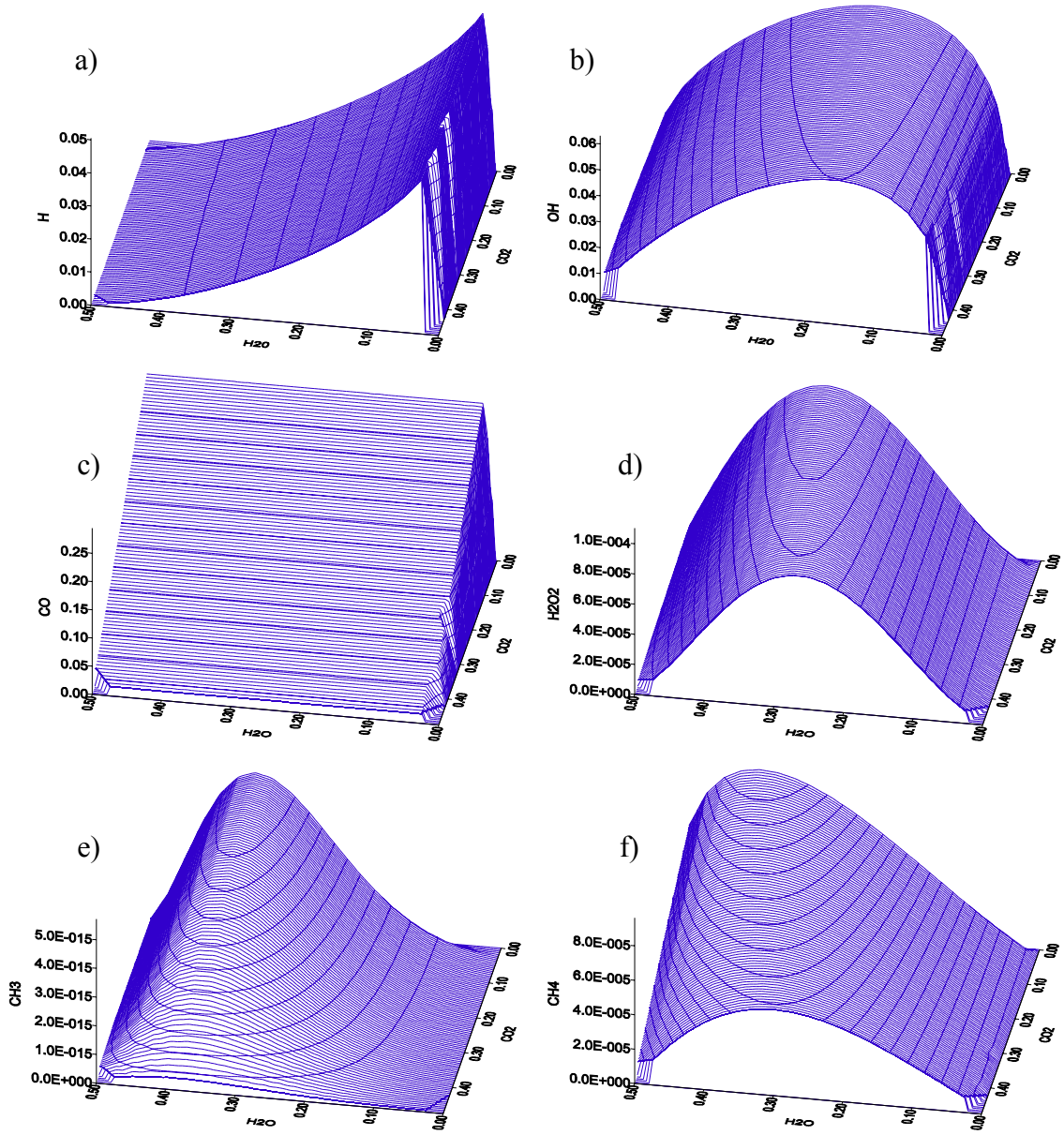


Figure 3.12 Mass fraction variation of the species projected into CO_2-H_2O space, for methane/air combustion. (ζ= 0.3)

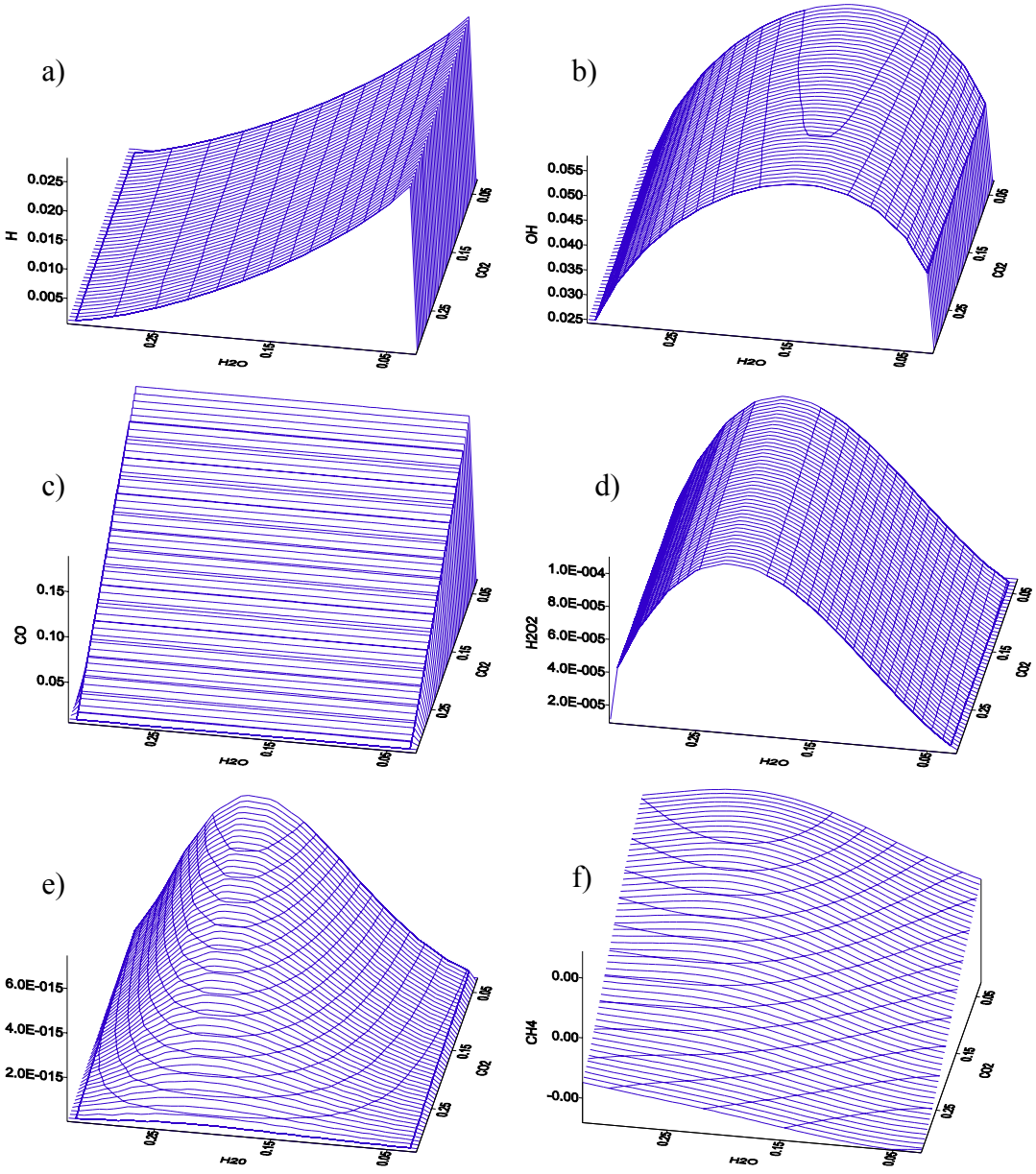


Figure 3.13 Mass fraction variation of the species projected into CO_2-H_2O space, for methane/air combustion. (ζ= 0.2)

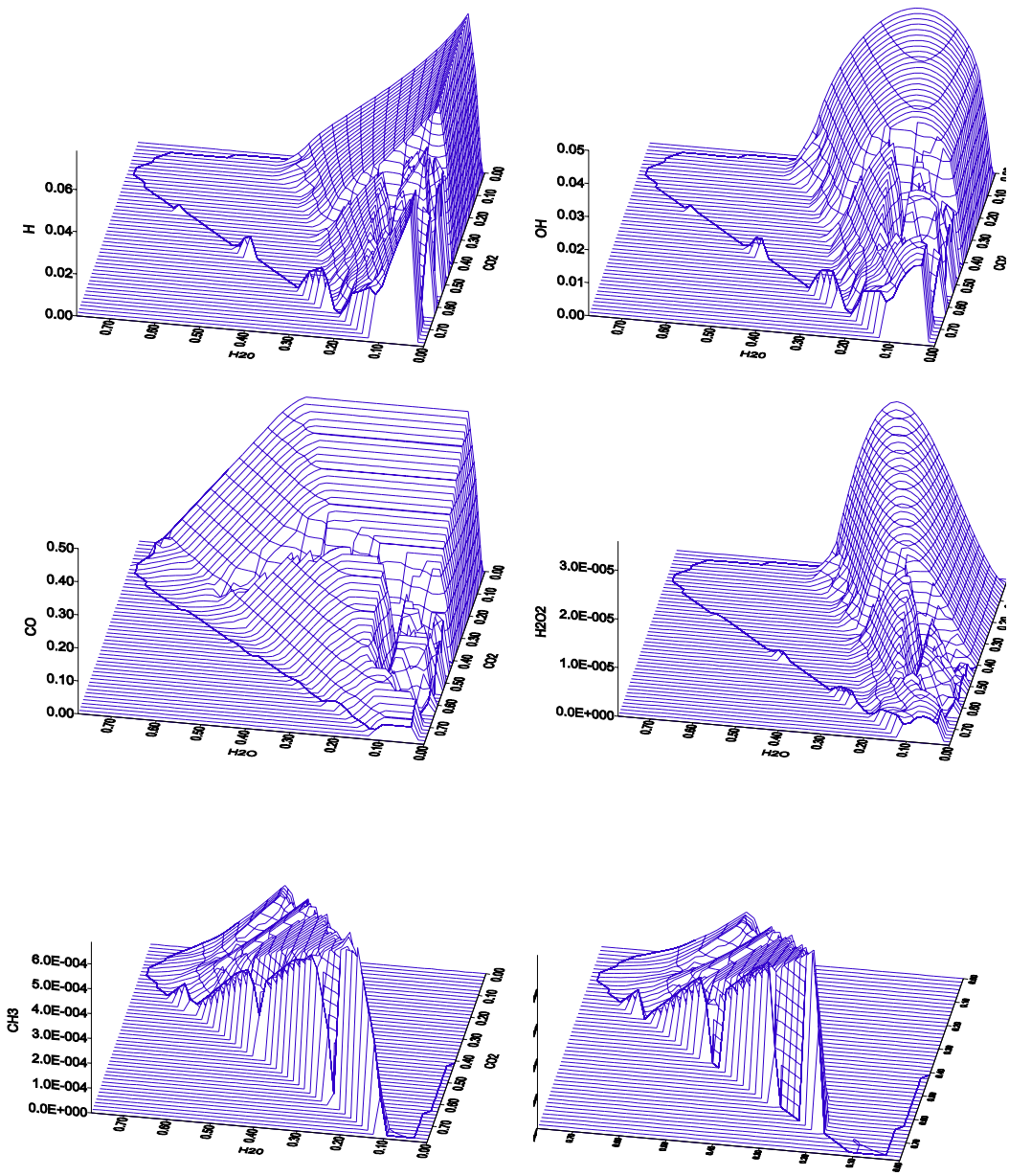


Figure 3.14 Mass fraction variation of the species projected into CO_2-H_2O space, for methane/air combustion. (ζ= 0.5)

3.3 Implementation of ILDM into CFD Solvers

The solution for the scalar field can be calculated by the ILDM methodology in terms of the RPVs, and tabulated in a look-up table. Different look-up tables can be calculated for different fuel/oxidizer combinations; number and choice of the RPVs. On the next step, the use and interpretation of the data, stored in the table, for different combustion processes should be determined. Since the data is tabulated with respect to the varying values of RPVs, the instantaneous mass fraction of each species and the reaction rates, can be easily read from the table. To calculate the variation of the species mass fraction in a combustor, the general idea is to track the composition of the RPVs just by solving the species mass transfer equation with flow solver, and then read and the reaction rate of the scalar field from the look-up tables (Correa 2000; Rawath 1997; Bedford 2001; Eggels 1996). Although the procedure seems easy, it has several difficulties in application, which will be outlined on the following section.

To get the composition of the species within the combustion zone, for a detailed calculation, one has to solve the species mass transfer equation, which can be seen in equation 4.64.

$$\rho \frac{\partial Y_i}{\partial t} + \rho \nabla \left(Y_i \vec{U} \right) = \rho D_{AB} \nabla^2 \left(Y_i \right) + \rho \dot{Y}_i \tag{3.64}$$

where, the consumption/production rate of the species *i* can be calculated as follows,

$$\dot{Y}_i = \frac{M_i}{\rho} \sum_{n_r} \left(b_{ir} - a_{ir} \right) \dot{w}_R \tag{3.65}$$

b_{ir} and a_{ir} denote the stoichiometric coefficients, M_i the molar mass of species *i*, and $\dot{w}_r$ denote the reaction rate.

$$w_R = k_f \prod_{j=1}^{n} \left[Y_j \right]^{v'_j} - k_b \prod_{j=1}^{n} \left[Y_j \right]^{v''_j} \tag{3.66}$$

For the solution of a non-turbulent reactive flow, the instantaneous reaction rates, which were calculated and tabulated by ILDM methodology, can be used to close the production term of the species mass transfer equation. However, most of the

applications require the solution for a turbulent flow. Thus, the Favre averaged equations should be used.

$$\frac{\partial \overline{\rho}\widetilde{Y}_i}{\partial t} + \nabla\left(\overline{\rho}\widetilde{Y}_i\widetilde{\vec{U}} \right) = \nabla\left(\overline{\rho D \nabla Y_i} - \overline{\rho \vec{U}'' Y''}_i \right) + \overline{\rho \dot{Y}_i} \tag{3.67}$$

In this case, the calculation of the time averaged source term is much more complicated and requires special techniques. Reaction rate can be either calculated by applying averaging rules to equation (3.66) or using a probability density function (PDF) (Goldin and Menon 1998; Pope 2000; Warnatz et. al. 2001; Veynante and Vervisch 2002). PDF solution approach is most widely used in simulation of reactive flow applications. In terms of PDF transport equation the source term can be calculated as follows,

$$\widetilde{\dot{Y}}_i = \int \dot{Y}_i\left(\zeta, T, Y_{rpv1}, Y_{rpv2}, ..., Y_{nrpv}\right) P\left(\zeta, T, Y_{rpv1}, Y_{rpv2}, ..., Y_{nrpv}\right) d\zeta . dT . d(Y_{rpv1}) . d(Y_{rpv2}) ... d(Y_{nrpv}) \tag{3.68}$$

where, $\dot{Y}_i$ is the instantaneous rate of species *i* which was calculated with ILDM methodology, and $P\left(\zeta, T, Y_{rpv1}, Y_{rpv2}, ..., Y_{nrpv}\right)$ denotes the PDF function which is a function of the mixture fraction ζ, Temperature *T*, and the specific mass fraction of the RPVs, and requires the construction of a *nrpv*+2 dimensional PDF. Although techniques to deal with multidimensional PDFs exist, (Correa 2000), they are not very suitable for complex systems, as their construction requires not only the variances, but also the cross correlations in between all the variables. That's why a more practical approach is to assume that a statistical independence of the each variable is valid, and hence to split, the PDF function in to *nrpv*+2 discrete functions

$$P\left(\zeta, T, Y_{rpv1}, Y_{rpv2}, ..., Y_{nrpv}\right) = P(\zeta) P(T) P(Y_{rpv1}) P(Y_{rpv2}) ... P(Y_{nrpv}) \tag{3.69}$$

The shapes of the one-dimensional PDFs can now be assumed, and they can be constructed based on the mean moments. Several shapes of PDF are possible to use. Gaussian function, Beta functions or Dirac-delta functions. For non-premixed combustion applications the fuel and oxidizer enter to the combustion zone with two different streams as can be seen in figure (3.15). Mixture fraction in the early stages of the mixing shows two distinct peaks of 0 and 1 in the vicinity of the oxidizer and fuel streams. In the dead zone, which is illustrated with symbol C in the figure, the

fuel and oxidizer streams could not make any effect yet, and it does not show any variance. On the other hand, if one is interested by the mixture fraction variation on point D, where the mixing process occurred effectively, a Gaussian distribution is likely to be occurring. This shows that a combination of a Dirac Delta function for the early stages, and a Gaussian distribution for well-stirred zones, is required. That's why, for mixture fraction a Beta function is chosen to construct the PDF.

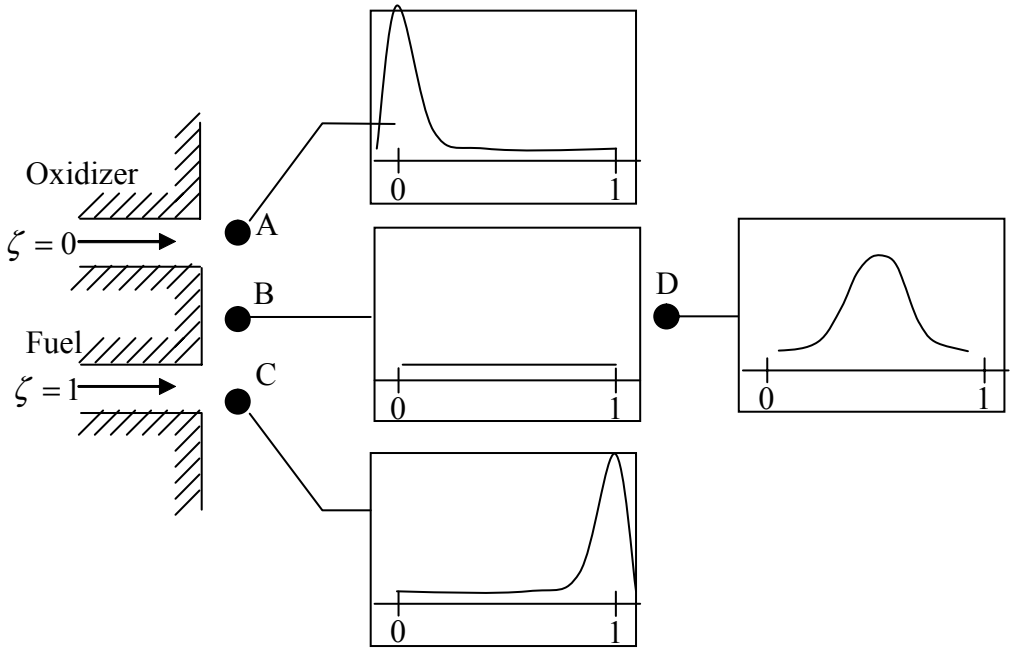


Figure 3.15 Schematic illustration for PDF of mixture fraction in a turbulent non-premixed combustion configuration.

The Beta function, for a variable *f*, can be constructed as follows,

$$P(f) = \gamma . f^{(a-1)} . (1-f)^{(b-1)} \tag{3.70}$$

with,

$$\gamma = \frac{G(a+b)}{G(a)+G(b)} \tag{3.71}$$

where, *G*, denotes the Gamma function. Thus only two parameters *a* and *b* need to be determined, form the mean and variance of the variable of *f* as,

$$a = \frac{b\bar{f}}{1-\bar{f}} \tag{3.72}$$

and

$$b = \frac{\bar{f}\left(1-\bar{f}\right)^2}{\overline{f''^2}} + \bar{f} - 1 \tag{3.73}$$

(Correa 2000). On the other hand the usual practical application for temperature is to maintain the temperature of the both fuel and oxidizer streams same, and then to start combustion by igniting a particular zone in the combustion chamber. Then, different from the variation of mixture fraction in the combustion chamber, temperature distribution shows a Gaussian distribution in the all stages of the combustion process. Both Gaussian and Beta functions are referred as two-parameter distribution, in that they need both the variance and mean values of their variables. So, the mean and variance of mixture fraction, $\widetilde{\zeta}$, $\widetilde{\zeta}''^2$, Temperature $\widetilde{T}$, $\widetilde{T}''^2$, and the specific mass fraction of the RPVs $\widetilde{Y}_{rpv1}$, $\widetilde{Y}''^2{}_{rpv1}$; $\widetilde{Y}_{rpv2}$, $\widetilde{Y}''^2{}_{rpv2}$; …. ; $\widetilde{Y}_{nrpv}$, $\widetilde{Y}''^2{}_{nrpv}$ are needed to proceed in the calculations. The variance of the mixture fraction can be simply calculated with the following formula,

$$\frac{\partial \overline{\rho}\widetilde{Y}''^2{}_i}{\partial t} + \nabla\left(\overline{\rho}\widetilde{\vec{U}}\widetilde{Y}''^2{}_i\right) = \nabla\left(\overline{\rho}D_T\nabla\widetilde{Y}''^2{}_i\right) + 2\overline{\rho}D_T\left(\nabla\widetilde{Y}_i\right)^2 - 2\overline{\rho}\frac{\widetilde{\varepsilon}}{\widetilde{k}}\widetilde{Y}''^2{}_i \tag{3.74}$$

For the variance of the Temperature, a transport equation can also be written and solved in order to get the PDF. But, the temperature variance equation is very difficult to solve and contains many unclosed terms due to the chemistry source terms, which makes the solution quite impossible. Hence, it can be assumed that the intensity of turbulence is the same for the mixture fraction and the temperature (Correa 2000), i.e.,

$$\frac{\widetilde{\zeta}''^2}{\widetilde{\zeta}} = \frac{\widetilde{T}''^2}{\widetilde{T}} \tag{3.75}$$

from which, the temperature variance $\widetilde{T}''^2$ can be calculated. This approach assumes that the temperature behaves like a conserved scalar, which is not physically reasonable. However, in non-adiabatic, variable-pressure engines, where enthalpy is

not a unique function of the mixture fraction, a PDF integration over the temperature has to be carried out, and the above equation is an approximation for the variance.

The PDF for the reaction progress variables is much more complicated to construct. The assumption of the statistical independence may be valid between the mixture fraction and the temperature in some particular cases. On the other hand the mass fraction of the RPVs are a function of the temperature and mixture fraction. In this respect applying the statistically independent assumption to construct a one-dimensional PDF for the RPVs is not valid. This difficulty is overcome by applying a simple variable change on the PDF, and will be shown for the case of fuel/oxidizer system is CH_4/Air and the selected RPV is CO_2.

The mixture fraction of the CO_2 is zero in the pure fuel (ζ=0) and pure oxidizer (ζ=1) conditions, where it reaches to its maximum value when the mixture is stoichiometric ($\zeta=\zeta_{st}$). Then Burke-Schumann solution for the variation of the mass fraction of CO_2 with respect to the mixture fraction can be easily calculated, and it can be seen in figure (3.16).

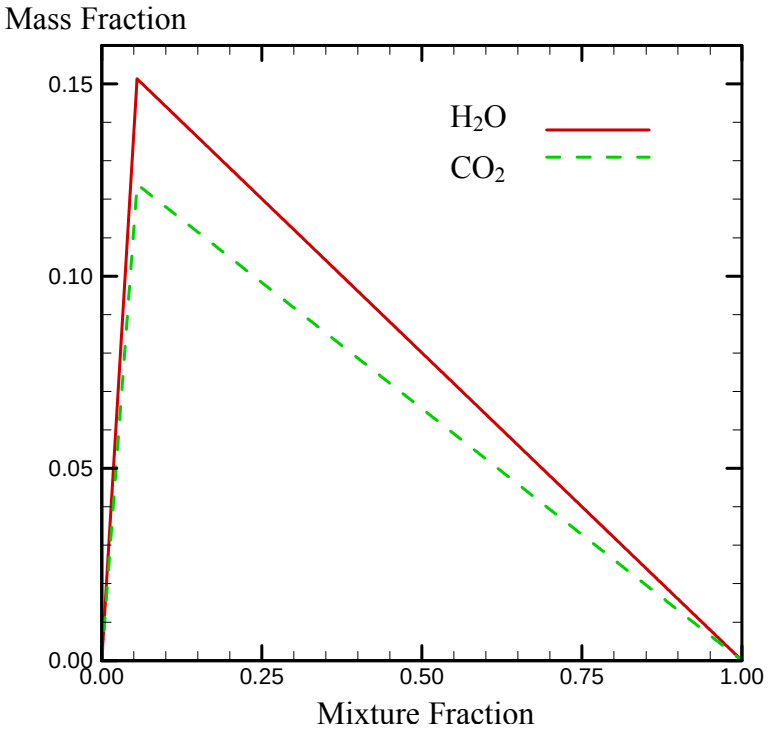


Figure 3.16 Burke – Schumann solution for the variation of CO_2 and H_2O with respect to mixture fraction.

Interested readers may refer Appendix IV for Burke - Schumann calculations of a methane/air combustion system. The conventional PDF method requires the integration of the mixture fraction on a straight line as it can be seen in figure (3.16) Infact the mass fraction is bounded by Burke-Schumann solution and must lie at least within the solution domain. Defining a new variable *b* instead of Y_{CO2} which is calculated as,

$$b = \frac{Y_{CO_2}}{Y_{CO_2,st}} \tag{3.76}$$

the mixture fraction can be normalized and kept in the physical domain. The mean of variable *b* can be determined as

$$\widetilde{b} = \frac{\widetilde{Y}_{CO_2}}{\widetilde{Y}_{CO_2,st}} \tag{3.77}$$

Here, the mean mass fraction value of CO_2 is calculated by solving the corresponding species mass transfer equation. For the mean values of the stoichiometric value of the CO_2, another PDF should be constructed.

$$\widetilde{Y}_{CO_2,st} = \int Y_{CO_2,st} \widetilde{P}(\zeta) \widetilde{P}(T) d\zeta . dT \tag{3.78}$$

Since, it is difficult to get the variance of the variable *b*, without causing a misleading result, the shape of the PDF can be assumed as Delta function, which does not require the calculation of the variance.

As a result the PDF $P\left(\zeta, T, Y_{CO_2}\right)$ is turned to be $P\left(\zeta, T, b\right)$, all the variables can be separated from each other to construct one dimensional PDFs, as

$$P\left(\zeta, T, b\right) = P(\zeta) P(T) P(b) \tag{3.79}$$

To sum up what we have at last, beta function is used for the construction of the PDF of mixture fraction and temperature, where the shape of the PDF used for *b* is assumed to be Delta. For the one-dimensional PDF of the mixture fraction, the mean and variance equations should be solved by the CFD code. On the other hand, for the PDF of Temperature, since it is difficult to solve its variance, it is assumed to change linearly with the variance of mixture fraction and is calculated from equation (3.75). The mean values of mass fraction is calculated by the CFD code. Although the

bounds of the PDF constructed for the mixture fraction is [0,1] and for Temperature is [0,∞], by using the ILDM technique, it is only possible to use the limits calculated with the method itself.

3.4 Hierarchical Structure of ILDM

In recent years ILDM methodology is tested and used for many combustion applications, and effective results have been taken (Xiao *et al.* 2002; Chen 2002; Correa 2000; Taut *et al.* 2000; Blasenbrey *et al.* 1998, Maas and Schmidt 1998). Even tough ILDM stems from a strong mathematical background (Bongers *et al.* 2002); practical use of the algorithm has some drawbacks, and they still need to be improved to increase the efficiency, and the speed, of the numerical calculations. One of the main difficulties imposed by the ILDM is that, a low dimensional manifold in the phase space, for the rich or lean values of the mixture fraction, or for the ignition, cannot be detected well. The idea of constructing a manifold that is governed by 2 or 3 slow processes, and all the other processes being in equilibrium, can be valid only for the partially burnt or burnt gases. However a large number of progress variables are needed in un-burnt gases and the early stages of combustion. In such configurations, the number of the RPVs should be increased, which needs a dynamic regulation within the code with respect to the variation of the mixture fraction and enthalpy. Another problem of ILDM is related with the complexity of the hydrocarbon fuels especially for those containing high number of Carbon in their structure (Correa 2000, Chen 2002, Warnatz 2002). As the complexity of the fuel increases, the number of the species and the reactions involved in the combustion also increases, resulting a much more stiff equation system, which is difficult to solve. Also, an increase in the order of the equation system, causes an ill conditioned assumption for the relaxation of all processes except those associated with the number of the RPVs. In order to not to loose the advantages obtained by ILDM, a numerical scheme, which allows the construction of low dimensional manifolds for high hydrocarbon fuels, is improved and tested within the thesis. The hierarchical structure of the combustion of hydrocarbon fuels and the equilibrium concept is exploited to change the code.

The classical approach in ILDM method is to start the calculation with an initial point which lies already on the manifold, and then to reach the desired state, by

changing the elements of the parameterization vector (Maas and Pope 1992a). In this respect, the program finds the way to the desired state by itself, and the code is written in such a manner that always the shortest path is preferred. Obviously this approach has some disadvantages, in that the program does not have any information about the trajectory that it is following. One can start the calculation from a region where ILDM is not capable of producing good results, and may face up with a huge computation time to wait the code find best trajectory to follow. The modification of the program by using the hierarchical structure of the hydrocarbon fuels also helps to overcome this disadvantage. For the calculation of the high hydrocarbon fuels, the subroutines of the ILDM is modified in such a way that instead of starting the calculation from a single point, the program looks for the result table which was prepared previously for simple fuels. The datasets containing information about the mass fractions of the species, temperature, rates of the RPVs, etc., are, read one by one, and used as initial guesses for the calculation. In this respect, approach of hierarchical calculation has two advantages. Since the datasets are read one by one, the program should have to obey the mesh generated for the simple fuel. So, the bad points for which ILDM failed to calculate even for the simple fuels are skipped a priori. The code does not have to spend the time to find its way on difficult or nonsense regions. Another advantage is, since the previously calculated datasets are on the manifold, the spectral gap between the slow and fast processes are already distinct, and the eigenvalues are relaxed. As a result, while the number of the calculations for the inner loop exhibits large values to relax the eigenvalues for classical ILDM approach, the current version will not spend too much time on this process. Thus, number of the eigenvalues that have to be relaxed for the high hydrocarbon fuels is decreased by the order imposed with the detailed mechanism of simple fuel. In this way, the time required for generating a result table for high hydrocarbon fuels decrease, and the capability of the calculation of intermediate species occurring in C_4 mechanism increases.

The chemical aspects of the modified version stems from the hierarchical structure of the hydrocarbons and the equilibrium concept. The combustion of the higher hydrocarbons generally shows the same hierarchical structure. An initial attack on the C-H bond of the fuel, by H, O, or OH, leads the formation of the H_2, OH, H_2O and the alkyl radical with the H-atom absorption processes. The alkyl radical is then

decomposed into relatively stable radicals of *methyl* (CH_3), *ethyl* (C_2H_5) by the *β*-decomposition reactions. Both processes follows two different chemical flow charts up to the formation of CO and CO_2, which eventually feed the C_1-C_4 oxidation system. The C_1-C_4 reaction mechanism performs further oxidation processes including the H_2, CO and CH_3OH subsystems. Sensitivity analyses, performed for different hydrocarbon fuels to understand the overall kinetics of the combustion processes, show that the rate-limiting, slow, part of the mechanism is the oxidation of the CH_3 and C_2H_5 radicals (Warnatz 2002). Then, the strategy in the development of detailed reaction mechanisms for high hydrocarbons can be to use the C_1-C_4 reaction mechanism and to add additional reactions for the specific system. It is possible to exploit this structure in the ILDM concept. In this way, mechanisms developed, for example, for CH_4 combustion will also be applicable to the calculation of the C_8H_{18} flames. If, the eigenvalues corresponding to the additional reactions to the small mechanisms exhibits small eigenvalues than the C_1-C_4 mechanism, both the original and the reduced schemes should represent the same topology on the phase space. In the concept of ILDM this means that, if the added extra reactions do not contain any significant slower reaction than those exist already in the previous mechanism, they can be also decoupled with the other fast reactions. It is because of this hierarchical structure, the ILDM calculation performed for different combustion systems usually show the same characteristic variation regardless of their detailed mechanism.

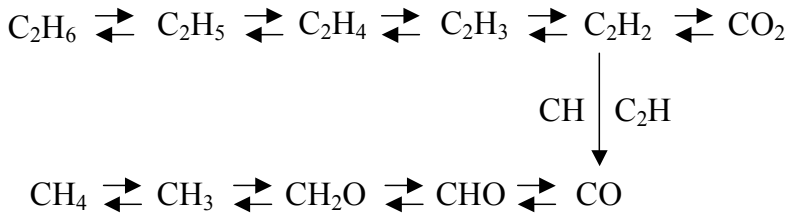


Figure 3.17 Schematic representation of the C_1 and C_2- hydrocarbon oxidation

Another important parameter which affects the structure of the different low-dimensional manifolds in the phase space is the equilibrium concept. The main idea is, the equilibrium point, being a solution of the scalar field equation system, is a stable point, and attracts the solution space into itself in the direction of the eigenvectors. It is well known that the equilibrium point is a function of the element

composition, enthalpy and mixture fraction of the combustion mixture (Blasenbrey and Maas 2000). Then, If two very different combustion system have the same equilibrium conditions, same enthalpy, mixture fraction and element composition, they have to use the same portion of the phase space in order to reach into their equilibrium point.

To sum up what we have, incase of their equilibrium points are same, a $C_{10}H_{22}$/air and CH_4/air system, regardless of the complexity of the complexity of the fuel mixture, have to share the same solution space, since the base point of both spaces are same and most of the eigenvectors denoting the direction of the variation of the space are identical. The place of the base point is affected by the equilibrium point, and, if the equilibrium points are same, then the portion of the space that they share should be same. But this does not mean that the both solution spaces may coincide perfectly, because their surface topology can be different. In this point, the direction of the eigenvectors of their governing equations distinguishes the differences. If, the eigenvectors, which are associated with their detailed mechanism, are same, then their topology should also be same. It was pointed out on the previous paragraph that the hierarchical structure of the detailed mechanisms show that most of the eigenvalues are indeed same for two different systems.

Within the scope of the thesis, several subroutines are written in FORTRAN programming language and implemented into the existing ILDM code to make use of this hierarchical structure. Modified version of the code reads the mass fractions of the species which belong to the previous calculation and stores them in the memory. Later, the species of the current calculation step is compared with the previous one, and the mass fractions for the species that match with those are equilibrated. The new initial guess values for the state vector contain zeros for the species corresponding to the new calculation, plus the mass fractions which belong to the calculation for simple fuel. In the classical approach, every calculated dataset is stored in the memory with the binary trees, which allows to sort the data and construct the result table in a ordered manner. In this way, whenever a dataset is needed by the CFD solver, it can be found very quickly. But, it should be noted that for an accurate CFD simulation, a typical methane/air result table should consist of millions of datasets, each dataset containing 49 data written in the format of double precision. Even though there are numerous attempts by the researchers to simplify the calculation

procedure to speed up the calculation time required for an ILDM point, the need for storing every calculated data in the memory require computers which have really big random access memories (RAM). Even in this case, after a certain number of calculations, RAM will be filled up and the computer will be slow down. The subroutines written for hierarchical calculation is free from this disadvantage. Since the datasets are already ordered in the result table calculated for the simple fuels, and are read one by one by as initial guesses by the modified version, the calculated datasets which belong to the new approach are also ordered. The increments occurring on the RPVs due to the new calculation is same for every dataset, and thus the order of the table should stay the same. The only difference is the values of the RPVs are shifted compared with the previous one. The new subroutines are written in such a manner that, whenever a new dataset is calculated, it is written into the result table. In this way, the memory allocations in the RAM are maintained in considerable relatively small numbers. Last thing to mention about is, the new version of ILDM code can be switch between the classical and modified versions by a flag that is read from the initialization file.

The H_2O_2 and OH specific mass fraction variations with respect to CO_2 and H_2O, calculated separately with ILDM simulations for different fuel compositions using C_1 C_1-C_2 and C_{10} mechanisms, but the same equilibrium point, can be seen in figures. (3.18) and (3.19) It is a common feature in both graphs that the variation of H_2O_2 and OH on the solution space are not affected from different fuel compositions. It is also possible to express that the effect of the change of detailed mechanism yield only small deviation from that of its value calculated with other mechanisms.

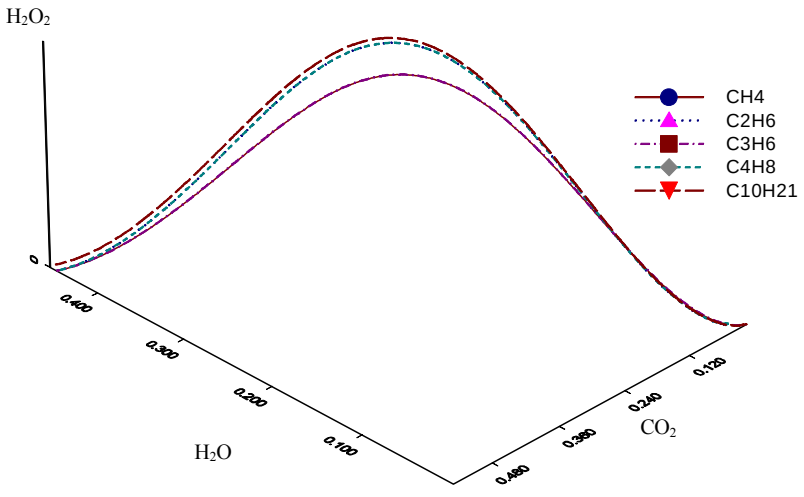


Figure 3.18 Low Dimensional Manifolds for different fuels projected into H_2O_2-CO_2-H_2O space

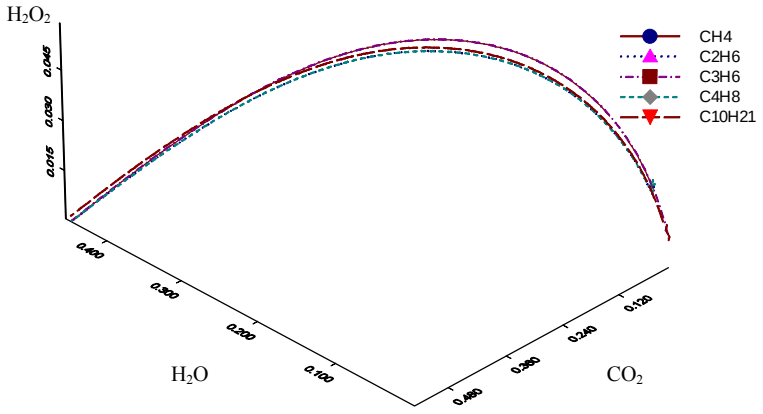


Figure 3.19 Low Dimensional Manifolds for different fuels projected into OH-CO_2-H_2O space

4. RESULTS AND DISCUSSION

The modified version of the ILDM code, which is capable of performing calculations based on the simplification procedure introduced by the hierarchical structure of the hydrocarbon fuels, is tested for a set of basic calculations. The calculations are performed for an isobaric non premixed combustion system where synthesis gas/oxygen and methane/oxygen mixtures are used for fuel/oxidizer mixtures. To validate the data obtained by the hierarchical calculation methodology, a methane/air table is produced by the classical approach of ILDM, with the same initial and boundary conditions.

To start the hierarchical calculation for methane/oxygen system an initialization table is generated for a synthesis gas/oxygen mixture with two RPVs being H_2O and CO_2. Temperature and pressure boundary conditions in the fuel and oxidizer inlets are assumed to be same, 330 K and 1 bar respectively. The fuel is a mixture of CO and H_2, with the mass fractions of 0.37 and 0.66, and oxygen is used as the oxidizer for the combustion. To initialize the calculation, equilibrium point is evaluated with ILDM. To maintain the element composition same for both calculations, the mixture fraction for methane/oxygen system is chosen 0.2, whereas it is 0.4 for synthesis gas/oxygen system. 3-D and 2-D tables generated for synthesis gas/oxygen mixture, projected into CO_2 and H_2O space can be seen in figure (5.1.), where 2-D ILDM is denoted with black squares on the surface. The stoichiometric mass fraction values of the species H_2O and CO_2 are, 0.454 and 0.528, which represents the limitation of the accessible area by the ILDM. In the stoichiometric mixture all intermediate species are consumed and there exists only the combustion products in the combustion zone. The figures obtained for OH, H_2O_2, CH_2O and CHO shows a Gaussian like variation with respect to CO_2 and H_2O, and all of them reach to their maximum values in the range of 0.30 – 0.20 for H_2O. The variation obtained for H and CO exhibits a linear distribution with respect to the rpvs with a constant slope. It was also interesting to see that the mass fraction of the all Carbon containing species shows an increase by the increasing values of CO_2.

It was possible to generate a methane/oxygen table by using the datasets calculated for synthesis gas table as initial guesses. The distribution of the various species obtained for methane/oxygen system and projected into the space formed by CO_2 and H_2O can be seen in figure (5.2.). As it was expected, the variances in general show similar patterns with those that were obtained for synthesis gas/oxygen mixture, except for the triangular area confined to the range of 0 – 0.30 for H_2O and 0 – 0.5 for CO_2, where ILDM failed to calculate points. The accessible area obtained for CH_2O and CHO is further decreased than those obtained for other four species. Both distributions show a peak value for the mass fraction of 0.10 and 0.20 for CO_2 and H_2O respectively, and then decrease suddenly to the values of the order 10^{-5}. Thus it is logical to say that CHO and CH_2O makes effect on the overall kinetics just for a triangular zone lying in the range of 0.30 – 0 for H_2O and 0.20 – 0 for CO_2. Another interesting feature can be spoken for the distribution of CO, which can be seen in (5.2.) (c). The distribution generally shows two distinct regions with different slopes. It is known that the formation of CO is dependent on different processes including the CH_2O - CHO and C_2H, - CH_2 systems. Thus, the different regimes of the variation represent the effects of the processes on the formation of CO. The valley which is placed in between two zones, and squeezed into the range of 0.3 – 0.20 for H_2O and 0.20 – 0 for CO_2, coincides with the area obtained for both CH_2O and CHO. It is therefore possible to say that the valley zone represents the amount of CO produced by CH_2O and CHO oxidation.

In order to verify the data obtained by the modified version, another simulation is done with the same boundary conditions, but by using the classical approach of ILDM. Equilibrium point is used for initializing the simulation. The corresponding distributions of the species can be seen in figure (5.3.). All the variations seem to match perfectly with the modified version, except for the triangular region where zero mass fraction values are encountered. Indeed, it was possible to find the existence of the same area with the modified version as well, but in that case it was confined to a rather smaller area. Another property, which can be observed in all distributions, is the roughness of the surface topology in comparison with the modified version. The reason for these problems can be explained as follows; the idea of using relaxed points as initial guesses helps the code to work more efficiently in the ranges where it is difficult to obtain a result. Since the initial conditions for the

state vector compromises of logical values, the newly calculated data should adopt itself into those values. On the other hand, in the classical approach, when ILDM fails to create a point, it refines the mesh, re calculates the points and forces itself to find the state. Sometimes it may not be possible to calculate the state by the program and mathematically true but chemically false states can be calculated and used as initial guesses for the calculation of other points. Thus, it is possible to a get a bad point as an initial guess, and in this way the error of the initial point would likely to propagate in to the other points. This is the main reason for the roughness of the distribution obtained for methane/oxygen calculation with the classical approach of ILDM. Also, since the relaxed points which belong to the previous set of calculation are used as initial guesses in hierarchical calculations, the code works fairly good in the ranges where it is difficult for the classical approach to construct low-dimensional manifold. That's why; the total area of the triangular region, where it was not possible to create points by conventional method, is decreased by the hierarchical calculation.

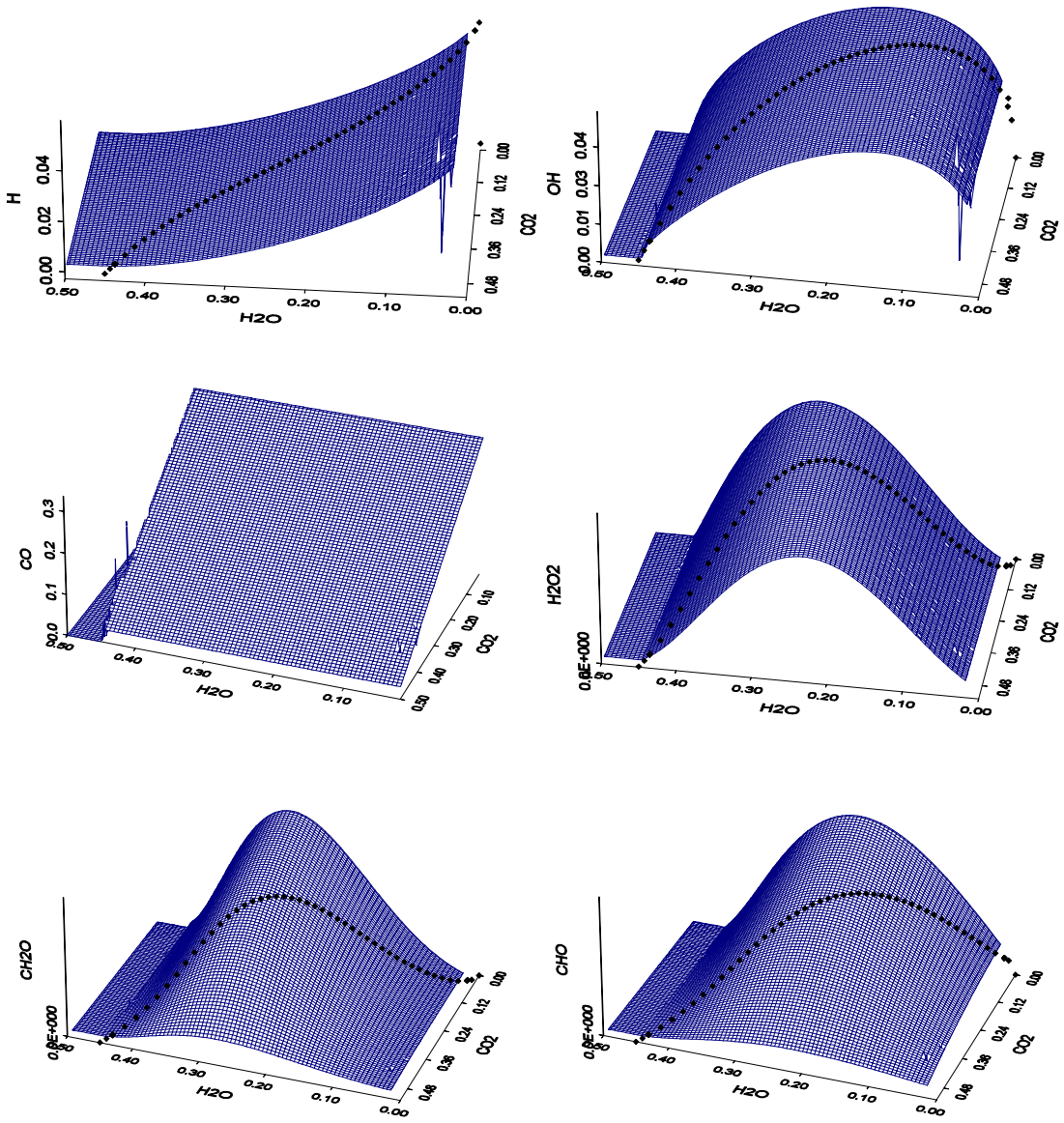


Figure 4.1 Mass fraction varition of the species projected into CO_2-H_2O space, calculated for synthesis gas with classical approach.

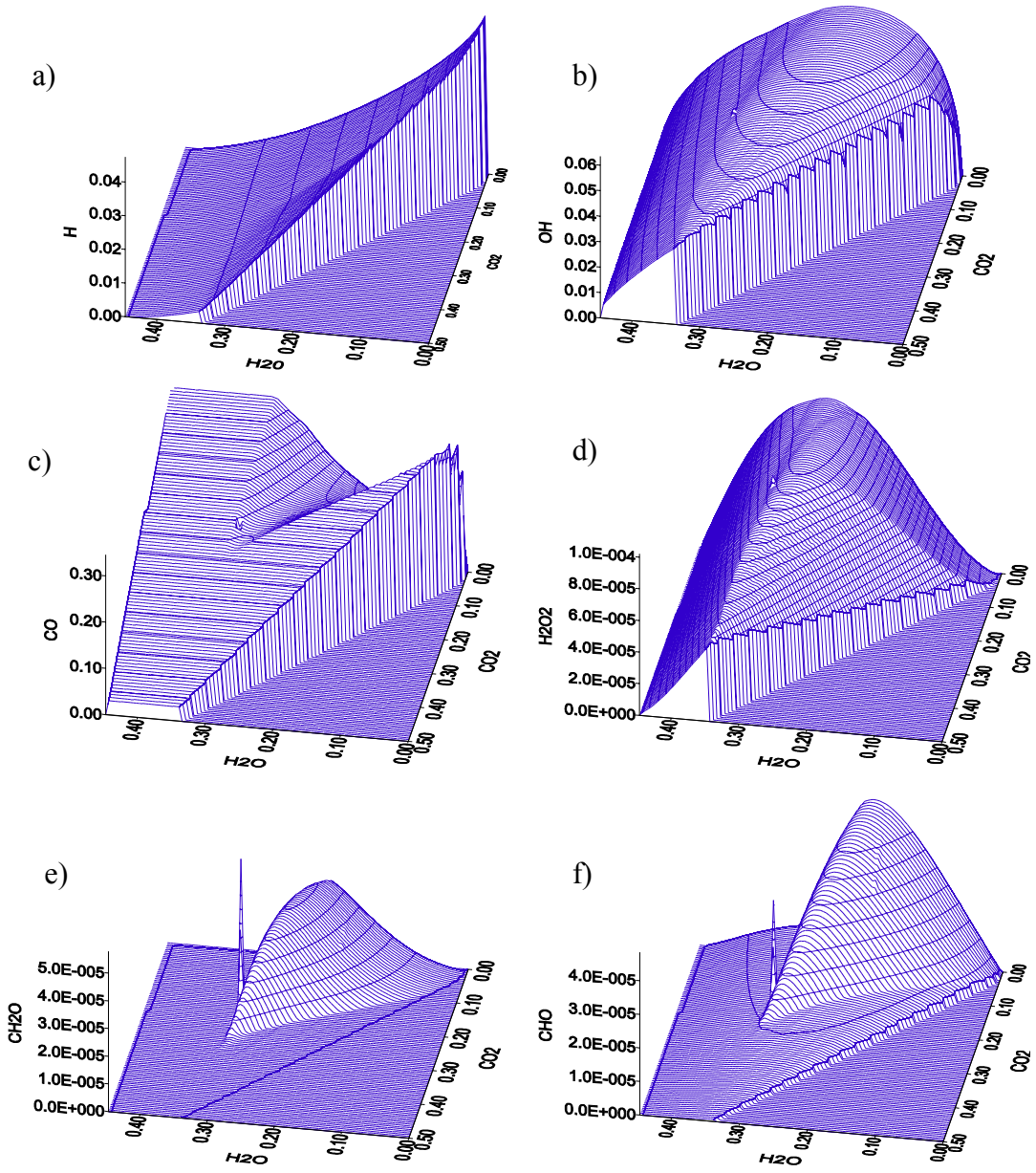


Figure 4.2 Mass fraction variation of the species projected into CO_2-H_2O space, calculated for methane with the hierarchical approach.

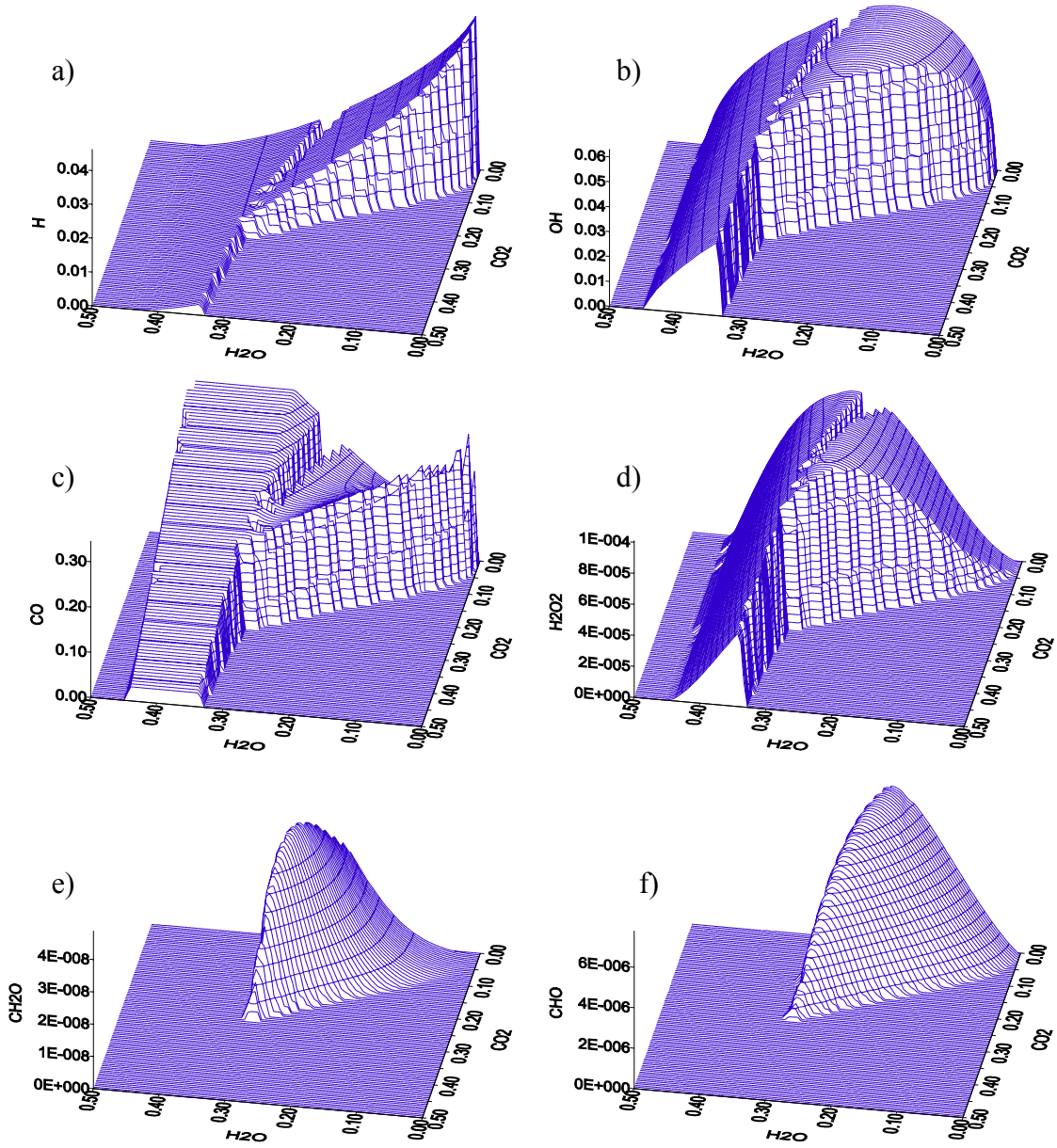


Figure 4.3 Mass fraction variation of the species projected into CO_2-H_2O space, calculated for methane with the classical approach.

The distributions obtained by synthesis gas/oxygen, methane/oxygen with hierarchical calculation and with the classical approach, were given separately in the figures above. Even tough the figures give a clue about the similarity between the simulations performed for hierarchical and classical approaches of ILDM, the exact comparison of the method can not be obtained. In order to demonstrate the accuracy of the modified version, a better way would be presenting the variances in the same figure for the range of same species. In this respect, the variation of H, OH, CO and $H_2O_2$with CO_2 are drawn for further error analyzing. In order to avoid confusion, the distribution of the species are calculated only at the cross sectional areas for H_2O being 0.1, 0.2, 0.3 and 0.4. In the figures the variances obtained by classical and modified method seem to show similar patterns and the error does not exceed a maximum of %3.8 for cross sections obtained at 0.1, 0.2 and 0.3. It is a common behavior in the figures that there is a strong similarity between the values calculated by both classical and modified method in the cross sectional areas of 0.1 and 0.2 for H_2O. Apart from that, the initial distribution given by the synthesis gas/oxygen system seems to have minor effect on the hierarchical calculations. As it can be seen in the figures, especially for the cross sections obtained at 0.1 and 0.2 of H_2O, even tough the initial distribution is linear, the modified version is capable of calculating the same parabolic profile of the methane/air system. The error in this region seems to be almost zero for the CO variation, whereas it reaches to its maximum value of %3.6 for H variation, which is still within the acceptable limits of error. On the other hand, except for the CO variation, local error increases for the cross sectional areas obtained for the increasing values of H_2O. A reason for this can be due to the similarity between the surface topologies obtained by the initial and normal calculations. Since both distributions exhibit the same topology, datasets read from the initial guesses forces the modified version to calculate points similar to them. Even tough the values obtained by modified version seem to be shifted from its normal value with a local error varying between %2 - %9; it can still evaluate the datasets within the same boundaries obtained by classical approach. Also, it is possible to say that, the error decreases with the increasing values of CO_2. The error seems to be minimum for all cross-sectional areas obtained for the CO distribution. One reason for this can be due to the order of the magnitude of the CO mass fraction values. A typical value for the CO mass fraction is on the order of 0.1, where an error on the order of 0.001 is acceptable. On the other hand an error with an order of 0.001

is very high for H or H_2O_2 since they exhibit values as small as 10^{-2} and 10^{-5} respectively. In this respect even tough the absolute error seems to be relatively high for those species, which is between %1 – 5, the absolute error does not make any sense because mass fractions are themselves small.

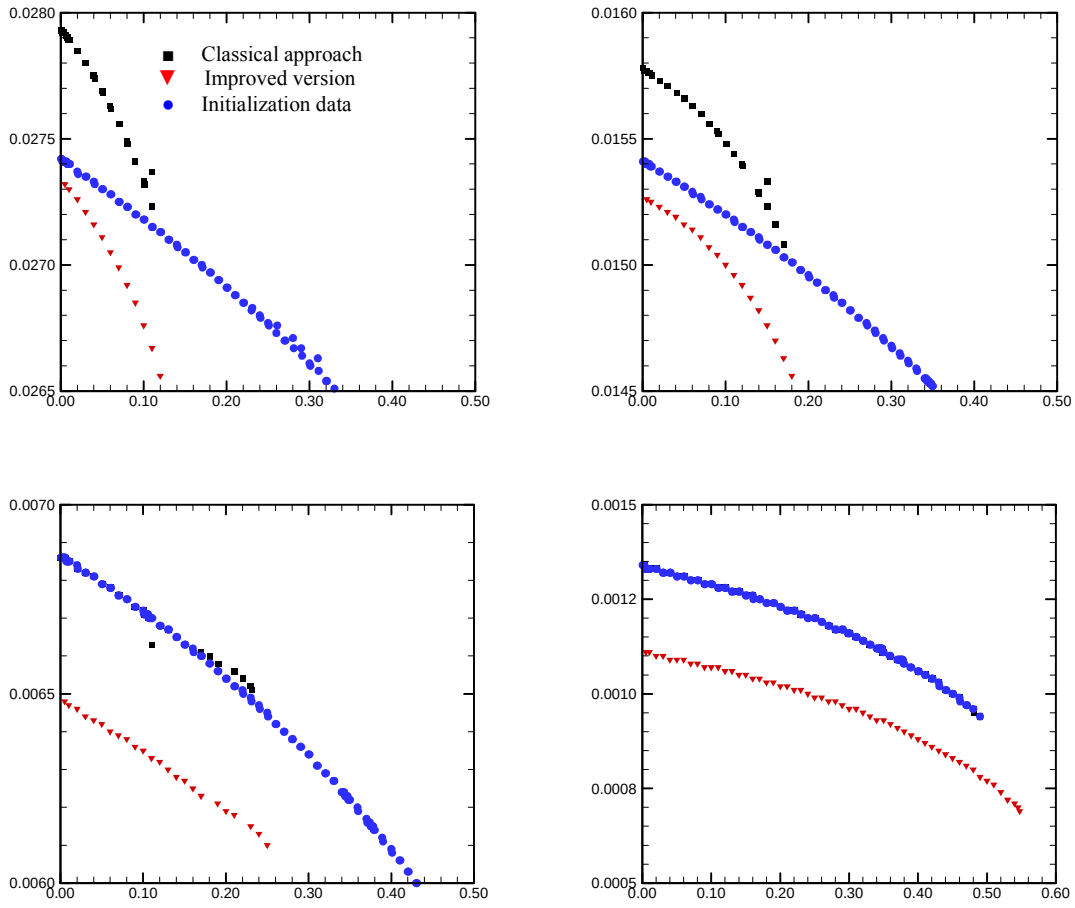


Figure 4.4 Mass fraction variation of H with respect to CO_2 obtained for four different cross-sections.

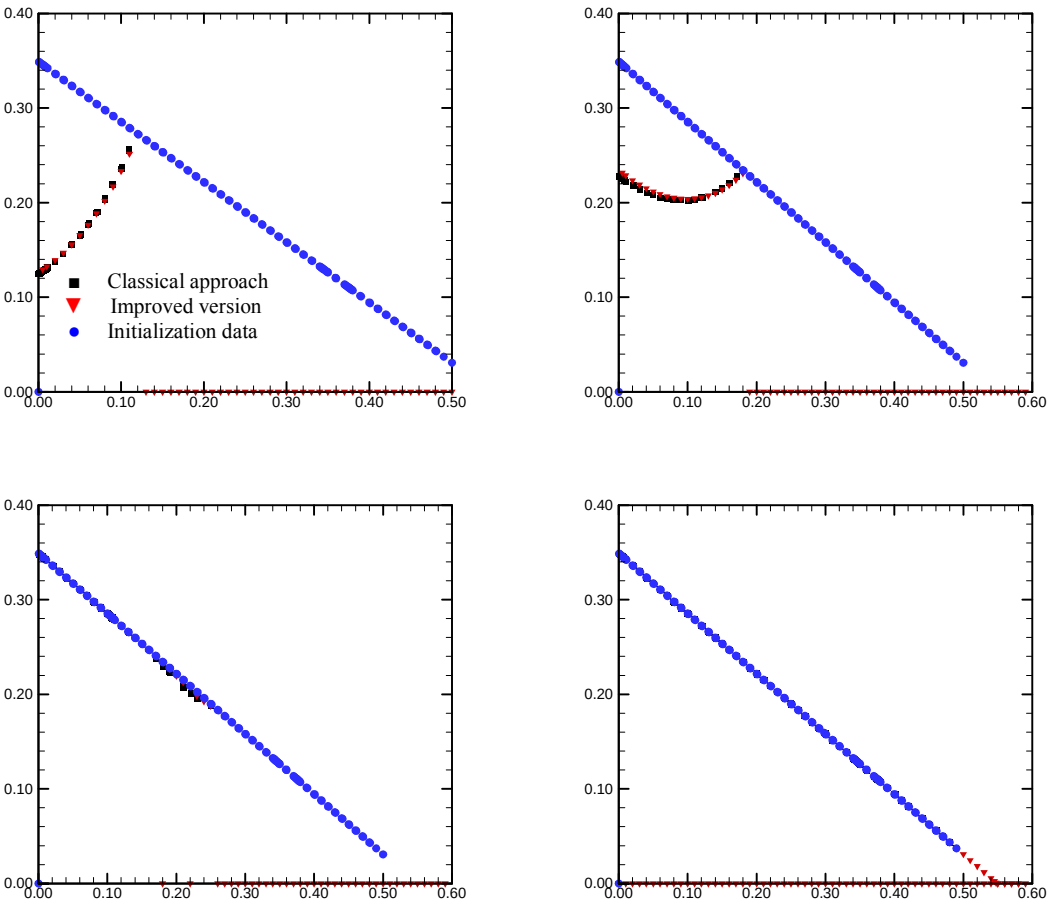


Figure 4.5 Mass fraction variation of CO with respect to CO_2 obtained for four different cross-sections.

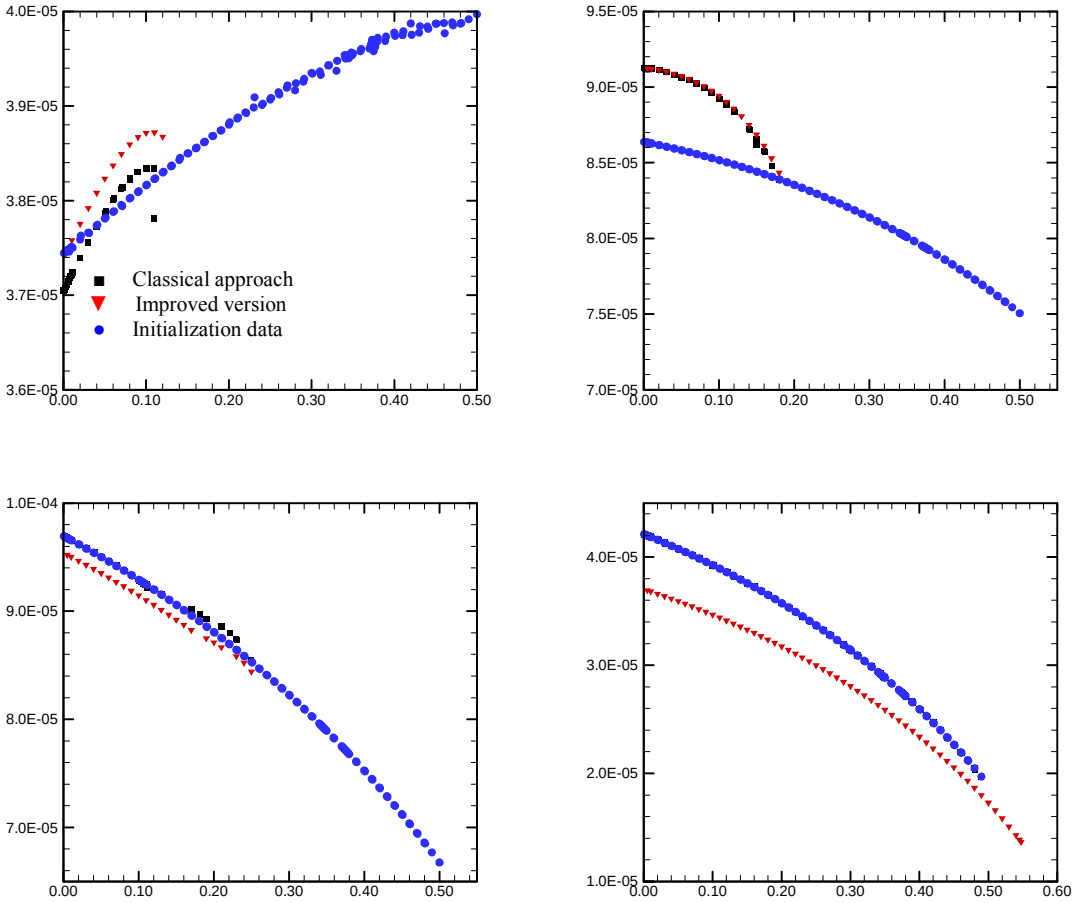


Figure 4.6 Mass fraction variation of H_2O_2 with respect to CO_2 obtained for four different cross-sections.

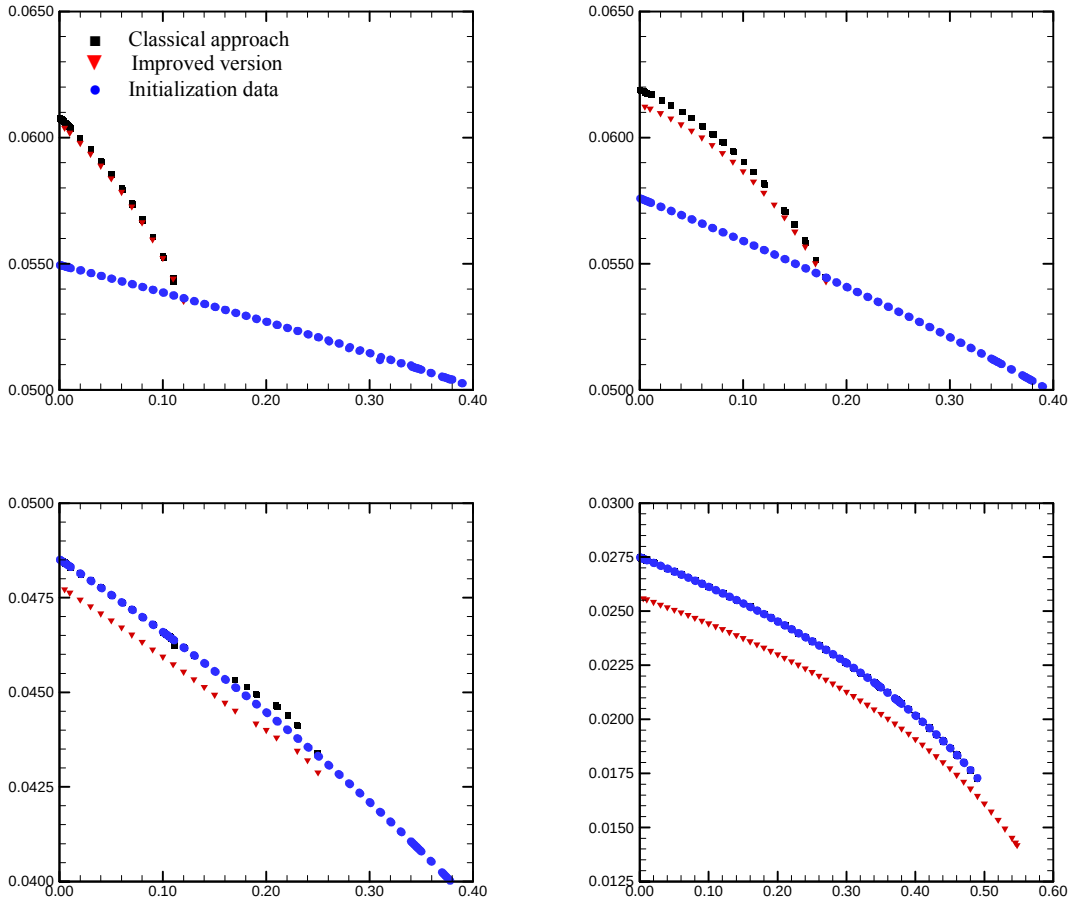


Figure 4.7 Mass fraction variation of OH with respect to CO_2 obtained for four different cross-sections.

5. CONCLUSIONS

The chemical and physical aspects of 3-D turbulent combustion processes have been investigated with special emphasis on the development of reduced models for simplification of the chemical kinetics by intrinsic low-dimensional manifolds method. In this respect in order to understand the main difficulties imposed by the chemical kinetics, the governing equations of reactive flows are studied and ILDM is compared with different simplification procedures, like steady state and partial equilibrium assumptions, based on simple examples. The use of ILDM with probability density functions and the limitations of the code were also defined in the second and third sections of the thesis.

One of the main problem related with the ILDM methodology is the construction of result tables for high hydrocarbon fuels. It is well known that the combustion of hydrocarbon fuels generally share the same basis, in that a detailed mechanism developed for dodecane or heptane includes the C_1-C_4 reactions with the additional reactions specific to the fuel composition. Within the concept of the thesis, without loss of the accuracy, ILDM code is modified in a way that it allows the construction of in situ tables, including mass fractions of species and the reaction rates of the reaction progress variables, for the high hydrocarbon fuels by exploiting the hierarchical structure of the combustion processes. The capabilities and the efficiency of the modified version of ILDM was investigated with a set of simulations based on the construction of result tables for synthesis gas/oxygen and methane/oxygen non premixed combustion systems with isobaric and adiabatic conditions. The results showed that even tough successive ILDM points can be calculated for a synthesis gas/oxygen system in an area defined in the range of 0.0 – 0.5 for mass fraction values of the reaction progress variables, the accessible area confines to a rather smaller region by the hierarchical calculation, which well coincides with the table obtained by classical approach of ILDM. Also, the variations in the phase space represent very similar patterns, even for the distribution of

the intermediate species, both in the classical approach and modified versions. The distribution obtained by modified version exhibits a smooth surface in that it does not include any bad point within the solution domain.

In order to get further insight for the effect of the initial distribution on the calculations, and the error between both methodologies, results are investigated in the same cross sectional areas obtained from the surface plots, and it is observed that the local error does not exceed a maximum value of % 4 for the mass fraction of H_2O being 0.1, 0.2 and 0.3. However for 0.4, the local error reaches to values as high as %10 for some intermediate species like H_2O_2 or OH. One of the reasons that cause such an error is directly related with the order of magnitude for mass fraction values of the species. H_2O_2 and OH mass fractions exhibit a peak value at 10^{-2} and 10^{-5} respectively, which is indeed very small compared with the mass fractions of RPVs or main species like CO. While an error as small as 10^{-2} will not cause any significant effect on those species, it nearly doubles the mass fraction of species like H_2O_2 and OH, resulting an error of %100. In this concept, an error of % 10 can be considered as still within the limitations of the error criteria. On the other hand, it was interesting to see that even in such regions where relatively large errors are encountered, the results obtained by the modified version were capable of representing the same distribution with the one obtained by classical approach.

It is possible to state that the modified version of ILDM code can generate result tables effectively with its accuracy close to that of acquired by the classical approach. This would help to overcome the large time requirements of ILDM to generate tables for high hydrocarbon fuels in two ways. First, since an initialization table is used for calculation, the code is aware of the chemical aspects of the combustion process, and do not spend its time to calculate ILDM points on the regions where there exists no result. The other advantage is, since all the points read by the code as initial guesses have already relaxed on to the manifold, it is much simpler to calculate new points associated with the new mechanism. As a result, more smooth, in other words filtered, result tables can be obtained, including mass fractions of the species related with the high hydrocarbon fuels.

REFERENCES

Bedford, F.C., 2001. Modelling Production and Abatement of Nitrogen Oxide Pollutants in Direct Injection Diesel Engines, *Dissertation,* University of Wisconsin-Madison

Blasenbrey, T., 2000. Entwicklung und Implementierung Automatisch Reduzierter Reaktionsmechanismen für die Verbrennung von Kohlenwasserstoffen, *Dissertation,* Institute für Technische Verbrennung der Universitat Stuttgart.

Blasenbrey, Maas, U., 2000. ILDMs of Higher Hydrocarbons and the Hierarchy of the Chemical Kinetics, Proceedings of the Combustion Institute,**28**:1623-1630

Blasenbrey, T., Schmidt, D., Maas, U., 1998. Automatically Simplified Chemical Kinetics and Molecular Transport and its Applications in Premixed and Non-Premixed Laminar Flame Calculations, Twenty-Seventh Symposium (International) on Combustion/The Combustion Institute 505-511

Blasenbrey, T., Schmidt, D., Maas, U., 1999. An Improved Tabulation Strategy for Reduced Chemical Kinetics Based on Intrinsic Low-Dimensional Manifold, Proceedings of the 17th ICDERS, Heidelberg.

Bongers, H., van Oijen, J.A., de Goey, L.P.H., 2002. Intrinsic Low-Dimensional Manifolds Method Extended with Diffusion, Twenty Ninth International Symposium on Combustion, Sapporo Japan

Chen, C-J, Jaw, S-Y, 1998. Fundamentals of Turbulent Modeling. Taylor&Francis, Washington D.C.

Chen, J.-Y., 2002, Challenges in Modelling and Simulation of Turbulent Combustion, Proceedings of the First International Workshop on Trends in Numerical and Physical Modelling for Turbulent Processes in Gas Turbine Combustors.

Chevalier, C., Pitz, W.J., Warnatz, J., westbrook, C.K., Melenk, H., 1992. Hydrocarbon Ignition: Automatic Generation of Reaction Mechanisms and Applications to Modelling of Engine Knock, Proceedings of the twenty-Fourth Symposium (International) on Combustion/The Combustion Institute 93-101

Correa, C., 2000. Combustion Simulations in Diesel Engines using Reduced Reaction Mechanisms, *Dissertation,* Interdisziplinares zentrum für Wissenschaftliches Rechnen Ruprecht-Karls-Universitat Heidelberg

Eggels, R.L.G.M., 1996. Modelling of Combustion Processes and NO Formation with Reduced reaction Mechanisms, *Dissertation,* Teschnische Universiteit Eindhoven

Goldin, G.M., Menon, S., 1998. A Comparison of Scalar PDF Turbulent Combustion Models, Combustion and Flame, **113**:442-452

Golub, G.H., van Loan, C.F., 1989. Matrix Computations. The Hopkins University Pres, Columbia, MD.

Hewson, J. C., 1997. Pollutant Emmissions From Nonpremixed Hydrocarbon Flames, *Dissertation,* University of California San Diego.

Maas, U., 1997. Efficient Calculation of Intrinsic Low-Dimensional Manifolds for the Simplification of Chemical Kinetics. Konrad-Zuse-Zentrum für Informationstechnik Berlin, Preprint SC 97-20

Maas, U., 2002. Intrinsic Low-Dimensional Manifolds – Recent Progress and Remaining Challenges, Computational Methods for Multidimensional Reactive Flows, COMREF 2002, Invited Speaker.

Maas, U., Schmidt, D., 1998. Analysis of the Intrinsic Low-Dimensional Manifolds of Strained and Unstrained Flames, Combustion Theory and Modelling, 2:135-152

Maas, U., Pope, S. B., 1992. Simplifying Chemical Kinetics: Intrinsic Low-Dimensional Manifolds in Composition Space, Combustion and Flame **88**:239-264

Maas, U., Pope, S. B., 1992. Implementation of Simplified Chemical Kinetics Based on Intrinsic Low-Dimensional Manifolds, Twenty-Fourth Symposium (International) on Combustion/The Combustion Institute pp. 103-112

Maas, U., Pope, S. B., 1994. Laminar Flame Calculations Using Simplified Chemical Kinetics Based on Intrinsic Low-Dimensional Manifolds Proceedings of the Combustion Institute, **25**:1349-1356

Niemann, H., 2002. Nierdigdimensionale Modellierung Dynamiscer Systeme am Beispiel Reduzierter Reaktionsmechanismen, *Dissertation*, Interdisziplinares zentrum für Wissenschaftliches Rechnen Ruprecht-Karls-Universitat Heidelberg

Okino, S. M., Mavrovouniotis, M. L., 2001. Simplification of Mathematical Models of Chemical Reaction Systems, Chemical Reviews, **98**, Number 2

Peters, N., 2000. Turbulent Combustion. Cambridge University Press., Cambridge.

Pope, S.B., 2000. Turbulent Flows. Cambridge Univeristy Press., Cambridge.

Percival, I, Richards, D., 1989. Introduction to Dynamics. Cambridge University Press, Cambridge.

Rawat, R., 1997. Modeling of Finite-Rate Chemistry in Turbulent Reacting Flows, *Dissertation,* The University of Utah

Schmidt, D., 1996. Modellierung Reaktiver Strömungen Unter Verwendung Automatisch Reduzierter Reaktionsmechanismen, *Dissertation*, Interdisziplinares zentrum für Wissenschaftliches Rechnen Ruprecht-Karls-Universitat Heidelberg

Schmidt, D., Segate, J., Riedel, U., Warnatz, J., 1996. Simulation of Laminar Methane-Air Flames Using Automatically Simplified Chemical Kinetics, Combustion Science Technology, **113-114**, 3-16

Stull, D.R., Prophet, H., 1971. JANAF Thermochemical Tables, U.S. Department of Commerce/National Bureau of Standards, NSRDS- NBS37

Şen, B.A., Özdemir, İ.B., Warnatz, J. 2003. Implementation of the Hierarchical Structure of High Hydrocarbon Fuels into Intrinsic Low-Dimensional Manifolds Method, International Symposium on Turbulence Heat and Mass Transfer, THMT - 03

Taut, C., Correa, C., Deutschmann, O., Warnatz, J., Einecke, S., Schulz, C., Wolfrum, J., 2000. 3D- Modelling with Monte-Carlo –PDF Methods and Laser Diagnostic of the Combustion in a Two-Stroke Engine, Twenty-Eighth Symposium (International) on Combustion/The Combustion Institute, **28,** 1153-1159

Tennekes H., Lumley, J.L., 1973. A first course in turbulence. MIT press, Massachusetts.

Versteeg, H.K., Malalasekera, W., 1996. An introduction to computational fluid dynamics The finite volume method. Longman, Malaysia.

Veynate, D., Vervisch, L., 2002. Turbulent Combustion Modelling, Progress in Energy and Combustion Science **28**, 193-266

Warnatz, J., 1992. Resulotion of Gas Phase and Surface Combustion Chemistry into Elementary Reactions, Twenty-Fourth Symposium (International) on Combustion/The Combustion Institute 553-579

Warnatz, J., 2002. Generation and Reduction of Reaction Mechanisms Relevant to Combustion in Turbines, Proceedings of the First International Workshop on Trends in Numerical and Physical Modelling for Turbulent Processes in Gas Turbine Combustors.

Warnatz, J., Maas, U., Dibble, R.W., 2001. COMBUSTION: Physical and Chemical Fundamentals, Modeling and Simulation, Experiments, Pollutant Formation 3rd edition. Springer-Verlag, Heidelberg.

Xiao, K., Schmidt, D., Maas, U., 2002. Implementation of Reduced Kinetic Models in Turbulent Flame Calculations, First International Workshop on Trends in Numerical and Physical Modelling for Turbulent Processes in Gas Turbine Combustors.

APPENDIX I

SPECIES:

1. H	6. O	11. CH_2O
2. H_2	7. HO_2	12. CHO
3. O_2	8. H_2O_2	13. N_2
4. OH	9. CO_2	14. M
5. H_2O	10. CO	

ELEMENTARY REACTIONS:	B_f	n_f	E_a
O_2 +H ↔O +OH	8.70E +07	0.00E +00	6.03E +04
O +H_2 ↔OH +H	5.06E -02	2.67E +00	2.63E +04
OH Reactions:			
OH +H_2 ↔H_2O +H	1.00E +02	1.60E +00	1.38E +04
OH +OH ↔O +H_2O	1.50E +03	1.14E +00	4.20E +02
M Reactions:			
M +H +H ↔M +H_2	1.80E +06	-1.00E +00	0.00E +00
M +O +O ↔M +O_2	2.90E +05	-1.00E +00	0.00E +00
M +OH +H ↔M +H2O	2.20E +10	-2.00E +00	0.00E +00
M +O_2 +H ↔M +HO2	2.30E +06	-8.00E -01	0.00E +00
HO_2 Reactions:			
HO_2 +H ↔OH +OH	1.50E +08	0.00E +00	4.20E +03
HO_2 +H ↔O_2 +H_2	2.50E +07	0.00E +00	2.90E +03
HO_2 +H ↔O +H_2O	3.00E +07	0.00E +00	7.20E +03
HO_2 +O ↔OH +O_2	1.80E +07	0.00E +00	-1.70E +03
HO_2 +OH ↔H2O+O_2	6.00E +07	0.00E +00	0.00E +00

HO_2	$+HO_2$	$\leftrightarrow H_2O_2+O_2$	2.50E +05	0.00E +00	-5.20E +03

H_2O_2 Reactions:

M	+OH	+OH $\leftrightarrow M+H_2O_2$	3.25E +10	-2.00E +00	0.00E +00
H_2O_2	+H	$\leftrightarrow HO_2+H_2$	1.70E +06	0.00E +00	1.57E +04
H_2O_2	+H	$\leftrightarrow H_2O+OH$	1.00E +07	0.00E +00	1.50E +04
H_2O_2	+O	$\leftrightarrow HO_2+OH$	2.80E +07	0.00E +00	2.68E +04
H_2O_2	+OH	$\leftrightarrow HO_2+H_2O$	5.40E +06	0.00E +00	4.20E +03

CO Reactions:

CO	+OH	$\leftrightarrow CO_2+H$	4.76E +01	1.23E +00	2.90E +02
CO	$+HO_2$	$\leftrightarrow CO_2+OH$	1.50E +08	0.00E +00	9.87E +04
M	+CO	+O $\leftrightarrow M+CO_2$	7.10E +01	0.00E +00	-1.90E +04
CO	$+O_2$	$\leftrightarrow CO_2+O$	2.50E +06	0.00E +00	2.00E +05

CHO Reactions:

M	+CHO	$\leftrightarrow$M +CO +H	7.10E +08	0.00E +00	7.03E +04
CHO	+H	$\leftrightarrow$CO $+H_2$	9.00E +07	0.00E +00	0.00E +00
CHO	+O	$\leftrightarrow$CO +OH	3.00E +07	0.00E +00	0.00E +00
CHO	+O	$\leftrightarrow CO_2+H$	3.00E +07	0.00E +00	0.00E +00
CHO	+OH	$\leftrightarrow$CO $+H_2O$	1.00E +08	0.00E +00	0.00E +00
CHO	$+O_2$	$\leftrightarrow$CO $+HO_2$	3.00E +06	0.00E +00	0.00E +00
CHO	+CHO	$\leftrightarrow CH_2O+CO$	3.00E +07	0.00E +00	0.00E +00

CH_2O Reactions:

M	$+CH_2O$	$\leftrightarrow$M +CHO +H	5.00E +10	0.00E +00	3.20E +05
CH_2O	+H	$\leftrightarrow CHO+H_2$	2.30E +04	1.05E +00	1.37E +04
CH_2O	+O	$\leftrightarrow$CHO+OH	4.15E +05	5.70E -01	1.16E +04
CH_2O	+OH	$\leftrightarrow$ $CHO+H_2O$	3.40E +03	1.20E +00	-1.90E +03
CH_2O	$+HO_2$	$\leftrightarrow CHO+H_2O_2$	3.00E +06	0.00E +00	5.47E +04
CH_2O	$+O_2$	$\leftrightarrow CHO+HO_2$	6.00E +07	0.00E +00	1.7070E+05

APPENDIX II

SPECIES:

1. H	12. CH_3	23. C_2H_6	34. C_3H_2
2. H_2	13. $3CH_2$	24. C_2H_6	35. C_3H_3
3. O_2	14. $1CH_2$	25. C_2H_6	36. C_3H_4
4. OH	15. CH	26. C_2H_6	37. C_3H_5
5. H_2O	16. CH_3OH	27. C_2H_6	38. C_3H_6
6. O	17. CH_3O	28. C_2H_6	39. $N\text{-}C_3H_7$
7. HO_2	18. CH_2OH	29. HCCO	40. $N\text{-}C_4H_9$
8. H_2O_2	19. CH_2O	30. CH_2CO	41. C_6H_6
9. CO_2	20. CHO	31. CH_2CHO	42. $N\text{-}C_7H_{16}$
10. CO	21. CH_3O_2H	32. CH_3CHO	43. N_2
11. CH_4	22. CH_3O_2	33. CH_3CO	44. M

ELEMENTARY REACTIONS:

					B_f	n_f	E_a
O_2	+H	↔O	+OH		8.70E +07	0.00E +00	6.03E +04
O	+H_2	↔OH	+H		5.06E -02	2.67E +00	2.63E +04
OH Reactions:							
OH	+H_2	↔H_2O	+H		1.00E +02	1.60E +00	1.38E +04
OH	+OH	↔O	+H_2O		1.50E +03	1.14E +00	4.20E +02
M Reactions:							
M	+H	+H	↔M	+H_2	1.80E +06	-1.00E +00	0.00E +00
M	+O	+O	↔M	+O_2	2.90E +05	-1.00E +00	0.00E +00
M	+OH	+H	↔M	+H2O	2.20E +10	-2.00E +00	0.00E +00
M	+O_2	+H	↔M	+HO2	2.30E +06	-8.00E -01	0.00E +00
HO_2 Reactions:							
HO_2	+H	↔OH	+OH		1.50E +08	0.00E +00	4.20E +03
HO_2	+H	↔O_2	+H_2		2.50E +07	0.00E +00	2.90E +03
HO_2	+H	↔O	+H_2O		3.00E +07	0.00E +00	7.20E +03
HO_2	+O	↔OH	+O_2		1.80E +07	0.00E +00	-1.70E +03
HO_2	+OH	↔H2O	+O_2		6.00E +07	0.00E +00	0.00E +00
HO_2	+HO_2	↔H_2O_2	+O_2		2.50E +05	0.00E +00	-5.20E +03
H_2O_2 Reactions:							
M	+OH	+OH	↔M+H_2O_2		3.25E +10	-2.00E +00	0.00E +00
H_2O_2	+H	↔HO_2	+H_2		1.70E +06	0.00E +00	1.57E +04
H_2O_2	+H	↔H_2O	+OH		1.00E +07	0.00E +00	1.50E +04
H_2O_2	+O	↔HO_2	+OH		2.8030E+07	0.00E +00	2.68E +04
H_2O_2	+OH	↔HO_2	+H_2O		5.40E +06	0.00E +00	4.20E +03
CO Reactions:							
CO	+OH	↔CO_2	+H		4.76E +01	1.23E +00	2.90E +02
CO	+HO_2	↔CO_2	+OH		1.50E +08	0.00E +00	9.87E +04
M	+CO	+O	↔M+CO_2		7.10E +01	0.00E +00	-1.90E +04
CO	+O_2	↔CO_2	+O		2.50E +06	0.00E +00	2.00E +05
CH Reactions:							
CH	+O	↔CO	+H		4.00E +07	0.00E +00	0.00E +00
CH	+O_2	↔CHO	+O		3.00E +07	0.00E +00	0.00E +00
CH	+CO_2	↔CHO	+CO		3.40E +06	0.00E +00	2.90E +03
CH	+OH	↔CHO	+H		3.00E +07	0.00E +00	0.00E +00
CHO Reactions:							
M	+CHO	↔M	+CO	+H	7.10E +08	0.00E +00	7.03E +04
CHO	+H	↔CO	+H_2		9.00E +07	0.00E +00	0.00E +00
CHO	+O	↔CO	+OH		3.00E +07	0.00E +00	0.00E +00
CHO	+O	↔CO_2	+H		3.00E +07	0.00E +00	0.00E +00
CHO	+OH	↔CO	+H_2O		1.00E +08	0.00E +00	0.00E +00

$CHO + O_2 \leftrightarrow CO + HO_2$	3.00E +06	0.00E +00	0.00E +00
$CHO + CHO \leftrightarrow CH_2O + CO$	3.00E +07	0.00E +00	0.00E +00

3CH2 Reactions:

$3CH_2 + H \leftrightarrow CH + H_2$	6.00E +06	0.00E +00	-7.50E +03
$3CH_2 + O \rightarrow CO + H + H$	8.40E +06	0.00E +00	3.6178E+03
$3CH_2 + 3CH_2 \leftrightarrow C_2H_2 + H_2$	1.20E +07	0.00E +00	3.40E +03
$3CH_2 + 3CH_2 \leftrightarrow C_2H_2 + H + H$	1.10E +08	0.00E +00	3.40E +03
$3CH_2 + CH_3 \leftrightarrow C_2H_4 + H$	4.20E +07	0.00E +00	0.00E +00
$3CH_2 + O_2 \leftrightarrow CO + OH + H$	1.30E +07	0.00E +00	6.20E +03
$3CH_2 + O_2 \leftrightarrow CO_2 + H_2$	1.20E +07	0.00E +00	6.20E +03

1CH2 Reactions:

$M + 1CH_2 \leftrightarrow M + 3CH_2$	1.20E +07	0.00E +00	0.00E +00
$1CH_2 + O_2 \leftrightarrow CO + OH + H$	3.10E +07	0.00E +00	0.00E +00
$1CH_2 + H_2 \leftrightarrow CH_3 + H$	7.20E +07	0.00E +00	0.00E +00

CH_2O Reactions:

$M + CH_2O \leftrightarrow M + CHO + H$	5.00E +10	0.00E +00	3.20E +05
$CH_2O + H \leftrightarrow CHO + H_2$	2.30E +04	1.05E +00	1.37E +04
$CH_2O + O \leftrightarrow CHO + OH$	4.15E +05	5.70E -01	1.16E +04
$CH_2O + OH \leftrightarrow CHO + H_2O$	3.40E +03	1.20E +00	-1.90E +03
$CH_2O + HO_2 \leftrightarrow CHO + H_2O_2$	3.00E +06	0.00E +00	5.47E +04
$CH_2O + CH_3 \leftrightarrow CHO + CH_4$	1.00E +05	0.00E +00	2.55E +04
$CH_2O + {}_{O2} \leftrightarrow CHO + HO_2$	6.00E +07	0.00E +00	1.7070E+05

CH_3 Reactions:

$M + CH_3 \leftrightarrow M + 3CH_2 + H$	1.00E +10	0.00E +00	3.79E +05
$CH_3 + O \leftrightarrow CH_2O + H$	8.43E +07	0.00E +00	0.00E +00
$CH_3 + H \leftrightarrow CH_4$	1.93E +30	-7.00E +00	3.80E +04
$CH_3 + OH \leftrightarrow CH_3O + H$	2.26E +08	0.00E +00	6.48E +04
$CH_3 + O_2 \rightarrow CH_2O + OH$	3.30E +05	0.00E +00	3.74E +04
$CH_3 + HO_2 \leftrightarrow CH_3O + OH$	1.80E +07	0.00E +00	0.00E +00
$CH_3 + HO_2 \leftrightarrow CH_4 + O_2$	3.60E +06	0.00E +00	0.00E +00
$CH_3 + CH_3 \rightarrow C_2H_4 + H_2$	1.00E +10	0.00E +00	1.34E +05
$CH_3 + CH_3 \leftrightarrow C_2H_6$	1.69E +47	-1.20E +01	8.12E +04

CH_3O Reactions:

$M + CH_3O \leftrightarrow M + CH_2O + H$	5.00E +07	0.00E +00	1.05E +05
$CH_3O + H \leftrightarrow CH_2O + H_2$	1.80E +07	0.00E +00	0.00E +00
$CH_3O + O2 \leftrightarrow CH_2O + HO_2$	4.00E +04	0.00E +00	8.90E +03
$CH_2O + CH_3O \leftrightarrow CHO + CH_3OH$	6.00E +05	0.00E +00	1.38E +04
$CH_3O + O \leftrightarrow CH_3 + O_2$	1.10E +07	0.00E +00	0.00E +00
$CH_3O + O \leftrightarrow CH_2O + OH$	1.40E +06	0.00E +00	0.00E +00

CH_2OH Reactions:

$M + CH_2OH \leftrightarrow M + CH_2O + H$	5.00E +07	0.00E +00	1.05E +05
$CH_2OH + H \leftrightarrow CH_2O + H_2$	3.00E +07	0.00E +00	0.00E +00
$CH_2OH + O_2 \leftrightarrow CH_2O + HO_2$	1.00E +07	0.00E +00	3.00E +04

CH3O2 Reactions:

$M + CH_3O_2 \leftrightarrow M + CH_3 + O_2$	7.24E +10	0.00E +00	1.1110E+05
$CH_3O_2 + CH_2O \leftrightarrow CH_3O_2H + CHO$	1.30E +05	0.00E +00	3.77E +04
$CH_3O_2 + CH_3 \leftrightarrow CH_3O + CH_3O$	3.80E +06	0.00E +00	-5.00E +03
$CH_3O_2 + HO_2 \leftrightarrow CH_3O_2H + O_2$	4.60E +04	0.00E +00	-1.09E +04
$CH_3O_2 + CH_3O_2 \leftrightarrow {}_{CH2O} + CH_3OH + O_2$	1.80E +06	0.00E +00	0.00E +00
$CH_3O_2 + CH_3O_2 \leftrightarrow CH_3O + CH_3O + O_2$	3.70E +06	0.00E +00	9.20E +03

CH_4 Reactions:

$CH_4 + H \leftrightarrow CH_3 + H_2$	1.30E -02	3.00E +00	3.36E +04
$CH_4 + O \leftrightarrow CH_3 + OH$	6.9230E+02	1.56E +00	3.55E +04
$CH_4 + OH \leftrightarrow CH_3 + H_2O$	1.60E +01	1.83E +00	1.16E +04
$CH_4 + HO_2 \leftrightarrow CH_3 + H_2O_2$	1.10E +07	0.00E +00	1.031E+05
$CH + CH_4 \leftrightarrow C_2H_4 + H$	3.00E +07	0.00E +00	-1.70E +03
$3CH_2 + CH_4 \leftrightarrow CH_3 + CH_3$	1.30E +07	0.00E +00	3.99E +04

CH_3OH Reactions:

$CH_3OH \leftrightarrow CH_3 + OH$	9.51E +29	-4.30E +00	4.04E +05
$CH_3OH + H \leftrightarrow CH_2OH + H_2$	4.00E +07	0.00E +00	2.55E +04
$CH_3OH + O \leftrightarrow CH_2OH + OH$	1.00E +07	0.00E +00	1.96E +04
$CH_3OH + OH \leftrightarrow CH_2OH + H_2O$	1.00E +07	0.00E +00	7.10E +03
$CH_3OH + HO_2 \leftrightarrow CH_2OH + H_2O_2$	6.20E +06	0.00E +00	8.11E +04
$CH_3OH + CH_3 \leftrightarrow CH_2OH + CH_4$	9.00E +06	0.00E +00	4.11E +04
$CH_3O + CH_3OH \leftrightarrow CH_2OH + CH_3OH$	2.00E +05	0.00E +00	2.93E +04
$CH_2O + CH_3OH \leftrightarrow CH_3O + CH_3O$	1.53E +06	0.00E +00	3.33E +05

CH_3O_2H Reactions:

$CH_3O_2H \leftrightarrow CH_3O + OH$	4.00E +15	0.00E +00	1.80E +05
$CH_3O_2H + OH \leftrightarrow CH_3O_2 + H_2O$	2.60E +06	0.00E +00	0.00E +00

C_2H Reactions:

$C_2H + O \leftrightarrow CH + CO$	1.00E +07	0.00E +00	0.00E +00
$C_2H + O_2 \leftrightarrow HCCO + O$	3.00E +06	0.00E +00	0.00E +00

HCCO Reactions:

$HCCO + H \leftrightarrow 3CH_2 + CO$	1.50E +08	0.00E +00	0.00E +00
$HCCO + O \rightarrow CO + CO + H$	9.60E +07	0.00E +00	0.00E +00
$HCCO + 3CH_2 \leftrightarrow C_2H_3 + CO$	3.00E +07	0.00E +00	0.00E +00

C_2H_2 Reactions:

$M + C_2H_2 \leftrightarrow M + C_2H + H$	3.60E +10	0.00E +00	4.46E +05
$C_2H_2 + O_2 \leftrightarrow HCCO + OH$	2.00E +02	1.50E +00	1.26E +05
$C_2H_2 + H \leftrightarrow C_2H + H_2$	6.0230E+07	0.00E +00	1.16E +05
$C_2H_2 + O \leftrightarrow 3CH_2 + CO$	2.1680E+00	2.10E +00	6.57E +03
$C_2H_2 + O \leftrightarrow HCCO + H$	5.0590E+00	2.10E +00	6.57E +03
$C_2H_2 + OH \leftrightarrow C_2H + H_2O$	6.0000E+07	0.00E +00	5.42E +04

CH_2CO Reactions:

$M + CH_2CO \leftrightarrow M + 3CH_2 + CO$	1.00E +10	0.00E +00	2.48E +05
$CH_2CO + H \leftrightarrow CH_3 + CO$	3.60E +07	0.00E +00	1.41E +04
$CH_2CO + O \leftrightarrow CHO + CHO$	2.30E +06	0.00E +00	5.70E +03

CH_2CO+OH $\leftrightarrow CHO+CH_2O$	1.00E +07	0.00E +00	0.00E +00
C_2H_3 Reactions:			
C_2H_3 $\leftrightarrow C_2H_2+H$	4.73E +40	-8.80E +00	1.9450E+05
C_2H_3 $+OH$ $\leftrightarrow C_2H_2+H_2O$	5.00E +07	0.00E +00	0.00E +00
C_2H_3 $+H$ $\leftrightarrow C_2H_2+H2$	1.20E +07	0.00E +00	0.00E +00
C_2H_3 $+O$ $\leftrightarrow C_2H_2+OH$	1.00E +07	0.00E +00	0.00E +00
C_2H_3 $+O$ $\leftrightarrow CH_3+CO$	1.00E +07	0.00E +00	0.00E +00
C_2H_3 $+O$ $\leftrightarrow CHO+3CH_2$	1.00E +07	0.00E +00	0.00E +00
CH_3CO Reactions:			
CH_3CO $\leftrightarrow CH_3+CO$	2.32E +26	-5.00E +00	7.5120E+04
CH_3CO+H $\leftrightarrow CH_2CO+H_2$	2.00E +07	0.00E +00	0.00E +00
CH_2CHO+H $\leftrightarrow CH_2CO+H_2$	2.00E +07	0.00E +00	0.00E +00
M Reactions:			
M $+C_2H_4 \leftrightarrow M+C_2H_2+H_2$	7.50E +11	0.00E +00	3.32E +05
M $+C_2H_4 \leftrightarrow M+C_2H_3+H$	8.50E +11	0.00E +00	4.04E +05
C_2H_4 Reactions:			
$C2H4$ $+H$ $\leftrightarrow C_2H_3+H_2$	5.40E +08	0.00E +00	6.29E +04
C_2H_4 $+O$ $\leftrightarrow CH_2CHO+H$	1.02E +00	2.08E +00	0.00E +00
C_2H_4 $+O$ $\leftrightarrow CHO+CH_3$	2.42E +00	2.08E +00	0.00E +00
C_2H_4 $+OH$ $\leftrightarrow C_2H_3+H_2O$	2.20E +07	0.00E +00	2.49E +04
CH_3CHO Reactions:			
$M+CH_3CHO$ $\leftrightarrow M+CHO+CH_3$	7.00E +09	0.00E +00	3.42E +05
CH_3CHO+H $\leftrightarrow CH_3CO+H_2$	2.10E +03	1.16E +00	1.01E +04
CH_3CHO+H $\leftrightarrow CH_2CHO+H_2$	2.00E +03	1.16E +00	1.01E +04
CH_3CHO+O $\leftrightarrow CH_3CO+OH$	5.00E +06	0.00E +00	7.60E +03
CH_3CHO+O $\leftrightarrow CH_2CHO+OH$	8.00E +05	0.00E +00	7.60E +03
CH_3CHO+O_2 $\leftrightarrow CH_3CO+HO_2$	4.00E +07	0.00E +00	1.64E +05
$CH_3CHO+OH \leftrightarrow CH_3CO+H_2O$	2.30E +04	7.30E -01	-4.70E +03
$CH_3CHO+HO_2 \leftrightarrow CH_3CO+H_2O_2$	3.00E +06	0.00E +00	5.00E +04
$CH_3CHO+3CH_2 \leftrightarrow CH_3CO+CH_3$	2.50E +06	0.00E +00	1.59E +04
$CH_3CHO+CH_3 \leftrightarrow CH_3CO+CH_4$	2.00E -12	5.64E +00	1.03E +04
C_2H_5 Reactions:			
C_2H_5 $\leftrightarrow C_2H_4+H$	1.02E +43	-9.10E +00	2.25E +05
C_2H_5 $+H$ $\leftrightarrow CH_3+CH_3$	3.00E +07	0.00E +00	0.00E +00
C_2H_5 $+O$ $\leftrightarrow CH_3CHO+H$	5.00E +07	0.00E +00	0.00E +00
C_2H_5 $+O$ $\leftrightarrow CH_2O+CH_3$	1.00E +07	0.00E +00	0.00E +00
C_2H_5 $+O_2$ $\leftrightarrow C_2H_4+HO_2$	1.10E +04	0.00E +00	-6.30E +03
C_2H_5 $+CH_3$ $\leftrightarrow C_2H_4+CH_4$	1.14E +06	0.00E +00	0.00E +00
C_2H_5 $+C_2H_5 \leftrightarrow C_2H_4 + C_2H_6$	1.40E +06	0.00E +00	0.00E +00
C_2H_6 Reactions:			
C_2H_6 $+H$ $\leftrightarrow C_2H_5+H_2$	1.40E +03	1.50E +00	3.11E +04
C_2H_6 $+O$ $\leftrightarrow C_2H_5+OH$	1.00E +03	1.50E +00	2.44E +04
C_2H_6 $+OH$ $\leftrightarrow C_2H_5+H_2O$	7.20E +00	2.00E +00	3.60E +03

C_2H_6 +HO_2 ↔C_2H_5 +H_2O_2	1.70E +07	0.00E +00	8.59E +04
C_2H_6 +O_2 ↔C_2H_5 + HO_2	6.00E +07	0.00E +00	2.17E +05
C2H6 +3CH_2↔C_2H_5 + CH_3	2.20E +07	0.00E +00	3.63E +04
C2H6 +CH_3 ↔C_2H_5 +CH_4	1.50E -13	6.00E +00	2.54E +04
M +CH_3 ↔M +CH +H_2	6.90E +08	0.00E +00	3.45E +05
1CH_2 +CH_3 ↔C_2H_4 +H	1.60E +07	0.00E +00	-2.38E +03

CH Reactions:

CH +H_2O ↔CH_2O +H	4.56E +06	0.00E +00	-3.20E +03
CH +H_2O ↔3CH_2 +OH	1.14E +06	0.00E +00	-3.20E +03
CH_3 +OH ↔1CH_2+H_2O	2.30E +07	0.00E +00	0.00E +00

C_2H_3 Reactions:

C_2H_3 +O_2 ↔CHO +CH_2O	5.42E +06	0.00E +00	0.00E +00
C_2H_3 +O_2 ↔CHO +CH_2O	-2.46E +09	-7.80E -01	1.31E +04
C_2H_3 +O_2 ↔CH_2CHO +O	2.46E +09	-7.80E -01	1.31E +04
C_2H_2 +CH ↔C_3H_2+H	1.00E +08	0.00E +00	0.00E +00

C_3H_2 Reactions:

C_3H_2 +O_2 ↔HCCO +CO +H	5.00E +07	0.00E +00	0.00E +00
C_3H_2 +OH ↔C_2H_2 +CHO	5.00E +07	0.00E +00	0.00E +00

C_3H_3 Reactions:

C_3H_3 +O_2 ↔CH_2CO+CHO	3.00E +04	0.00E +00	1.20E +04
C_3H_3 +O ↔C_2H +CH_2O	2.00E +07	0.00E +00	0.00E +00
C_3H_3 +H ↔C_3H_2+H_2	5.00E +07	0.00E +00	1.2560E+04
C_3H_3 +OH ↔C_3H_2+H_2O	2.00E +07	0.00E +00	0.00E +00
C_3H_3 +C_3H_3↔C_6H_6	3.40E +07	0.00E +00	0.00E +00

C_2H_2 Reactions:

C_2H_2 +CH →C_3H_3	2.00E +08	0.00E +00	0.00E +00
HCCO +C_2H_2↔C_3H_3 +CO	1.00E +05	0.00E +00	1.2560E+04
C_2H_2 +3CH_2↔$_{C3H3}$ +H	1.20E +07	0.00E +00	2.7630E+04
C_2H_2 +1CH_2↔C_3H_3+H	1.50E +08	0.00E +00	0.00E +00

C_2H_4 Reactions:

C_2H_4 +O ↔C_2H_2+CH_2O	1.00E +06	0.00E +00	0.00E +00
C_2H_4 +O ↔C_2H_3+CHO	1.00E +06	0.00E +00	0.00E +00
C_2H_4 +OH ↔ C_2H_3+CH_2O	1.00E +06	0.00E +00	0.00E +00
C_2H_4 +OH ↔C_2H_4+CHO	1.00E +06	0.00E +00	0.00E +00

C_3H_4 Reactions:

M +C_3H_4↔M +C_3H_3+H	1.00E +11	0.00E +00	2.93E +05
C_3H_4 +H ↔C_2H_2+CH_3	2.00E +07	0.00E +00	1.00E +04
C_3H_4 +H ↔C_3H_3+H_2	1.00E +06	0.00E +00	6.30E +03
C_3H_4 +C_2H ↔C_3H_3+C_2H_2	1.00E +07	0.00E +00	0.00E +00
C_3H_4 +CH_3 ↔C_3H_3+CH_4	2.00E +06	0.00E +00	3.22E +04

C_3H_5 Reactions:

C_3H_5 ↔C_3H_4+H	3.98E +13	0.00E +00	2.9310E+05

C_3H_5 +H	↔C3H4+H_2	1.00E +07	0.00E +00	0.00E +00
C_3H_5 +O_2	↔C_3H_4+HO_2	6.00E +05	0.00E +00	4.19E +04
C_2H_4 +1CH_2	↔C_3H_5+H	1.30E +08	0.00E +00	0.00E +00

C3H6 Reactions:

C_3H_6	↔C_3H_5+H	1.00E +13	0.00E +00	3.26E +05
C_3H_6	↔C_2H_3+CH_3	3.15E +15	0.00E +00	3.59E +05
C_3H_6 +H	↔C_3H_5+H_2	5.00E +06	0.00E +00	6.30E +03
C_3H_6 +O	↔C_2H_4+CH_2O	5.90E +07	0.00E +00	2.10E +04
C3H_6 +O	↔C_2H_5+CHO	3.60E +06	0.00E +00	0.00E +00
C_3H_6 +O	↔CH_3CO+CH_3	5.00E +06	0.00E +00	2.50E +03
C_3H_6 +OH	↔C_2H_5+CH_2O	7.90E +06	0.00E +00	0.00E +00
C_3H_6 +OH	↔CH_3CHO+CH_3	5.10E +06	0.00E +00	0.00E +00
C_3H_6 +OH	↔C_3H_5+H_2O	4.00E +06	0.00E +00	0.00E +00
C_3H_6 +CH_3	↔C_3H_5+CH_4	8.96E +06	0.00E +00	3.56E +04
C_3H_6 +C_2H_5	↔C_3H_5 +C_2H_6	1.00E +05	0.00E +00	3.85E +04

N-C_3H_7 Reactions:

N-C_3H_7	↔C_2H_4+CH_3	9.60E +13	0.00E +00	1.2980E+05
N-C_3H_7	↔C_3H_6+H	1.25E +14	0.00E +00	1.5490E+05
N-C_3H_7+O_2	↔C_3H_6+HO_2	1.00E +06	0.00E +00	2.09E +04

N-C_7H_{16} Reactions:

N-C_7H_{16}+H	↔N-C_4H_9+C_3H_6+H_2	5.63E +01	2.00E +00	3.22E +04
N-C_7H_{16}+H	↔N-C_4H_9+C_3H_6+H_2	4.50E +01	2.00E +00	2.09E +04
N-C_7H_{16}+O	↔N-C_4H_9+C_3H_6+OH	1.00E +08	0.00E +00	3.29E +04
N-C_7H_{16}+O	↔N-C_4H_9+C_3H_6+OH	1.30E +08	0.00E +00	2.18E +04
N-C_7H_{16}+OH	↔N-C_4H_9+C_3H_6+H_2O	8.58E +03	1.05E +00	7.60E +03
N-C_7H_{16}+OH	↔N-C_4H_9+C_3H_6+H_2O	6.50E +03	1.25E +00	2.90E +03
N-C_4H_9	↔C_2H_4+C_2H_5	9.60E +13	0.00E +00	1.29E +05

APPENDIX III

Mixture fraction is a useful tool to understand the composition of the mixture in any part of the domain, and can be represented as,

$$\zeta = \frac{\dot{m}_1}{\dot{m}_1 + \dot{m}_2} \tag{C.1}$$

In this expression subscript 1 denotes the fuel stream, where as the subscript 2 is for the oxidizer stream. Thus, the mass fractions of fuel and oxidizer in the unburned side can be calculated as follows,

$$Y_{F,u} = Y_{F,1}\zeta \tag{C.2}$$

$$Y_{Ox,u} = Y_{Ox,2}(1-\zeta) \tag{C.3}$$

The mass does not change with the chemical reactions, so the total mass in the unburned side and in the burned side should be equal to each other,

$$\upsilon Y_F - Y_{Ox} = \upsilon Y_{F,u} - Y_{Ox,u} \tag{C.4}$$

where the coefficient υ is given by the expression,

$$\upsilon = \left.\frac{Y_{Ox,u}}{Y_{F,u}}\right|_{st} = \frac{\upsilon'_{Ox} W_{Ox}}{\upsilon'_F W_F} \tag{C.5}$$

Replacing equations (C.1) and (C.2) into equation (C.3) yields,

$$\upsilon Y_F - Y_{Ox} = \upsilon Y_{F,1}\upsilon\zeta - Y_{Ox,1}(1-\zeta) \tag{C.6}$$

and by a fair amount of algebra, one can get the following expression for the mixture fraction,

$$\zeta = \frac{\upsilon Y_F - Y_{OX} + Y_{OX,2}}{\upsilon Y_{F,1} + \upsilon Y_{OX,2}} \tag{C.7}$$

It is known that, for a stoichiometric mixture,

$$\upsilon Y_{F,u} = Y_{Ox,u} \tag{C.8}$$

$$\upsilon Y_F = Y_{OX} \tag{C.9}$$

The mixture fraction can be further simplified, with the assumption of a stoichiometric mixture, in to a form of,

$$\zeta_{st} = \frac{Y_{Ox,2}}{\upsilon Y_{F,1} + Y_{Ox,2}} \tag{C.10}$$

Now let us investigate the termination of the combustion process in the fuel lean and fuel rich conditions,

1) Fuel-lean Condition $\left(\zeta \le \zeta_{st}\right)$

Combustion terminates when all the fuel is consumed within the domain. In the limiting case, $Y_{F,b}=0$

$$\zeta = \frac{-Y_{Ox,b} + Y_{Ox,2}}{\upsilon Y_{F,1} + Y_{Ox,2}} \tag{C.11}$$

$$Y_{Ox,b} = Y_{Ox,2} - \zeta\left(\upsilon Y_{F,1} - Y_{Ox,2}\right) \tag{C.12}$$

$$= Y_{Ox,2}\left[1 - \zeta - \zeta\left(\frac{\upsilon Y_{F,1}}{Y_{Ox,2}}\right)\right] \tag{C.13}$$

$$= Y_{Ox,2}\left[1 - \zeta\left(1 + \frac{\upsilon Y_{F,1}}{Y_{Ox,2}}\right)\right] \tag{C.14}$$

$$Y_{O,b} = Y_{O,2}\left(1-\frac{\zeta}{\zeta_{st}}\right) \text{ for } \left(\zeta \le \zeta_{st}\right) \tag{C.15}$$

2) Fuel-rich Condition $\left(\zeta > \zeta_{st}\right)$

Combustion terminates when all the oxidizer is consumed within the domain. In the limiting case of, $Y_{Ox,b}=0$

$$\zeta = \frac{\upsilon Y_{F,b} + Y_{Ox,2}}{\upsilon Y_{F,1} + Y_{Ox,2}} \tag{C.16}$$

$$Y_{F,b} = \frac{\zeta\left(\upsilon Y_{F,1} + Y_{Ox,2}\right) - Y_{Ox,2}}{\upsilon} \tag{C.17}$$

$$Y_{F,b} = Y_{F,1}\left[\zeta + \frac{\zeta Y_{Ox,2}}{\upsilon Y_{F,1}} - \frac{Y_{Ox,2}}{\upsilon Y_{F,1}}\right] \tag{C.18}$$

$$\frac{1}{\zeta_{st}} = 1 + \frac{\upsilon Y_{F,1}}{Y_{Ox,2}} \tag{C.19}$$

so,

$$\frac{\upsilon Y_{F,1}}{Y_{Ox,2}} = \frac{\zeta_{st}}{1-\zeta_{st}} \tag{C.20}$$

Replacing this expression into the equation (C.18) yields,

$$Y_{F,b} = Y_{F,1}\left[\zeta + \zeta\left(\frac{\zeta_{st}}{1-\zeta_{st}}\right) - \left(\frac{\zeta_{st}}{1-\zeta_{st}}\right)\right] \tag{C.21}$$

and finally we can get,

$$Y_{F,b} = Y_{F,1}\left(\frac{\zeta-\zeta_{st}}{1-\zeta_{st}}\right) \tag{C.22}$$

for the condition $\left(\zeta > \zeta_{st}\right)$

Now let us consider a specific example, for the combustion of methane/air system,

$$CH_4 + 2\ O_2 + 7.52\ N_2 \longrightarrow CO_2 + 2\ H_2O + 7.52\ N_2$$

The element mass fractions in the unburned mixture,

$$Z_C = \frac{W_C}{W_F} Y_{F,u} \tag{C.23}$$

$$Z_H = \frac{4W_H}{W_F} Y_{F,u} \tag{C.24}$$

$$Z_O = \frac{W_O}{W_{Ox}} Y_{Ox,u} \tag{C.25}$$

$$Z_N = \frac{2W_N}{W_{Ox}} Y_{Ox,u} \tag{C.26}$$

Element mass fractions in the burned mixture,

$$Z_C = \frac{W_C}{W_F} Y_{F,b} + \frac{W_C}{W_{CO_2}} Y_{CO_2,b} \tag{C.27}$$

$$Z_H = \frac{4W_H}{W_F} Y_{F,b} + \frac{2W_H}{W_{H_2O}} Y_{H_2O,b} \tag{C.28}$$

$$Z_O = \frac{2W_O}{W_{Ox}} Y_{Ox,b} + \frac{W_O}{W_{H_2O}} Y_{H_2O,b} + \frac{2W_O}{W_{CO_2}} Y_{CO_2,b} \tag{C.29}$$

$$Z_N = \frac{2W_N}{W_{N_2}} Y_{N_2,b} \tag{C.30}$$

1) When $\zeta \le \zeta_{st}$, $Y_{F,b} = 0$

$$\frac{W_C}{W_{CO_2}} Y_{CO_2,b} = \frac{W_C}{W_F} Y_{F,u} \tag{C.31}$$

$$Y_{CO_2,b} = \frac{W_C}{W_F} Y_{F,u} \tag{C.32}$$

$$Y_{CO_2,b} = \frac{W_C}{W_F} Y_{F,1} \zeta \tag{C.33}$$

$$Y_{CO_2,st} = \frac{W_C}{W_F} Y_{F,1} \zeta_{st} \tag{C.34}$$

$$Y_{CO_2,b} = Y_{CO_2,st} \frac{\zeta}{\zeta_{st}} \tag{C.35}$$

Similarly for the mass fraction of the H_2O in the burned part with respect to the mixture fraction can be written as follows,

$$\frac{4W_H}{W_F} Y_{F,u} = \frac{2W_H}{W_{H_2O}} Y_{H_2O,b} \tag{C.36}$$

$$Y_{H_2O,b} = \frac{2W_{H_2O}}{W_F} Y_{F,1} \zeta \tag{C.37}$$

$$Y_{H_2O,st} = \frac{2W_{H_2O}}{W_F} Y_{F,1} \zeta_{st} \tag{C.38}$$

$$Y_{H_2O,b} = Y_{H_2O,st} \frac{\zeta}{\zeta_{st}} \tag{C.39}$$

1) When $\zeta \ge \zeta_{st}$, $Y_{O_z,b} = 0$

$$\frac{W_C}{W_F} Y_{F,b} + \frac{W_C}{W_{CO_2}} Y_{CO_2,b} = \frac{W_C}{W_F} Y_{F,u}$$

Replacing equation (C.22) inplace of $Y_{F,b}$, and (C.2) for $Y_{F,u}$ we can get the expression,

$$\frac{W_C}{W_F}Y_{F,1}\left(\frac{\zeta-\zeta_{st}}{1-\zeta_{st}}\right)+\frac{W_C}{W_{CO_2}}Y_{CO_2,b}=\frac{W_C}{W_F}Y_{F,1}\zeta \tag{C.41}$$

$$Y_{CO_2,b}=\frac{W_{CO_2}}{W_F}Y_{F,1}\zeta-\frac{W_{CO_2}}{W_F}Y_{F,1}\left(\frac{\zeta-\zeta_{st}}{1-\zeta_{st}}\right) \tag{C.42}$$

$$Y_{CO_2,b}=\frac{W_{CO_2}}{W_F}Y_{F,1}\left(\zeta-\left(\frac{\zeta-\zeta_{st}}{1-\zeta_{st}}\right)\right) \tag{C.43}$$

$$Y_{CO_2,st}=\frac{W_{CO_2}}{W_F}Y_{F,1}\zeta_{st} \tag{C.44}$$

$$Y_{CO_2,b}=Y_{CO_2,st}\left(\frac{1-\zeta}{1-\zeta_{st}}\right) \tag{C.45}$$

For H in the burned and unburned size mass fractions should be equal,

$$Z_H=\frac{4W_H}{W_F}Y_{F,b}+\frac{2W_H}{W_{H_2O}}Y_{H_2O,b}=\frac{4W_H}{W_F}Y_{F,u} \tag{C.46}$$

Replace $Y_{F,b}$ $Y_{F,u}$ with the equations (C.22) and (C.2),

$$Z_H=\frac{4W_H}{W_F}Y_{F,1}\left(\frac{\zeta-\zeta_{st}}{1-\zeta_{st}}\right)+\frac{2W_H}{W_{H_2O}}Y_{H_2O,b}=\frac{4W_H}{W_F}Y_{F,1}\zeta \tag{C.47}$$

$$Y_{H_2O,b}=\frac{2W_{H_2O}}{W_F}Y_{F,1}\zeta-\frac{2W_{H_2O}}{W_F}Y_{F,1}\left(\frac{\zeta-\zeta_{st}}{1-\zeta_{st}}\right) \tag{C.48}$$

$$Y_{H_2O,b}=\frac{2W_{H_2O}}{W_F}Y_{F,1}\left(\zeta-\left(\frac{\zeta-\zeta_{st}}{1-\zeta_{st}}\right)\right) \tag{C.49}$$

$$Y_{H_2O,b}=\frac{2W_{H_2O}}{W_F}Y_{F,1}\zeta_{st} \tag{C.50}$$

BIOGRAPHY

Barış Ali Şen was born in 1979 in Kassel-Germany. He completed his primary and secondary school education in Ordu. Following graduation from Ordu Anatolian High School he started his undergraduate study at the School of Mechanical Engineering in the İ.T.Ü. and received his B.Sc. degree in 2001. Since 2001, he is a graduate student in İ.T.U. Applied Science and Technology Institute –Energy Programme. In 2002 he was involved in a research on intrinsic low-dimensional manifolds method at the interdisziplinäres Zentrum für wissenschaftliches Rechnen at the Ruprecht – Karls - Universität Heidelberg.

Since 2000, Barış Ali Şen has been working as a researcher in the Fluids Laboratories of the School of Mechanical Engineering, İTÜ.